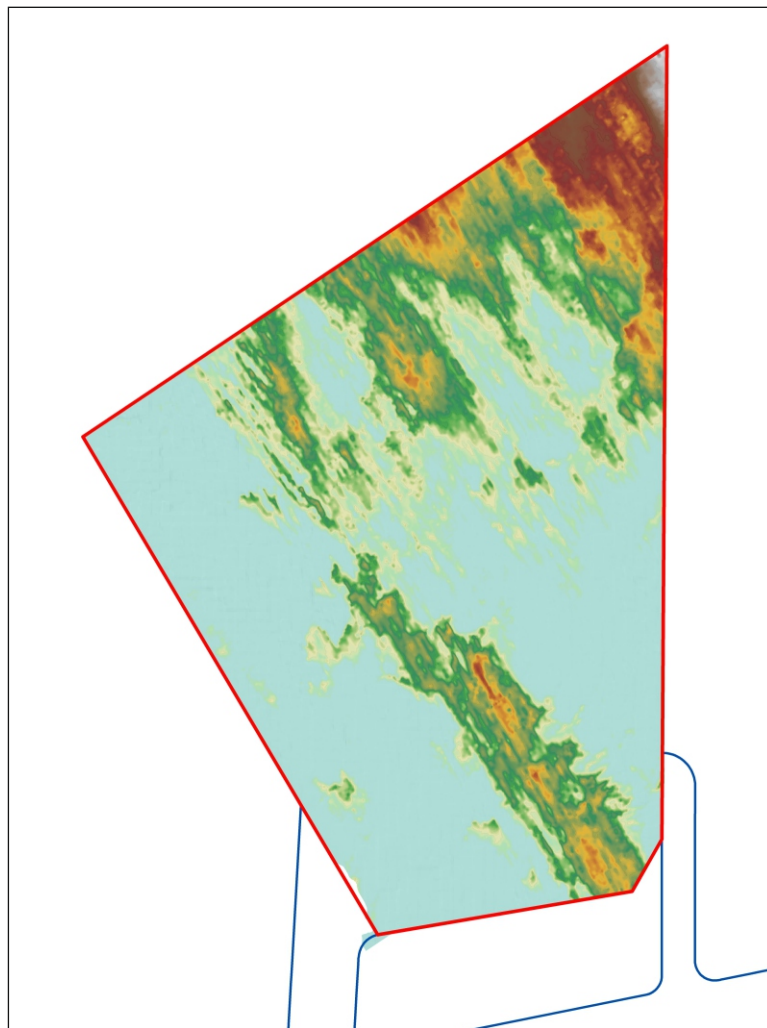




# Norfolk Vanguard Offshore Wind Farm

Stage 4 Palaeoenvironmental Assessment



Ref: 114844.01  
May 2019



© Wessex Archaeology Ltd 2019, all rights reserved.

Portway House  
Old Sarum Park  
Salisbury  
Wiltshire  
SP4 6EB

[www.wessexarch.co.uk](http://www.wessexarch.co.uk)

Wessex Archaeology Ltd is a Registered Charity no. 287786 (England & Wales) and SC042630 (Scotland)

#### Disclaimer

The material contained in this report was designed as an integral part of a report to an individual client and was prepared solely for the benefit of that client. The material contained in this report does not necessarily stand on its own and is not intended to nor should it be relied upon by any third party. To the fullest extent permitted by law Wessex Archaeology will not be liable by reason of breach of contract negligence or otherwise for any loss or damage (whether direct indirect or consequential) occasioned to any person acting or omitting to act or refraining from acting in reliance upon the material contained in this report arising from or connected with any error or omission in the material contained in the report. Loss or damage as referred to above shall be deemed to include, but is not limited to, any loss of profits or anticipated profits damage to reputation or goodwill loss of business or anticipated business damages costs expenses incurred or payable to any third party (in all cases whether direct indirect or consequential) or any other direct indirect or consequential loss or damage.

## Document Information

Document title	Norfolk Vanguard Offshore Wind Farm
Document subtitle	Stage 4 Palaeoenvironmental Analysis
Document reference	114844.01
Client name	Royal HaskoningDHV
Address	2 Abbey Gardens Great College Street Westminster London SW1P 3NL
On behalf of	Norfolk Vanguard Limited
Address	First Floor, 1 Tudor Street London EC4 YOAH
Site location	Southern North Sea
Planning authority	Marine Management Authority
WA project name	Vanguard Offshore Stage 4
WA project codes	114844 (114840, 114841, 114842, 114843)
Project management by	Dave Norcott
Document compiled by	Claire Mellett
Contributions from	Alex Brown, Ines Lopez-Doriga, Dave Howell, Megan Metcalfe, Andrew Shaw, Louise Tizzard, John Whittaker and Phil Toms
Graphics by	Nancy Dixon

## Quality Assurance

Issue and date	Status	Author	Approved by
1 01/02/2019	External draft	CLM	DRN
2 11/02/2019	Revised draft after RHDHV comments	CLM	DRN
3 14/03/2019	Revised after client comments	CLM	DRN
4 02/05/2019	Revised after Historic England comments	CLM	DRN

### DATA LICENCES

This product has been derived in part from material obtained from the UK Hydrographic Office with the permission of the UK Hydrographic Office and Her Majesty's Stationery Office.

© Crown copyright, [2019]. Wessex Archaeology Ref. HA294/007/316-01.

The following notice applies:

**NOT TO BE USED FOR NAVIGATION**

**WARNING:** The UK Hydrographic Office has not verified the information within this product and does not accept liability for the accuracy of reproduction or any modifications made thereafter.

Contains Ordnance Survey data © Crown copyright and database rights [2019]







## Contents

<i>Non-technical summary</i> .....	<i>iii</i>
<i>Acknowledgements</i> .....	<i>v</i>
<b>1 INTRODUCTION</b> .....	<b>1</b>
1.1 Project background.....	1
1.2 Summary of previous works.....	1
<b>2 AIMS AND OBJECTIVES</b> .....	<b>3</b>
<b>3 GEOARCHAEOLOGICAL BACKGROUND</b> .....	<b>4</b>
3.1 Geological baseline .....	4
3.2 Archaeological record .....	6
<b>4 METHODS</b> .....	<b>9</b>
4.1 Stage 4 analysis .....	9
4.2 Foraminifera and ostracods .....	9
4.3 Pollen and charcoal .....	10
4.4 Plant macrofossils.....	10
4.5 Radiocarbon dating and chronological modelling .....	11
4.6 Optical stimulated luminescence dating .....	11
4.7 Palaeogeographic reconstructions.....	13
<b>5 RESULTS</b> .....	<b>15</b>
5.1 Deposit model.....	15
5.2 Foraminifera and Ostracods.....	16
5.3 Pollen and charcoal .....	18
5.4 Plant macrofossils.....	20
5.5 Radiocarbon dating and chronological modelling .....	22
5.6 Optical stimulated luminescence dating .....	24
5.7 Palaeogeographic reconstructions.....	26
<b>6 DISCUSSION</b> .....	<b>27</b>
6.1 Introduction.....	27
6.2 Middle to Upper Palaeolithic (Early-Mid Devensian) [MIS 5e – MIS 3] .....	27
6.3 Late Upper Palaeolithic to Mesolithic (Late Devensian to Holocene) [MIS 2-1] .....	30
<b>7 CONCLUSIONS</b> .....	<b>36</b>
<b>8 RECOMMENDATIONS</b> .....	<b>38</b>
<b>REFERENCES</b> .....	<b>39</b>
<b>APPENDICES</b> .....	<b>47</b>
Appendix 1 – list of sub-samples.....	47
Appendix 2 – Foraminifera and ostracod results .....	2
Appendix 3 – raw pollen data VC074 .....	1
Appendix 4 – radiocarbon reports .....	1
Appendix 5 – OSL report.....	1
Appendix 6 – Norfolk Vanguard site stratigraphy (deposit model) .....	2

## List of Figures

<b>Figure 1</b>	Location of Norfolk Vanguard site
<b>Figure 2</b>	Chronostratigraphic timeline for the last 1 million years
<b>Figure 3a</b>	Norfolk Vanguard East extent and location of deposits showing palaeogeographic features mapped from geophysical data



- Figure 3b** Norfolk Vanguard West extent and location of deposits showing palaeogeographic features mapped from geophysical data
- Figure 4** Pleistocene ice limits
- Figure 5** Location of geotechnical boreholes showing stages of geoarchaeological assessment/analysis
- Figure 6** Vibrocore log and geophysical palaeolandscape assessment showing palaeoenvironmental and dating results and interpretation, for VC074
- Figure 7** Vibrocore log and geophysical palaeolandscape assessment showing palaeoenvironmental and dating results and interpretation, for VC076
- Figure 8** Vibrocore log and geophysical palaeolandscape assessment showing palaeoenvironmental and dating results and interpretation, for VC079
- Figure 9** Vibrocore log and geophysical palaeolandscape assessment showing palaeoenvironmental and dating results and interpretation, for VC085
- Figure 10** Vibrocore log and geophysical palaeolandscape assessment showing palaeoenvironmental and dating results and interpretation, for VC107
- Figure 11** Pollen diagram for VC074
- Figure 12** Bayesian modelling of radiocarbon dates
- Figure 13** Palaeogeography of Norfolk Vanguard West during the early Devensian, PalaeoDEM taken from Fugro (2017), sea level from Waelbroeck et al. (2002)
- Figure 14** Middle to Upper Palaeolithic sea-level and palaeolandscape history of Norfolk Vanguard West
- Figure 15** Schematic cross section of site stratigraphy (deposit model)
- Figure 16** Preservation of palaeolandscape features
- Figure 17** Upper Palaeolithic to Mesolithic sea-level and palaeolandscape history of Norfolk Vanguard West

#### List of Tables

- Table 1** Previous marine archaeological works in support of the Norfolk Vanguard Project Area
- Table 2** Stages of geoarchaeological assessment and recording.
- Table 3** Parameters used in palaeogeographic model
- Table 4** Shallow-stratigraphy of the Norfolk Vanguard site (deposit model)
- Table 5** Foraminifera and ostracod assessment, vibrocore VC074
- Table 6** Foraminifera and ostracod assessment, vibrocore VC085
- Table 7** Plant macrofossils
- Table 8** AMS radiocarbon dates
- Table 9** Dose Rate ( $D_r$ ) and Equivalent Dose ( $D_e$ ) and resulting OSL age estimates. Age estimates expressed in ka relative to year of sampling. Uncertainties in age are quoted at  $1\sigma$  confidence and include combined systematic and experimental variability.
- Table 10** Palaeogeography of the NV West site during Early to Mid-Devensian
- Table 11** Archaeological potential of deposits studied within the Norfolk Vanguard site



## Non-technical summary

Wessex Archaeology (WA) were commissioned by Royal HaskoningDHV to undertake Stage 4 palaeoenvironmental analysis and dating of vibrocore sample retrieved from the Norfolk Vanguard site, comprising Norfolk Vanguard West (NV West) and Norfolk Vanguard East (NV East).

The results presented in this report build upon previous geoarchaeological and geophysical works that included a review of geotechnical vibrocore logs, geoarchaeological recording, deposit modelling, palaeoenvironmental assessment, dating and palaeolandscape feature mapping from seismic data (WA 2017a; 2017b; 2018a; 2018b). Additional results presented here for the first time include additional foraminifera and ostracod assessment, and optical stimulated luminescence (OSL) dating of sub-samples from Upper Brown Bank deposits, and high-resolution pollen analysis and radiocarbon dating of an Early Holocene peat sequence.

The principle aim of this report is to assess the submerged palaeolandscape resource within the Norfolk Vanguard project area by integrating the results from all stages of marine geoarchaeological and geophysical works. The report focusses on two key periods; Middle to Upper Palaeolithic, and late Upper Palaeolithic to Mesolithic, which are represented by deposits belonging to Upper Brown Bank (Unit 5) and Elbow Formation (Unit 7), respectively.

The age and depositional history of Upper Brown Bank deposits is of archaeological interest as it can help establish if the southern North Sea was marine or terrestrial during the early parts of the last glacial period, which is of importance considering there is no evidence of hominins in Britain at this time.

The results suggest Upper Brown Bank was deposited in a shallow embayment fringed by open estuaries between 82 ka and 57 ka, during a period of climatic instability and fluctuating sea levels in the Early Devensian. Palaeogeographic modelling shows that at times of low sea level, there is potential for parts of NV West to become partially exposed creating an irregular coastal geography characterised by isolation basins, barriers/spits and lagoons. The Brown Bank embayment appears to have been a persistent feature in the landscape until ~57 ka when sea levels fell low enough to fully expose the southern North Sea. Interestingly, this broadly correlates to the timing of reoccupation of Britain (~60 ka). Therefore, it could be argued that the presence of the Brown Bank embayment created a significant geographic barrier to migration pathways through the southern North Sea during the Middle Palaeolithic.

Doggerland, the area of the southern North Sea that was previously sub-aerially exposed, is known for its potential to preserve prehistoric archaeology. Reconstructing environmental change using submerged palaeolandscapes is important for targeting where archaeology is most likely preserved, but also for providing a landscape context for any prehistoric activity. For this reason, Early Holocene minerogenic and peat deposits belonging to the Elbow Formation (Unit 7) were targeted for palaeoenvironmental analysis and dating.

An extensive submerged palaeolandscape characterised by a network of meandering river channels fringed by wetland and woodland areas has been identified within NV West. Radiocarbon dates indicate two possible phases of peat development; the first during the Windermere Interstadial as climate warmed at the end of the last glacial period, and the second in the Early Holocene after a period of hiatus associated with the Loch Lomond Stadial.

The peat deposits document up to ~3,500 years of environmental history and show the vegetation was largely woodland which was initially dominated by birch, and later by pine which was succeeded by hazel. The presence of charcoal in peat deposits provides evidence of repeated fire-events which can be caused by human activity or natural processes.



The results from two new sea-level limiting points suggest NV West was flooded by rising sea levels after ~10,000 cal. BP. Rates of sea-level rise were rapid at this time, which is thought to be a significant factor in the exceptional preservation observed. Subsequent burial of submerged palaeolandscape features by marine sand banks also appears to have played a role in protecting them from erosion.

By integrating marine geoarchaeological and geophysical techniques, we have identified an extensive, previously unknown submerged palaeolandscape resource within the Norfolk Vanguard site. The results have been used to reconstruct vegetation and environmental history over a period of up to 3,500 yrs, from the late Upper Palaeolithic to early Mesolithic. They have also been used to reappraise the formation history of Middle to Upper Palaeolithic deposits in relation to southern North Sea palaeogeography at a time when humans are apparently absent from Britain. To maximise the impact of this work, it is recommended the results are published as two period-specific articles in a peer-reviewed journal.



## **Acknowledgements**

This work was commissioned by Royal HaskoningDHV on behalf of Vattenfall. We would like to thank Victoria Cooper and David Tarrant of Royal HaskoningDHV for their support during production of this report, as well as Fugro and Joseph Hine of Vattenfall for provision of seismic interpretations.

This report was compiled by Dr Claire Mellett, Wessex Archaeology (WA). Foraminifera and ostracod assessment was carried out by Dr John Whittaker. Optical stimulated luminescence dating was undertaken at University of Gloucestershire by Prof. Phil Toms. Radiocarbon dating was carried out at 14 Chrono Centre, Queens University, Belfast. Pollen analysis was undertaken by Dr Alex Brown (WA), plant macrofossil assessment and chronological modelling was undertaken by Dr Ines Lopez Doriga (WA) and Nicki Mulhall (WA) carried out sub-sampling and macrofossil extraction. Geophysical data assessment was undertaken by Megan Metcalfe (WA) and Dave Howell (WA). Palaeogeographic modelling was carried out by Dr Claire Mellett (WA). Dr Louise Tizzard (WA) and Dr Andrew Shaw provided technical review. Illustrations were prepared by Nancy Dixon (WA). Quality control and project management was provided by Dave Norcott (WA).

# Norfolk Vanguard Offshore Wind Farm

## Stage 4 Palaeoenvironmental Analysis

### 1 INTRODUCTION

#### 1.1 Project background

1.1.1 Wessex Archaeology (WA) have been commissioned by Royal HaskoningDHV to undertake Stage 4 paleoenvironmental analysis and dating of vibrocores within the proposed Norfolk Vanguard project area comprising the offshore wind farm array (the site), the offshore cable corridor, and area of project interconnector cables (**Figure 1**).

1.1.2 The Norfolk Vanguard site is located in the southern North Sea (**Figure 1**). It comprises two separate tranches, Norfolk Vanguard West (NV West) and Norfolk Vanguard East (NV East) which lie 47 km and 89 km respectively, east of Bacton, north Norfolk. An Offshore Cable Corridor joins the NV West and NV East sites to the landfall site at Happisburgh South, on the Norfolk coast (**Figure 1**).

1.1.3 The location of the Norfolk Vanguard site is of prehistoric archaeological interest, located in an area that at the end of the last ice age formed part of a vast habitable plain connecting Britain with the rest of the European continent. This landscape was later submerged by rising post-glacial sea levels with full marine conditions occurring across the southern North Sea basin by ca. 8,000 yrs before present (BP) (**Figure 2**).

#### 1.2 Summary of previous works

1.2.1 Marine archaeological works in support of the Norfolk Vanguard Offshore Wind Farm project have been ongoing since 2017 (**Table 1**) and include assessments of marine geotechnical (WA 2017a; 2018a; 2018b) and geophysical site-specific surveys (WA 2017b) undertaken in support of the proposed development.

**Table 1** Previous marine archaeological works in support of the Norfolk Vanguard Project Area

Report type	Title	Report no.	Reference
Stage 1	Vanguard Offshore Wind Farm Stage 1 Geoarchaeological Review	114840.01	WA 2017a
Marine geophysics	Norfolk Vanguard Offshore Wind Farm Marine Archaeological Technical Report	112380.02	WA 2017b
Stage 2	Vanguard Offshore Wind Farm Stage 2 Geoarchaeological Recording and Deposit Modelling	112380.03	WA 2018a
Stage 3	Vanguard Offshore Wind Farm Stage 3 Geoarchaeological Sampling and Assessment	114843.01	WA 2018b

1.2.2 An assessment of marine geophysical data, principally sub-bottom seismic data, identified 171 features with paleogeographic potential within the Norfolk Vanguard site (18 in the NV East site, 110 in the NV West site and 43 in the Offshore Cable Corridor (WA 2017b). These included high amplitude reflectors and acoustic blanking, possibly indicative of peat and/or shallow gas, and cut and fill features interpreted to be palaeochannels (**Figure 3**).

- 1.2.3 Geotechnical data collected from the Norfolk Vanguard site included 65 vibrocores which provide a near-continuous record of the deposits within 6 m of the seabed. A Stage 1 review of geotechnical logs identified 22 vibrocores that were recommended for Stage 2 geoarchaeological recording as they potentially comprised deposits of archaeological interest (WA 2017a).
- 1.2.4 The results of geoarchaeological recording, interpreted alongside the geophysical data, were used to develop an outline deposit model for the Norfolk Vanguard site (WA 2018a). Given the relatively large distance between vibrocores (~3-6 km), a series of 2D cross sections were produced to represent the extent and depth of deposits across the site. Three Units were identified as having archaeological potential, Upper Brown Bank, Twente Formation and Holocene sediments. Recommendations were made for Stage 3 palaeoenvironmental assessment on five vibrocores (VC074, VC076, VC079, VC085 and VC107) to determine the age and depositional history of these deposits, and the potential for preservation of palaeoenvironmental material.
- 1.2.5 Stage 3 palaeoenvironmental assessment included pollen, diatom, foraminifera, ostracod and plant macrofossil assessment, particle size analysis, and radiocarbon and optical stimulated luminescence (OSL) dating (WA 2018b). The key results are summarised in Section 5 and 6 of this report. Recommendations included additional radiocarbon dating and pollen analysis from a peat deposit in VC074 to provide a high-resolution record of vegetation development. Additional OSL dating of Upper Brown Bank in VC074 and VC107 was recommended, combined with further foraminifera and ostracod assessment in VC079 and VC085, to refine the chronology and depositional history of Upper Brown Bank in relation to periods of hominin presence/absence in Britain.
- 1.2.6 Concurrently, a series of geophysical and geoarchaeological works were undertaken in support of the proposed Norfolk Boreas site which lies directly adjacent to the Norfolk Vanguard site (**Figure 1**). A palaeolandscapes assessment of geophysical data was undertaken and identified features of archaeological interest that included palaeochannels and areas of shallow gas possibly indicative of organic deposits (WA 2018c). A total of 61 vibrocores were recovered from the Norfolk Boreas site and after a Stage 1 geoarchaeological review (WA 2018d), followed by Stage 2 geoarchaeological recording (WA 2018e), Upper Brown Bank and Holocene pre-transgression deposits from five vibrocores were selected for further palaeoenvironmental work. The results from Stage 3 palaeoenvironmental assessment (WA 2018f) reveal the deposits at the Norfolk Boreas site are contemporaneous with those in the Norfolk Vanguard site suggesting the features and deposits identified are part of a much larger submerged landscape that has not previously been identified. At the time of writing, results from Stage 4 palaeoenvironmental analysis of deposits from the Norfolk Boreas site are pending.

### 1.3 Scope of report

- 1.3.1 To help frame geoarchaeological investigations of this nature, WA has developed a five-stage approach, encompassing different levels of investigation appropriate to the results obtained, accompanied by formal reporting of the results at the level achieved. The stages are summarised below (**Table 2**).
- 1.3.2 This report presents the results of Stage 4 palaeoenvironmental analysis and integrates the results of the previous geoarchaeological and geophysical assessments to reconstruct palaeoenvironmental evolution of the Norfolk Vanguard site in relation to the submerged palaeolandscapes resource.



**Table 2** Stages of geoarchaeological assessment and recording.

Stage	Method	Description
1	Review	A desk-based archaeological review of the borehole, vibrocore and CPT logs generated by geotechnical contractors. Aims to establish the likely presence of horizons of archaeological interest and broadly characterise them, as a basis for deciding whether and what Stage 2 archaeological recording is required. The Stage 1 report will state the scale of Stage 2 work proposed.
2	Geoarchaeological recording and deposit modelling	Archaeological recording of selected retained or new core samples will be undertaken. This will entail the splitting of the cores, with each core being cleaned and recorded. The Stage 2 report will state the results of the archaeological recording and will indicate whether any Stage 3 work is warranted.
3	Sampling assessment and	Dependent upon the results of Stage 2, sub-sampling and palaeoenvironmental assessment (pollen, diatoms and foraminifera) may be required. Subsamples will be taken if required. Assessment will comprise laboratory analysis of the samples to a level sufficient to enable the value of the palaeoenvironmental material surviving within the cores to be identified. Subsamples will also be taken and/or retained at this stage in case scientific dating is required during Stage 4. Some scientific dating (e.g. radiocarbon or Optically Stimulated Luminescence (OSL)) may be undertaken at this stage to provide chronological context. The Stage 3 report will set out the results of each laboratory assessment together with an outline of the archaeological implications of the combined results, and will indicate whether any Stage 4 work is warranted.
4	Analysis dating and	Full analysis of pollen, diatoms and/or foraminifera assessed during Stage 3 will be undertaken. Typically, Stage 4 will be supported by scientific dating (e.g. radiocarbon or OSL) of suitable subsamples. Stage 4 will result in an account of the successive environments within the coring area, a model of environmental change over time, and an outline of the archaeological implications of the analysis.
5	Final report	If required Stage 5 will comprise the production of a final report of the results of the previous phases of work for publication in an appropriate journal. This report will be compiled after the final phase of archaeological work, whichever phase that is.

## 2 AIMS AND OBJECTIVES

2.1.1 The principle aim of this report is to assess the submerged palaeolandscape resource within the Norfolk Vanguard site by integrating the results from all stages of marine geoarchaeological and geophysical works (see section 1.2).

2.1.2 This will be achieved through the following objectives;

- Present the results from Stage 4 palaeoenvironmental analysis and dating;
- Refine the deposit model, outlining the stratigraphy, depositional environment, age, extent and depth of deposits;
- Reconstruct palaeogeographic and palaeoenvironmental evolution, and;

- Assess the archaeological resource, its preservation potential, and the implications for prehistoric archaeology.

2.1.3 A series of period-specific research questions are proposed below, building upon previous works (WA 2018a; 2018b) and taking into account the regional research framework (Medlycott 2011) and the national maritime research framework (Ransley et al. 2013).

#### *Middle to Upper Palaeolithic*

- What is the age and depositional history of Brown Bank Formation?
- What is the palaeogeography of the area during deposition of Brown Bank Formation?
- How do the findings relate to the presence or absence of hominins in Britain during the Middle Palaeolithic?

#### *Late Upper Palaeolithic to Mesolithic*

- What is the age and formation history of the preserved peat deposits?
- What is the landscape and vegetation history?
- Is there evidence for hominin activity?
- What is the timing and nature of landscape inundation?

### **3 GEOARCHAEOLOGICAL BACKGROUND**

#### **3.1 Geological baseline**

- 3.1.1 Geoarchaeological assessments are typically undertaken with reference to geological periods (e.g. Quaternary), epochs (e.g. Pleistocene) and sub-epochs (e.g. Devensian) that reflect major climate, sea-level or environmental changes. Here we adopt British nomenclature correlated to the Marine Isotope Stage (MIS) record to distinguish between different climatic periods, with dates given as ka (thousands of years before present). Marine Isotope Stages are deduced from marine palaeoclimatic records and reflect alternating warm (interglacial) and cold (glacial) periods throughout the Quaternary. Some Marine Isotope Stages can be subdivided into sub-stages reflecting relatively warmer (interstadial) or cooler (stadial) periods within a single stage.
- 3.1.2 The Norfolk Vanguard site is located in an area characterised by Pleistocene and Holocene sediments (Cameron et al. 1992), comprising clays, silts, sands and gravels with occasional organic-rich deposits (peats), overlain by recent unconsolidated marine shelly sands.
- 3.1.3 The Pleistocene geological history of the North Sea basin is dominated by repeated glacial/interglacial cycles, resulting in rising and falling sea levels (**Figure 2**) and deposition of terrestrial, marine and glacially-derived sediments. The Norfolk Vanguard site, and southern North Sea in general, is known to contain an important sedimentary archive including material dating from the earliest occupation of North Western Europe (Parfitt et al. 2010) up to more recent post-glacial reoccupation of Britain (Waddington 2015).
- 3.1.4 Only one glacial episode is thought to have directly affected the area. This was during the Anglian period (MIS 12, 480-423 ka) when ice extended into the southernmost North Sea (**Figure 4**). During subsequent glacial episodes, ice sheets terminated further north so did not directly affect the region. However, indirect affects resulting from changing sea levels

and cold periglacial conditions will have influenced the region. The exact southern extent of the Anglian glaciation is debatable. However, bathymetric data suggests part of the Anglian ice sheet may have extended as far south as offshore from Felixstowe (Emu 2009), and Dix and Sturt (2011) argue for an Anglian glacial origin for over-deepened valleys (tunnel valleys) identified within the Outer Thames estuary.

- 3.1.5 As the area off East Anglia, including the study area, has only experienced one glacial advance during the Pleistocene (**Figure 4**), palaeolandscape features from periods of low relative sea level are more likely to be preserved here rather than further north (approximately north of the north Norfolk coast), where they have been removed during the subsequent Saalian and Devensian glacial advances. Any surviving Pleistocene deposits may have been reworked or redeposited to a certain extent during subsequent marine transgressions (Cameron et al. 1992), but there is potential for them to survive on the seabed.
- 3.1.6 Potential superficial deposits of geoarchaeological significance likely to be encountered within the Norfolk Vanguard site area include the Brown Bank Formation, tentatively dating from the late Ipswichian interglacial to early Devensian glaciation (Limpenny et al. 2011).
- 3.1.7 The Brown Bank Formation includes deposits of silty sand, sandy silt and sandy silty clay, which is in places up to 20 m thick. The sandy silty clay deposits are here termed the Upper Brown Bank, to distinguish them from the underlying deposits of silty sand and sandy silt that characterise both the Lower Brown Bank (Early Devensian) and underlying Eem Formation (Ipswichian) (Limpenny et al. 2011; Bicket and Tizzard 2015).
- 3.1.8 The Brown Bank Formation is present as a blanket deposit across the general area and has traditionally been interpreted to represent a shallow lagoon environment, comprising clayey silty sands (Cameron et al. 1992; Limpenny et al. 2011).
- 3.1.9 Brown Bank Formation has been previously dated using OSL (WA 2008; Limpenny et al. 2011; Tizzard et al. 2014; 2015) and ages fell into two broad ranges: MIS 3 and MIS 5d-5c. Based on this evidence, it is not clear if Brown Bank Formation was deposited over the duration of the early Devensian, or if deposition was more episodic punctuated by periods of hiatus and sub-aerial exposure (Tizzard et al. 2015). The date of the Brown Bank Formation therefore has significant implications both for our understanding of the palaeogeographic development of the North Sea as well as the nature and significance of any archaeology, if preserved.
- 3.1.10 In places across the southern North Sea a sequence of early Holocene deposits are mapped overlying Pleistocene sediments. The Holocene sediments include organic-rich peats along with more minerogenic fluvial and alluvial sediments, most often infilling channels (Limpenny et al. 2011; Tappin et al. 2011; Tizzard et al. 2015; Gearey et al. 2017; Brown et al. 2018), but also preserved on the Brown Bank Formation or overlying periglacial aeolian sediment. The peats are of high geoarchaeological potential, preserving a range of palaeoenvironmental remains and material suitable for radiocarbon dating.
- 3.1.11 Pleistocene and early Holocene sediments are capped by post-transgression marine sands. The progressive inundation of the North Sea occurred over an extended time scale, with particularly rapid sea-level rise during the early Holocene (11.5-7 ka), and with fully marine conditions occurring by around 6 ka (Sturt et al. 2013). However, limitations in the availability of reliable sea-level index-points (Hazell 2008, WA 2013a), combined with uncertainty around the glacio-isostatic response of the southern North Sea, make it difficult to

accurately reconstruct sea-level history and the timing of inundation across the Norfolk Vanguard site.

### 3.2 Archaeological record

- 3.2.1 The southern North Sea off the east coast of East Anglia is known to contain relatively well preserved palaeolandscape features such as fluvial channels that formed during periods of lower sea level when the southern North Sea was free of ice. The remains of these terrestrial landscapes are frequently recovered by dredging and fishing activities in numerous areas around the southern North Sea, generally in the form of the remains of extinct megafauna (e.g. woolly mammoths, woolly rhinoceros, bison, horse, lion and hyena).
- 3.2.2 The discovery of actual human artefacts, such as stone tools and worked bone, and even remains is a rarer occurrence, but artefacts have been recovered (e.g. Hublin et al. 2009). Reported finds from offshore activity has, to date, produced a range of early prehistoric lithic artefacts indicating early prehistoric activity in submerged palaeolandscapes from Lower, Middle, and Upper Palaeolithic periods (Tizzard et al. 2015; WA 2011; 2013b), with notable collections of more recent Mesolithic artefacts from submerged palaeolandscape contexts (Momber et al. 2011; WA 2013a).
- 3.2.3 The earliest records of Lower Palaeolithic archaeology from northern Europe are associated with terrestrial deposits on the margins of the North Sea basin in East Anglia, most notably from Pakefield (Parfitt et al. 2005) and Happisburgh Site 3 (Parfitt et al. 2010). Whilst the archaeology at Pakefield was created during a fully interglacial, more Mediterranean climate, at around MIS 17 (**Figure 2**), the remains at Happisburgh Site 3 are older (MIS 21 or MIS 25) and the environmental evidence is indicative of cool conditions at the edge the boreal zone (Candy et al. 2011) which implies that these early hominins were capable of surviving in northern Europe in periods not associated with fully interglacial environments (Parfitt et al. 2010). The importance of these sites is international, as they are currently unique at this latitude for this early date (WA 2013a).
- 3.2.4 Cohen et al. (2012) highlighted the North Sea basin as a key region for understanding Pleistocene hominins within a northerly, coastal environment. The east of England, particularly East Anglia, but also the southeast of England, are important regions for later Middle Pleistocene, Lower Palaeolithic archaeology (MIS 13-MIS 9). During this timeframe British archaeology reflects repeated episodes of hominin occupation during temperate interglacial and cool conditions, separated by phases of hominin absence during fully glacial periods.
- 3.2.5 Archaeological evidence is particularly abundant during MIS 13 and MIS 11 (**Figure 2**) (Wymer 1999; Pettitt and White 2012) when warmer climate conditions meant Britain was again available to be recolonised by hominin communities, after a period of absence during the preceding Anglian glaciation (MIS 12). Lower Palaeolithic archaeological assemblages of this date tend to be characterised by handaxes, although during the earlier part of MIS 11, collections lacking handaxes (termed Clactonian) have been recognised. The foreshore, cliffs and hinterland at Clacton-on Sea (Essex) comprise an important Lower Palaeolithic site which is a designated geological Site of Special Scientific Interest (SSSI). Channel sediments from the area are also an important site for the Lower Palaeolithic Clactonian flint industry and have yielded a rare wooden spear alongside lithic artefacts. This archaeology dates from the Hoxnian interglacial period (MIS 11, c. 423 – 380 ka, **Figure 2**) (Sumbler 1996; Bridgland et al. 1999), and the type site for the Hoxnian (the Hoxne Brick Pit) is located a relatively short distance inland outside of Diss, Suffolk (Ashton et al 2008).

- 3.2.6 During the MIS 10 glaciation (**Figure 2**) there appears to have been a hiatus in hominin activity in Britain (Pettitt and White 2012). The post MIS 10 occupation Britain is associated with the emergence of the Neanderthals and their associated archaeology and patterns of behaviour. From the later part of MIS 9 the archaeological record attests to the development of Levallois core working strategies (White and Ashton 2003). This is also seen to mark the end of the Lower Palaeolithic and the beginning of the Middle Palaeolithic. The Levallois technique comes to dominate the British archaeological record during the early Middle Palaeolithic (late MIS 8 and MIS 7), with handaxe production occurring infrequently (Scott and Ashton 2011).
- 3.2.7 The international importance of early Middle Palaeolithic archaeology in the southern North Sea is highlighted by the numerous sites preserved within the Thames river terraces (White 2006; Scott et al. 2011) and, in particular, by the submerged prehistoric Levallois lithic assemblage from marine aggregate licence Area 240 in the palaeo-Yare catchment. Over 120 artefacts have now been recovered from this locale, some of which are identifiable as Levallois, with many recovered from in situ or minimally disturbed contexts (Tizzard et al. 2014; 2015; WA 2013a; 2013b).
- 3.2.8 The substantial, mixed assemblage of handaxes also recovered from Area 240 may be of older Lower Palaeolithic origin (e.g. >MIS 9, **Figure 2**), or may date to the Later Middle Palaeolithic when handaxes re-emerge as one of the key components of the archaeological record (late MIS 4-MIS 3, **Figure 2**) (Boismier et al. 2012). However, based on palaeoenvironmental and sedimentological evidence an early Middle Palaeolithic date is most likely (Tizzard et al. 2015).
- 3.2.9 Palaeogeographically, Area 240 is one of the most northerly Neanderthal sites in northwest Europe and of primary archaeological importance for defining Middle Palaeolithic potential and the contemporary palaeogeography across the southern North Sea basin (Tizzard et al. 2014). The site highlights the archaeological potential of preserved Pleistocene fluvial deposits within the southern North Sea.
- 3.2.10 Currently there is no definitive evidence of a hominin presence in Britain during the Ipswichian (MIS 5e) or the early Devensian (MIS 5d-a; Lewis et al. 2011). Within the context of early prehistory and submerged palaeogeography, however, substantial areas of the southern North Sea basin would have been dry land during the warming and cooling limbs of the various sub-stages (MIS 5d to 5a, **Figure 2**) and archaeological sites of this age are relatively abundant in northern France (Lewis et al. 2011; Pettitt and White 2012). Therefore, the potential exists for human activity to have occurred sporadically both within Britain and in any sub-aerially exposed parts of the southern North Sea basin, during the early Devensian.
- 3.2.11 From late MIS 4 to MIS 3 there is evidence in Britain for Neanderthal recolonization. This late Middle Palaeolithic archaeological record is associated with morphologically and technologically distinctive handaxes (White and Jacobi 2002). A key site belonging to this period is Lynford Quarry, Norfolk where a palaeochannel containing mammoth remains and associated late Middle Palaeolithic stone tools and debitage have been recovered (Boismier et al. 2012).
- 3.2.12 Climatically, MIS 3 was significantly colder than now but did not attain the glacial conditions of later or earlier glacial periods (e.g. MIS 6 or 2, **Figure 2**) (Pettitt and White 2012). For the Neanderthals that may have occupied the region at this time, surviving in the southern North Sea during this period may have been subject to a variety of technological and cultural adaptations (White 2006).



- 3.2.13 In the early Upper Palaeolithic, at the end of the Late Pleistocene, Neanderthals were replaced in northern Europe by modern humans who, occupying and moving through the southern North Sea, were present in Britain from around 34 ka (Jacobi and Higham 2011; Bicket and Tizzard 2015). Archaeological evidence for this period consists of blade point/leaf point assemblages, thought to be associated with the final Neanderthal occupation of Britain, and small number of findspots associated with Evolved Aurignacian and Gravettian lithic artefacts which were produced by modern humans (Jacobi and Higham 2011).
- 3.2.14 During the last glacial period, the study area will have been close to the maximum Devensian ice margin (**Figure 4**). At the maximum of the last glacial period, the environment within the southern North Sea was relatively poor for human colonisation, with humans absent from Britain during these peak cold conditions. However, there was increasing human exploitation after ~15 ka. Humans at this time were hunting game, such as mammoth and deer, and evidence of these animals has been reported through marine aggregate dredging, and the associated reporting requirements (Bicket and Tizzard 2015).
- 3.2.15 The onshore archaeological record of later Upper Palaeolithic activity is marked by Creswellian/Final Magdalenian stone tool assemblages associated with the later Upper Palaeolithic recolonization of Britain (Higham and Jacobi 2011b), and offshore locations may provide unique and important context for coastal and lowland human activity during this period (WA 2013b).
- 3.2.16 The Mesolithic period began in the early Holocene and at around 10 ka, sea levels were approximately 35 m below current levels (Shennan et al. 2018) sub-aerially exposing large parts of the southern North Sea and English Channel making them suitable for human occupation. Archaeological and palaeoenvironmental material from this period has been reported from North Sea contexts for over a century (Reid 1913; Godwin and Godwin 1933). For example, a Maglemosian harpoon artefact was trawled in the early 20th century and was later radiocarbon dated to around 12,000 years ago (Housely 1991).
- 3.2.17 Between 8 and 5 ka, much of the landscape was inundated by eustatically driven sea level change, and by 6 ka sea level was only approximately 7 m below the present level (Shennan et al. 2018). Around this time, Britain became an island again (Coles 1998). Settlements at the time were often transitory and seasonal, and therefore leave little trace in the archaeological record. It is possible that the now submerged environment within the Norfolk Vanguard site was occupied up until the final marine transgression thought to have occurred around 8,000 years ago.
- 3.2.18 It is clear from numerous research and development-led investigations that postglacial marine transgression has not destroyed Pleistocene and Holocene palaeogeography by default (WA 2013b). Areas of preserved palaeogeographic features do remain, and detailed reconstructions of palaeoenvironments and palaeogeography can be achieved for large parts of the North Sea basin (Tappin et al. 2011; Limpenny et al. 2011; Dix and Sturt, 2011).
- 3.2.19 Considerable attention has been paid to Mesolithic landscapes of the southern North Sea (Gaffney et al. 2007; Tappin et al. 2011) as the now-submerged palaeolandscapes provide key contextual evidence for recovered artefacts and a background landscape within which to place these human communities. Increasingly, a maritime perspective has developed for understanding the early prehistoric archaeological record, where coasts, estuaries and wetlands are key landscape elements (Ransley et al. 2013).

## 4 METHODS

### 4.1 Stage 4 analysis

- 4.1.1 Of the five vibrocores subject to Stage 3 assessment (WA 2018) (**Figure 5**), three vibrocores (VC074, VC085 and VC107) were recommended for additional palaeoenvironmental analysis and dating as part of these Stage 4 works.
- 4.1.2 Recommended works included additional OSL dates from Upper Brown Bank deposits in VC074 and VC107 to test if dates are conformable. Foraminifera and ostracod assessment on Upper Brown Bank deposits from VC074 and VC085 was also proposed as these cores were not assessed as part of the Stage 3 works.
- 4.1.3 To provide a higher resolution record of vegetation development during the early Holocene, VC074 was selected for pollen analysis and additional radiocarbon dating.
- 4.1.4 Full analytical methods for each palaeoenvironmental and dating technique are described below. All sub-sample depths are quoted as metres below sea floor (mbsf). In some cases, the elevation of sub-samples has been corrected to Lowest Astronomical Tide (LAT).
- 4.1.5 A full list of sub-samples is presented in **Appendix 1** and shown on **Figures 6-10**.

### 4.2 Foraminifera and ostracods

- 4.2.1 Previous Stage 3 assessment of foraminifera and ostracods from Upper Brown Bank deposits in VC079 and VC107 revealed a rich and diverse assemblage indicative of deposition in a marine embayment or open estuary (WA 2018). To assess potential variations in depositional environment, additional samples from Upper Brown Bank deposits, comprising four sub-samples from VC074 and three from VC085 (itemised in **Appendix 1**), were submitted for foraminifera and ostracod assessment.
- 4.2.2 The sub-samples were weighed, then broken into small pieces by hand, placed into ceramic bowls, and dried in an oven. Boiling-hot water was then poured over them and a small amount of sodium carbonate added to help disaggregate the clay fraction. Each sub-sample was left to soak overnight. Washing was with hand-hot water through a 75 micron sieve, with the remaining residue being returned to the ceramic bowl for final drying in the oven. The residues were then stored in labelled plastic bags.
- 4.2.3 For examination, each sample was placed in a nest of sieves (>50, >250, >150µm, and base pan) and thoroughly shaken. Each grade was then sprinkled onto a picking tray, a little at a time, and viewed under a binocular microscope. "Contained material" were logged on a presence(x)/absence basis as shown in **Table 5** and **Table 6**.
- 4.2.4 The abundance of each foraminiferal and ostracod species was estimated semi-quantitatively (one specimen, several specimens, common and abundant/superabundant) by experience and by eye. Full results, including those from the Stage 3 assessment (WA 2018) are presented in **Appendix 2**.
- 4.2.5 Species identification comes from Murray (2006) for the foraminifera, Athersuch et al. (1989) for the brackish and marine ostracods, and Meisch (2000) for the freshwater ostracods, in addition to expert judgement. For Pleistocene fauna, Whittaker & Horne (2009) was used for ostracod identification, and Jones & Whittaker (2010) for foraminifera identification.

### 4.3 Pollen and charcoal

- 4.3.1 Eight sub-samples from VC074 previously assessed as part of the Stage 3 works (WA 2018) were selected for pollen analysis. An additional eight new sub-samples taken for pollen analysis to increase the resolution of the record. These sub-samples were processed using standard pollen extraction methods (Moore et al. 1991).
- 4.3.2 Pollen was identified and counted using a Nikon eclipse E400 biological research microscope. A target of 500 terrestrial pollen grains was counted for each sub-sample in addition to aquatics and fern spores. In the sub-sample at 1.58 mbsf, lower pollen concentration meant a 500 count was not possible and 300 grains were counted instead.
- 4.3.3 One *Lycopodium* tablet was added to enable calculation of pollen concentrations. Pollen and spores were identified to the lowest possible taxonomic level.
- 4.3.4 Plant nomenclature followed Stace (1997) and Bennett et al. (1994). Pollen sums are based on total land pollen (TLP) excluding aquatics and fern spores which are calculated as a percentage of TLP plus the sum of the component taxa within the respective category. Identification of indeterminable grains was according to Cushing (1967).
- 4.3.5 Plant taxa are assigned to one of the following groups (trees and shrubs, dwarf shrubs, herbs, fern spores and aquatics) based on their most likely ecological affinity, although many plant taxa occur in a range of environmental niches (see Stace 1997 for specific plant taxa).
- 4.3.6 Pollen diagrams were constructed using the software Tilia version 1.7.16 (Grimm 2011), and the diagram was subdivided into local pollen assemblage zones (LPAZ) by eye (**Figure 11**).
- 4.3.7 Pollen data for VC074 are presented in **Appendix 3**.
- 4.3.8 Microscopic charcoal was quantified for each pollen sample using the point count method of Clark (1982). The point count method expresses the total charcoal count as an estimate of the area of charcoal on any given pollen slide for a standard 1 cm<sup>3</sup> volume of sediment.
- 4.3.9 Randomly spaced parallel transects were analysed to ensure that a representative portion of the slide was examined. This is important as pollen and microscopic charcoal are not distributed evenly across a microscope slide. Charcoal is identifiable as highly angular, usually opaque black fragments of varying size and shape, sometimes preserving cellular structure. Humified plant matter may appear very dark brown black under the microscope, but unlike charcoal, usually exhibits translucent and rounded edges.
- 4.3.10 Charcoal data are presented in **Appendix 3** and plotted alongside pollen results in **Figure 11**.

### 4.4 Plant macrofossils

- 4.4.1 Six sub-samples were previously assessed for plant macrofossils as part of Stage 3 works (WA 2018). Two additional sub-samples from VC074 were processed for plant macrofossils to recover material suitable for radiocarbon dating (itemised in **Appendix 1**).
- 4.4.2 All sub-samples were processed by standard methods for the recovery of waterlogged plant remains; the flots were retained on a 0.25 mm mesh. Flots were stored in sealed containers with water. The flots were scanned under a x10–x40 stereo-binocular microscope and the



preservation and nature of the plant remains recorded in **Table 7**. Nomenclature follows Stace (1997).

- 4.4.3 Additional sub-samples other than those to be submitted for radiocarbon dating were not assessed for plant macrofossils. This was due to the large volume of material that would be required to undertake the assessment given the highly compacted and decomposed nature of the peat deposits.

#### **4.5 Radiocarbon dating and chronological modelling**

- 4.5.1 Two sub-samples from VC074 were taken for radiocarbon dating (itemised in **Appendix 1**).

- 4.5.2 Suitable material was identified under microscope (see **4.4**), stored in glass tubes, and sent to the <sup>14</sup>CHRONO Centre at Queens University Belfast for dating. Calibrated age ranges were calculated with OxCal 4.2.3 (Bronk-Ramsey and Lee 2013) using the IntCal13 curve (Reimer et al. 2013). All radiocarbon dates are quoted as uncalibrated years before present (BP), followed by the lab code and the calibrated date-range (cal. BP) at the 2σ (95.4%) confidence.

- 4.5.3 The new dates from VC074, were combined with existing dates acquired during the Stage 3 works (WA 2018) resulting in a total of eight dates, from three separate peat sequences (VC074, VC076 and VC085) (**Table 8**).

- 4.5.4 Radiocarbon dates from VC074 and VC076 were modelled using Bayesian statistics implemented through the software OxCal 4.1 (Bronk-Ramsey and Lee 2013). This approach enables the integration of multiple dates to refine probability distributions for individual ages when the series is presented in relative order governed by the principle of superimposition or other prior knowledge (e.g. biostratigraphy, expert judgement).

- 4.5.5 The model generates a probability for each sub-sample, called a posterior density estimate, which is essentially a product of the prior information (e.g. relative order of dates in a sequence) and likelihood probabilities. The modelled posterior density estimates (*italicised* to differentiate them from the original dating information) (2 sigma) typically reduce uncertainty ranges by 40–50%. An agreement index for individual dates is calculated to assess the difference between the modelled posterior density distribution (dark grey; **Figure 12**) and the original age probability distributions (light grey; **Figure 12**). Thresholds for acceptable agreement are an index of >60% (Ramsey 2009).

- 4.5.6 Model outputs are presented in **Figure 12** and the modelled posterior density estimates are given in **Table 8**.

- 4.5.7 Radiocarbon dating reports are presented in **Appendix 4**.

#### **4.6 Optical stimulated luminescence dating**

##### *Core handling and storage*

- 4.6.1 Vibrocores had been collected in transparent liners, and were split offshore into ~1 m sections, which were then sealed for onshore analysis. Vibrocores with geoarchaeological potential, identified during a Stage 1 review (WA 2017a), were transported to Wessex Archaeology for assessment.

- 4.6.2 At this stage, the ends of each core section and the outer surface of the core had already been exposed to light. Upon receipt, vibrocores were held in a dark core storage facility at Wessex Archaeology prior to geoarchaeological recording and sub-sampling.

- 4.6.3 When opened for geoarchaeological recording, plastic core liners were cut using a hand held vibrating multitool, cutting lengthways through the liner along either side of the core. Care was taken to minimise penetration into the sediment.
- 4.6.4 Depending on the nature of the sediment (cohesion, grain size etc.), the cores either naturally broke apart lengthways into two equal halves (2 x half round cores) or remained intact with minimal disturbance (whole round core).
- 4.6.5 During the geoarchaeological recording process, c.1-2 mm of sediment was removed from exposed core surfaces.
- 4.6.6 To avoid repeated disturbance of deposits, cores were opened and then immediately photographed and described. They were then sealed, wrapped in cling film and secured with Gorilla tape before being returned to the core storage facility. Unnecessary handling of cores was avoided.

#### *Sample selection*

- 4.6.7 Given the cohesive and compacted nature of Upper Brown Bank deposits recovered in cores, there was potential for these cores to be sub-sampled for OSL dating if a sample from the centre of the core could be extracted, avoiding the outer exposed surfaces.
- 4.6.8 Core photographs and geoarchaeological descriptions were used to identify potential core sections suitable for OSL dating, using the following criteria;
- Sediment must be undisturbed with no evidence of cracks, deformation slumping etc. as this could let light into the centre of the core or could allow reworked material to become incorporated into sample taken from the centre. By taking core photographs immediately after the core was opened, the opening/closing of any cracks could be monitored;
  - Sediment must be cohesive to avoid movement or disturbance of loose grains minimising the potential of exposed material becoming mixed with material from the centre of the core during sampling, and;
  - The core must not show evidence of drying out as this will affect water content calculations.
- 4.6.9 Additional sub-samples from VC074 and VC107 were targeted for OSL dating to be considered alongside the existing OSL dates acquired during Stage 3 works (WA 2018).

#### *Sample preparation and analysis*

- 4.6.10 Once suitable deposits were identified for OSL dating, a sub-section of the entire core was removed for delivery to the OSL lab. This was achieved by cutting through both the core liner and the sediment to create a ~30 cm cylinder of sediment still sealed within the core liner. Care was taken to minimise the exposure of new surfaces to light by taking a section from the top or bottom of a core where possible. These sub-sections were sealed in cling film and black liners for transport to the OSL laboratory for sample preparation and analysis.
- 4.6.11 All sample preparation and analysis was undertaken by OSL specialists at the University of Gloucester. Sub-sections were opened and prepared under controlled laboratory illumination provided by Encapsulite RB-10 (red) filters. To isolate any material potentially exposed to light, i.e. the outer core surface, sediment located within 10 mm of each core face was carefully removed to target the centre of the core that had been shielded from

light. Once the OSL sample was isolated, the remaining core material was used to calculate Dose Rate ( $D_r$ ) and moisture content.

- 4.6.12 The remaining sample was dried and then sieved. The fine sand fraction was segregated and subjected to acid and alkaline digestion (10% HCl, 15% H<sub>2</sub>O<sub>2</sub>) to attain removal of carbonate and organic components respectively. A further acid digestion in hydrofluoric acid (HF) (40%) for 60 mins was used to etch the outer 10-15  $\mu\text{m}$  layer affected by  $\alpha$  radiation and degrade each samples' feldspar content. During HF treatment, continuous magnetic stirring was used to effect isotropic etching of grains. 10% HCl was then added to remove acid soluble fluorides. Each sample was dried, resieved and the quartz isolated from the remaining heavy mineral fraction using a sodium polytungstate density separation at 2.68  $\text{g cm}^{-3}$ . Twelve 8 mm multi-grain aliquots (c. 3-6 mg) of quartz from each sample were then mounted on aluminium discs for determination of Equivalent Dose ( $D_e$ ) values.
- 4.6.13 All drying was conducted at 40°C to prevent thermal erosion of the signal. All acids and alkalis were Analar grade. All dilutions (removing toxic-corrosive and non-minerogenic luminescence-bearing substances) were conducted with distilled water to prevent signal contamination by extraneous particles.
- 4.6.14  $D_e$  values were quantified using a single-aliquot regenerative-dose (SAR) protocol (Murray and Wintle 2000; 2003). Weighted (geometric) mean  $D_e$  values were calculated from 12 aliquots using the central age model outlined by Galbraith et al. (1999) and are quoted at 1 $\sigma$  confidence (**5.6.1**). Lithogenic  $D_r$  values were defined through measurement of U, Th and K radionuclide concentration and conversion of these quantities into  $\beta$  and  $\gamma$   $D_r$  values (Adamiec and Aitken, 1998), accounting for  $D_r$  modulation forced by grain size (Mejdahl, 1979) and present moisture content (Zimmerman, 1971) (**5.6.1**). Cosmogenic  $D_r$  values were calculated on the basis of sample depth, geographical position and matrix density (Prescott and Hutton, 1994). Note, no in situ  $\gamma$  spectrometry was undertaken due to these samples being collected offshore, therefore the level of U disequilibrium was estimated by laboratory-based Ge  $\gamma$  spectrometry.
- 4.6.15 The accuracy with which  $D_e$  equates to total absorbed dose and that dose absorbed since burial was assessed. The former can be considered a function of laboratory factors, including feldspar contamination, preheating, irradiation and internal consistency, the latter, one of environmental issues such as incomplete zeroing and the influence of post-depositional turbation. Diagnostics were deployed to estimate the influence of these factors and criteria instituted to optimise the accuracy of  $D_e$  values. The analytical validity of each sample is presented in **5.6.1**.
- 4.6.16 Ages reported in **5.6.1** provide an estimate of sediment burial period based on mean  $D_e$  and  $D_r$  values and their associated analytical uncertainties. Full OSL results are presented in **Appendix 5**.

## 4.7 Palaeogeographic reconstructions

### *Introduction*

- 4.7.1 A series of palaeogeographic reconstructions showing the geography of NV West at different time intervals in the past were produced (**Figure 13**).
- 4.7.2 To model palaeogeography, two key inputs are required;
- a digital elevation model (DEM) showing the topography of the area at a point in time (palaeoDEM), and;

- information on the approximate sea level (relative to the present day) during the same time period.

#### *PalaeoDEM*

- 4.7.3 A palaeoDEM was created by Fugro as part of the site investigation process to inform the siting of individual wind turbines (Fugro 2017).
- 4.7.4 Ultra-high resolution (UHR) shallow seismic data was interpreted to identify boundaries between key stratigraphic units. These boundaries (horizons) were mapped along each seismic line, and the data interpolated to create a 3D isopach showing changes in the elevation of key horizons across the site. Corrections were applied to the mapped horizons to reduce them to meters below Lowest Astronomical Tide (mLAT). Full processing details are outlined in Fugro (2017).
- 4.7.5 At NV West, a horizon representing the boundary between Brown Bank Formation and the underlying Swarte Bank and Yarmouth Roads Formations, was mapped. This horizon represents the topography of NV West prior to the deposition of Brown Bank Formation thus providing a palaeoDEM for the early Devensian (MIS 5d-5a).
- 4.7.6 The PalaeoDEM was provided in raster format for interrogation in ArcGIS.
- 4.7.7 A PalaeoDEM was not created by Fugro for the horizon representing the Late Devensian to Early Holocene transition as these units are locally restricted and more complex making it difficult to correlate horizons across seismic lines.
- 4.7.8 Horizons from the time periods/stratigraphic units of interest at the NV East site were not mapped during production of the engineering ground model. Therefore, palaeogeographic reconstructions presented in this report are limited to NV West.

#### *Sea-level data*

- 4.7.9 Sea-level data was extracted from a global oxygen isotope based sea-level reconstruction outlined in Waelbroeck et al. (2002) (**Figure 14**). For each MIS stage, approximate sea level relative to the present day was extracted. To account for changes in sea level within a single MIS, the lowest and/or highest sea level during each MIS was taken (**Figure 14**).

#### *Palaeogeographic model*

Two sea-level scenarios were selected for palaeogeographic modelling as outlined below in **Table 3**. The choice of scenarios was based on a review of sea-level data in comparison to the elevation range of the palaeoDEM (39-60 mLAT).

Palaeogeographic modelling was undertaken for two time periods during the Early Devensian when sea level was potentially low enough to expose NV West. Reconstructions were not undertaken for time periods of high sea level as the site would have been completely submerged, nor were they undertaken for MIS 4-3 when the site is expected to have become sub-aerially exposed as a PalaeoDEM for the top of the Brown Bank Formation was not created by Fugro (2017).

**Table 3** Parameters used in palaeogeographic model

Scenario	Age (MIS)	<sup>1</sup> Sea level (relative to present day)	<sup>2</sup> Tidal range
B	~88 ka (MIS 5b)	-50 m (low)	2 m
A	~110 ka (MIS 5d)	-45 m (low)	2 m

Scenario	Age (MIS)	<sup>1</sup> Sea level (relative to present day)	<sup>2</sup> Tidal range
<sup>1</sup> Waelbroeck et al. (2002)			
<sup>2</sup> Tidal range inferred as no model data available for these time periods			

4.7.10 Palaeogeographic reconstructions were undertaken in ArcGIS. The palaeoDEM was contoured and shaded to show areas above and below sea level at given time periods. An arbitrary tidal range of 2 m was applied to the data to show possible extents of an intertidal zone based on the topography. The palaeogeographic reconstructions are shown in **Figure 13**.

## 5 RESULTS

### 5.1 Deposit model

5.1.1 Earlier geological reviews of the Norfolk Vanguard site defined the site stratigraphy (deposit model) using geophysical and geotechnical assessments undertaken for the East Anglia One Offshore Project Area, and Cameron et al. (1992). Recent site specific geophysical and geoarchaeological assessments at the Norfolk Vanguard site (WA 2017b; 2018a) have allowed this stratigraphic model to be refined so it fully represents the deposits likely to be encountered in the shallow sub-surface (**Table 4**).

5.1.2 A comparison between the updated deposit model (**Table 4**) and previous iterations produced by Wessex Archaeology (WA 2017b and 2018a) and Fugro (Fugro 2017) is presented in **Appendix 6**. The deposit model is considered alongside the British Geological Survey lithostratigraphic framework for UK continental shelf deposits (Stoker et al. 2011). Where possible, the same Formation names have been adopted, but in some cases, they have been refined to reflect subtle changes in depositional environment and age within a Formation/Unit (e.g. Units 7a, 7b and 7c).

5.1.3 Note, the stratigraphic scheme presented here (**Table 4**) is based on interpretations of shallow geophysics and geotechnical data and thus doesn't capture deeper, older deposits that are beyond the period of archaeological interest.

5.1.4 From herein, deposits are referred to according to the Unit Number and Unit Name presented in **Table 4**. A schematic 2D cross section showing the representative stratigraphy of the site is presented in **Figure 15**.

**Table 4** Shallow-stratigraphy of the Norfolk Vanguard site (deposit model)

WA Unit	WA Unit Name Age (MIS)	Geophysical characteristics <sup>1</sup>	Sediment type and depositional environment <sup>2</sup>
8	Seabed sediments <i>Holocene post-transgression (MIS 1)</i>	Generally observed as a veneer or thickening into large sand wave and bank features up to 6 m in height. Boundary between surficial sediments and underlying units not always discernible.	Medium to coarse sand with frequent shell fragments – marine.
7c	Elbow Formation – intertidal <i>Early Holocene (MIS 1)</i>	Not identified within the geophysical data as deposit thickness is lower than geophysical data resolution.	Laminated sand, silt and clay – intertidal.
7b	Elbow Formation – organic <i>Late Devensian to Early Holocene (MIS 2-1)</i>	Extensive areas of intermittent, relatively flat, high amplitude reflectors. Often associated with shallow channelling.	Peat ranging from strongly to weakly decomposed with plant fragments (reeds) roots and wood preserved – terrestrial/coastal wetland.



WA Unit	WA Unit Name Age (MIS)	Geophysical characteristics <sup>1</sup>	Sediment type and depositional environment <sup>2</sup>
7a	Elbow Formation – fluvial <i>Late Devensian to Early Holocene (MIS 2-1)</i>	Small, shallow, infilled channels. Fill characterised as acoustically chaotic or transparent, or by sub-parallel internal reflectors. Incises into the top of Upper Brown Bank.	Sand with silt and clay laminations, occasionally organic, may comprise plant/root or shell fragments – fluvial/alluvial, possible reworking of older deposits.
6	Twente Formation – <i>Late Devensian (MIS 2)</i>	Not identified in shallow geophysical data	Not identified in geotechnical core logs.
5	Upper Brown Bank <i>Early-Mid Devensian (MIS 5d-3)</i>	Observed as a blanket deposit across much of the area, either acoustically transparent or characterised by sub-horizontal layered reflectors. Contains numerous internal erosion surfaces, occasional fluid escape structures, and areas of acoustic blanking.	Silty clay and clayey silt with closely spaced fine laminations. May be sandy in places or comprise sand partings/laminations – restricted marine/open estuary.
4	Lower Brown Bank/Eem Formation <i>Ipswichian to Early Devensian (MIS 5e-5d)</i>	Observed within large topographically controlled depressions. Characterised by low relief basal reflector and either an acoustically transparent or well-layered fill.	Not identified in geotechnical data.
3	Swarte Bank <i>Anglian (MIS 12)</i>	Not identified in shallow geophysical data.	Not identified in geotechnical data.
2	Yarmouth Roads <i>Early to Mid-Pleistocene (&gt;MIS 13)</i>	Thick unit either seismically chaotic or containing numerous areas of well-defined cross cutting channel complexes characterised by layered sub-parallel internal reflectors. Top of unit generally a well-defined regional erosion surface.	Not identified in geotechnical data.
1	Westkapelle Ground Formation <i>Late Pliocene to Early Pleistocene (MIS 63-103)</i>	No identified in shallow geophysical data	Not identified in geotechnical data
<sup>(1)</sup> Based on geophysical data (WA 2017b)			
<sup>(2)</sup> Based on Stage 1-3 geoarchaeological works (WA 2017a; 2018a; 2018b)			

## 5.2 Foraminifera and Ostracods

- 5.2.1 Foraminifera and ostracod assessment was undertaken on four sub-samples from VC074 (Unit 5) and three from VC085 (Unit 5).
- 5.2.2 Foraminifera and ostracods are recorded on a presence (x) or absence (-) basis, either as (o) one specimen, several specimen (x), abundant (xx) or superabundant (xxx). Where other palaeoenvironmental material (e.g. plant fragments) was observed within the sample residue, this was also noted in the assessment.
- 5.2.3 A summary of the assessment results is presented in **Table 5** and **Table 6** with full details on species and abundance given in **Appendix 2**.

### VC074

- 5.2.4 The three lowermost sub-samples (2.80, 3.60 and 4.60 mbsf) from VC074 all contain a rich and diverse foraminifera and ostracod fauna of primarily marine species, although the presence of large numbers of the brackish euryhaline foraminifer, *Elphidium williamsoni* and the outer-estuarine ostracod *Leptocythere psammophila* (**Appendix 2**) strongly suggests the salinity was lower than expected for a fully marine environment.

- 5.2.5 The two commonest foraminifera are large, ornate and beautifully preserved specimens of *Ammonia batavus* which appear to be in situ, and abundant miliolids. Both species would be at home in marine lagoons which are slightly brackish (for example in the Fleet lagoon in Dorset, today). According to Funnell (1989), ornate *Ammonia batavus* is restricted in the North Sea to interglacial periods and is typically indicative of warmer climates. The presence of these ornate *Ammonia batavus* is at odds with the other foraminifera and ostracods species recorded which are all cold/cool climate indicators (**Appendix 2**).
- 5.2.6 The assemblages indicate Unit 5 deposits in the lower part of VC074 were laid down during cool/cold climate conditions in a largely shallow marine environment with slightly lower salinity, possibly along the margins of a large embayment.
- 5.2.7 The upper sub-sample at 1.90 mbsf differs slightly from the sub-samples below. The fauna appears worn and fragmented indicating reworking, and it comprises only a few of the species recorded below. The assemblage in this sub-sample likely reflects the transition between Unit 5, and overlying deposits, previously interpreted to represent a freshwater channel (Unit 7a) (WA 2018). Stage 2 geoarchaeological recording placed the boundary between Unit 5 and Unit 7 at 4.75 mbsf in VC074 (WA 2018a). However, the results from this assessment suggest it is much shallower, at approximately 2.00 mbsf (**Figure 6**).

**Table 5** Foraminifera and ostracod assessment, vibrocore VC074

Depth in core (mbsf)	1.90	2.80	3.60	4.60
<b>Deposit</b>	<b>Clayey silty sand</b>			
Peat/plant debris/seeds/megaspores		x	x	x
Molluscs	wf	j	f	j
Echinoderm fragments				
Marine foraminifera	x	x	x	x
Freshwater ostracods		x		
Reworked Crag foraminifera	x			
Bithynia opercula				
Fish remains				
Insect remains				
Marine ostracods	x	x	x	x
Brackish foraminifera		x	x	x
Brackish ostracods		x	x	x
Environment	Freshwater body or channel alluvium, with reworking initially	Large near-marine shallow embayment; microfauna for the most part indicative of cold climate (Devensian) but with some warmer indicators (interstadial?)		
j – juveniles; f – fragmentary; w - worn; x - present				

#### VC085

- 5.2.8 Three sub-samples taken from Unit 5 in VC085 comprise an almost identical fauna to the sub-samples from VC074. The assemblages are dominated by marine foraminifera and ostracods indicative of a cool/cold environment that would be found further north today. The presence of some brackish ostracods and foraminifera implies salinity is slightly lower than

expected for a marine environment. Again, the presence of large, ornate *Ammonia batavus* is of interest as these typically thrive in warm interglacial climates.

- 5.2.9 Based on foraminifera and ostracod assessments, Unit 5 in VC085 have been interpreted to represent a large near-marine shallow embayment (**Figure 9**).

**Table 6** Foraminifera and ostracod assessment, vibrocore VC085

Depth in core (mbsf)	3.50	4.40	5.60
Deposit	Silty clay		
Molluscs		f	
Echinoderm fragments			
Marine foraminifera	x	x	x
Marine ostracods	x	x	x
Brackish ostracods	x		
Freshwater ostracods			
Reworked Crag foraminifera			
Peat/plant debris/seeds/megaspores	x	x	x
Charophyte oogonia			
Brackish foraminifera	x	x	
Environment	Large near-marine shallow embayment; microfauna for the most part indicative of cold climate (Devensian) but with some warmer indicators (interstadial?)		
j – juveniles; f - fragmentary/worn; x - present			

### 5.3 Pollen and charcoal

- 5.3.1 Pollen and charcoal analysis was undertaken on 16 sub-samples from Unit 7b in VC074. The results when plotted on a pollen diagram (**Figure 11**), allow the subdivision of the sequence into two local pollen assemblage zones (LPAZ).

#### *LPAZ VC074-1, 1.58–1.20m 'Pinus sylvestris'*

- 5.3.2 Zone VC074-1 has been sub-divided into two sub-zones (VC074-1A and B), largely on the basis of the curve for pollen of *Pinus sylvestris* (pine). The zone is dominated by pollen of trees (max 71.8% at 1.38 mbsf), principally *Pinus sylvestris* which increases in sub-zone VC074-1A from 32.2% (1.58 mbsf) to a peak of 59.4% (1.38 mbsf) before declining within subzone VC074-1B to < 40%. *Betula* (birch) frequencies decline through the zone from 23% to <10%. There are smaller quantities of *Ulmus* (elm) and *Quercus* (oak) <5% increasing through the zone, particularly the latter from sub-zone VC074-1B.
- 5.3.3 Pollen of shrubs are represented largely by *Corylus avellana*-type (hazel) (10-21%) with smaller quantities of *Salix* (willow) (<3%) and occasional *Ilex aquifolium* (holly) (<0.5%).
- 5.3.4 Herbaceous pollen frequencies are represented largely by Poaceae (grass family) which decline within the base of the zone (sub-zone VC07-1A) from 22.7% to 10%, accompanied by a range of herb taxa, including Cyperaceae (sedge family) (<3%) and occasional Rosaceae (rose family), *Filipendula* (meadowsweet), Chenopodiaceae (goosefoot family), Brassicaceae (cabbage family), Apiaceae (carrot family) and *Aster* (daisies) (<1%).



- 5.3.5 Fern spores are present in variably quantities (2-22%), primarily Pteropsida monolet undiff (undifferentiated fern spores) with smaller quantities of *Dryopteris filix-mas* (male fern spore) (<1.5%) and *Thelypteris palustris* (marsh fern) (max. 4.5%).
- 5.3.6 Aquatic pollen taxa are present in moderate quantities, represented largely by *Potamogeton natans* type (pondweed) (3-10%) with smaller quantities of *Sparganium emersum* type (unbranched bur-reed) (<1.5%) and *Typha latifolia* (bulrush) (<1.5%).
- 5.3.7 Microscopic charcoal area values vary through the zone (0.61 – 7.55 cm<sup>2</sup> cm<sup>3</sup>), increasing to a maximum of 7.55 cm<sup>2</sup> cm<sup>3</sup> (1.42 mbsf) The majority of the charcoal is angular opaque black with little sign of preservation of cellular structure.

*LPAZ VC074-2, 1.20 – 0.88m 'Pinus sylvestris – Corylus avellana-type'*

- 5.3.8 The zone is characterised by decreasing quantities for *Pinus sylvestris*, declining from 48.4% (1.23 mbsf) to 33.8% (1.18 mbsf), with values not exceeding 41%. Values for *Betula* remain constant through the zone, with a minor increase in *Ulmus* and *Quercus* (up to 4%).
- 5.3.9 Shrub pollen increases through the zone, principally *Corylus avellana*-type (max 32.8% at 0.88m). Values for herbaceous pollen taxa remain relatively constant, as do those for fern spores and aquatic.
- 5.3.10 Microscopic charcoal area values are generally lower through this zone, but with a peak at 0.98m (6.25 cm<sup>2</sup> cm<sup>3</sup>). The charcoal is angular opaque black with little sign of preservation of cellular structure.

*Vegetation reconstruction*

- 5.3.11 Trees and shrubs dominate the pollen sequence from VC074 reflecting the vegetation of the dry ground at the local-regional scale. The woodland is characterised initially by *Pinus* and *Betula*, with *Pinus* subsequently becoming the dominant canopy component and *Corylus avellana*-type most likely growing both as an understorey component and along woodland edges which may have existed near to the channel. Both *Pinus* and *Betula* are light demanding species suggesting that the woodland may have been relatively open rather than closed (e.g. Giesecke et al. 2011). Stands of *Salix* may have formed a component of this woodland, along with declining stands of *Betula*, likely also growing on wetter soils adjacent to and within areas of wetland.
- 5.3.12 Some of the herbaceous plants may reflect those taxa growing within the woodland floor, along the woodland edge and also within the peat-infilled palaeochannel. Pollen of Poaceae and Cyperaceae, along with aquatics and fern spores are likely to reflect the vegetation growing within the palaeochannel, which had ceased to be active with peat formation. Stands of reeds and sedges are likely to have formed an important component of the wetland flora, intermixed with Pteropsida (most probably *Thelypteris palustris*) growing at a lower level underneath the taller canopy of reeds. Among these a variety of herbaceous plants, some perhaps growing on sedge tussocks or as sprawlers and climbers, are represented by pollen of Rosaceae, *Filipendula*, Rubiaceae (bedstraw family) and Apiaceae.
- 5.3.13 Aquatic pollen of *Potamogeton natans*-type, *Sparganium emersum*-type and *Typha latifolia* suggests still or possible slow-moving water. There are some indications of possible nearby saltmarsh environments within the base of zone VC074-1A represented by the small quantities of Chenopodiaceae and Aster-type pollen.

- 5.3.14 *Corylus avellana*-type becomes a more important component of the woodland canopy into zone VC074-2, thriving in an environment where shade-producing trees (e.g. *Tilia*) were absent or otherwise present in only small quantities. This woodland may represent a mosaic of both open woodland, largely comprising *Pinus* and *Corylus avellana*-type and a forest floor of grasses and other light-demanding herbs (although these may also reflect the vegetation growing within the channel), interspersed with patches of denser canopy.

## 5.4 Plant macrofossils

- 5.4.1 The plant macrofossil evidence from eight sub-samples from Unit 7b (VC074, VC076 and VC085) is dominated by the remains of aquatic or wetland plants (**Table 7**). These are mostly remains from vegetative parts, particularly *Sphagnum* spp. moss leaves, but also other mosses, wood fragments, and reed (*Phragmites australis*) stem fragments.
- 5.4.2 Abundant fruiting parts were also present; these included taxa such as lilies (*Nuphar lutea* and *Nymphaea alba*), rushes (*Juncus* sp.), sedges (Cyperaceae and *Carex* sp.), gypsywort (*Lycopus europaeus*), birch (*Betula* sp.), pondweed (*Potamogeton* sp.), pinks (Caryophyllaceae), goosefoot (Chenopodiaceae and *Chenopodium* sp.), buttercups (*Ranunculus* sp.), composites (Asteraceae), water-plantain (*Alisma* sp.), hornwort (*Ceratophyllum* sp.) and bog bean (*Menyanthes trifoliata*). Small fragments of wood charcoal were noted in small quantities in a few of the samples.
- 5.4.3 Remains of invertebrates, such as ostracods, insects, crustaceans (*Daphnia* sp. egg cases), aquatic molluscs (including cf. *Bithynia* sp.), foraminifera, and earthworm eggs were present in the samples. No other environmental evidence was preserved.
- 5.4.4 The macrofossil assemblages recovered are generally consistent with wetland deposits former during the Early Holocene. The reconstruction of vegetation patterns through the study of plant macrofossils from wetland environments is biased by the overrepresentation of plant parts that are more resistant to erosion, such as certain coated seeds, that may have been transported and accumulated as a result of alluvial processes, or winged seeds easily transported by wind (e.g. birch seeds). In addition, many aquatic plants reproduce vegetatively and therefore seed production is low, but non-woody vegetative plant parts are more rarely identifiable by binocular microscopy. Still, there are some vegetational landscape traits that can be gained through the study of plant macrofossils, and this is complementary to the pollen evidence, which also has biases.

### VC074

- 5.4.5 The bottom part of this sequence indicates an initial wetland environment, with *Sphagnum* mosses and plants typical of low-flowing or stagnant water (e.g. banks of rivers, streams and lakes), such as gypsywort (*Lycopus europaeus*), sedges (Cyperaceae), white water-lily (*Nymphaea alba*), and pondweed (*Potamogeton* sp.) with some terrestrial plants, including trees, such as birch (*Betula* sp.) and low growing plants of nutrient rich soils, such as nightshade (*Solanum* sp.), goosefoot (*Chenopodium* sp.) and pinks (Caryophyllaceae).
- 5.4.6 The middle part of the sequence indicates wetter conditions, with a progressive disappearance of terrestrial plants and the appearance of rushes (*Juncus* sp.) and water plantains (*Alisma* spp.), that normally grow in shallow waters or on exposed mud at the edges of eutrophic, nutrient rich water bodies. *Sphagnum* mosses and *Phragmites australis* reeds, typical of swamps and fens, dominated the assemblage.

5.4.7 The top of the sequence was characterised by the presence of *Sphagnum* mosses and wetland species of mildly acidic or basic conditions typical of lakes and ponds, or slowly flowing rivers (*Nuphar lutea*, *Nymphaea alba*, *Juncus* spp., Cyperaceae).

VC076

5.4.8 At the base of the sequence, very degraded plant material was recovered. Poorly preserved moss leaves, not identifiable to *Sphagnum* were found. The only identifiable seeds were of *Potamogeton* sp. (pondweed). The many species of pondweed are rhizomatous perennials which grow in still or slow-flowing bodies of fresh-water in a diversity of substrates, usually in shallow waters and edges, although some species are of deep-water.

5.4.9 Several wetland taxa and *Sphagnum* mosses could be identified at the top of this sequence, including gypsywort (*Lycopus europaeus*) rushes (*Juncus* sp.), composites (Asteraceae), sedges (*Carex* sp.), and buttercups (*Ranunculus* sp.). These taxa are indicative of wet habitats such as the banks of rivers, streams and lakes.

VC085

5.4.10 The plant macrofossils in this peat sequence were mostly composed of degraded vegetative plant parts, including *Sphagnum* spp. moss leaves. Seeds were generally rare, particularly at the bottom of the sequence, but could be identified to a few taxa at the top of the sequence. These taxa are typical of bodies of still-water or slow-flowing rivers, such as sedges (*Carex* sp.), rigid hornwort (*Ceratophyllum* cf. *demersum*) and bogbean (*Menyanthes trifoliata*). The presence of seeds of rigid hornwort is particularly indicative of still fresh-water, the only circumstances in which seeds are occasionally produced by this plant which mostly reproduces vegetatively. Bogbean indicates unshaded shallow edges.

**Table 7** Plant macrofossils

Sample Code	Bulk volume (ml)	Vegetative plant parts	Fruiting plant parts	Wood charcoal	Invertebrates
114843_VC074_0.9	70	A*** (inc. <i>Sphagnum</i> sp. leaves)	C ( <i>Nuphar lutea</i> , <i>Nymphaea alba</i> , <i>Juncus</i> spp., Cyperaceae)	C	Ostracods, Insects, <i>Daphnia</i> sp. egg cases
114844_VC074_1.18	40	A*** - <i>Sphagnum</i> sp. leaves, <i>Phragmites</i> sp. stems and small degraded wood fragments	B (Cyperaceae, <i>Solanum</i> sp., <i>Alisma</i> sp., Poaceae husks)	C	B - Indet insect parts
114844_VC074_1.45	42	A*** - <i>Sphagnum</i> sp. leaves, <i>Phragmites</i> sp. stems and small degraded wood fragments	B ( <i>Juncus</i> sp., <i>Betula</i> sp., Caryophyllaceae, <i>Alisma</i> sp., Chenopodiaceae, <i>Carex</i> sp., indets.)	C	B - Indet insect parts, C - <i>Daphnia</i> sp. egg cases
114843_VC074_1.56	70	A*** (inc. <i>Sphagnum</i> sp. leaves)	A ( <i>Betula</i> sp., <i>Solanum</i> sp., <i>Chenopodium</i> sp., Caryophyllaceae, <i>Betula</i> sp., <i>Lycopus europaeus</i> , Cyperaceae, <i>Nymphaea alba</i> , <i>Potamogeton</i> sp.)	-	Insects
114843_VC076_3.61-3.63	200	A*** (inc. <i>Sphagnum</i> sp. leaves)	C ( <i>Lycopus europaeus</i> , <i>Juncus</i> sp., Asteraceae, <i>Carex</i> sp., <i>Ranunculus</i> sp., indet.)	C	Moll-m and poss. f (inc. cf. <i>Bithynia</i> ), Foraminifera,

Sample Code	Bulk volume (ml)	Vegetative parts	plant	Fruiting plant parts	Wood charcoal	Invertebrates
						Earthworm eggs, insects
114843_VC076_3.91-3.93	100	A*** (inc. Lycopsideae leaves)		C ( <i>Potamogeton</i> sp.)	-	-
114843_VC085_1.75-1.77	70	A*** (inc. <i>Sphagnum</i> sp. leaves)		B ( <i>Carex</i> sp., <i>Ceratophyllum</i> sp. and <i>Menyanthes trifoliata</i> )	-	Moll-m and poss. f (inc. cf. <i>Bithynia</i> ), Ostracods, Foraminifera
114843_VC085_2.07-2.09	70	A**		C ( <i>Menyanthes trifoliata</i> )	-	-

Key: A\*\*\* = exceptional, A\*\* = 100+, A\* = 30-99, A = >10, B = 9-5, C = <5

## 5.5 Radiocarbon dating and chronological modelling

- 5.5.1 Two sub-samples were taken for radiocarbon dating from Unit 7b in VC074 to supplement existing radiocarbon dates acquired during Stage 3 assessment (WA 2018) (**Table 8**).
- 5.5.2 A total of four radiocarbon dates were acquired from Unit 7b in VC074, and when all dates are considered together the sequence is unconformable. The date acquired from the top of Unit 7b (0.90 mbsf) is the youngest of the four dates (UBA-36846; 10230-9910 cal. BP), as would be expected. However, dates from lower in the sequence, although older, are inverted as the oldest date (UBA-39469; 11230-10810 cal. BP) is from a depth of 1.18 mbsf and becomes progressively younger towards the base of Unit 7b (UBA-36847; 10420-10190 cal. BP).
- 5.5.3 Bayesian chronological modelling of dates from VC074 confirm the sequence is internally inconsistent showing a poor overall agreement (A=0.0%). The modelling shows that the two intermediate dates (UBA-39469 and UBA-39470) are out of sequence (A=<60%) with the dates from the top and bottom of the sequence (UBA-36846 and UBA-36847) which show good agreement (Amodel: 107) (**Figure 12a**). The intermediate dates UBA-39469 and UBA-39470 are therefore questionable and the more reliable dates from the sequence are UBA-36846 and UBA-36847 which indicate Unit 7b in VC074 formed over ~500 years between 9122 ± 49 BP (10420-10190 cal. BP) and 8955 ± 46 BP (10230-9920 cal. BP).
- 5.5.4 The disagreement between the dates from the middle of the sequence and those from the top and base of Unit 7b may be related to formation processes. A review of core logs shows that the two intermediate dates correspond to depths where the peat is sandier (**Figure 6**). Given VC074 is located on the margin of a palaeochannel according to the geophysical assessment (WA 2017b), this may reflect a wash of material from the river channel which could have introduced reworked older carbon into the peat deposit. Of interest, there are subtle changes in the pollen assemblage at the same depths as the sandy peat (**Figure 11**), one of them being an increase in the amount of indeterminate pollen grains which may suggest reworking or incorporation of residual plant material. To test this, the two intermediate dates were modelled as outliers (**Figure 12a**) in time and the results increased the overall agreement of the model (Amodel:101) thus indicating there is a high probability this hypothesis is true.
- 5.5.5 Two dates, one from the top, and one from the base of Unit 7b in VC076 are conformable and the modelling results show they are internally consistent (Amodel:99) (**Figure 12b**). They are therefore considered to be reliable. In VC076, Unit 7b was deposited between 11863 ± 55 BP (UBA-36849; 13790-13540 cal. BP) and 8936 ± 47 BP (UBA-36848; 10220-

9910 cal. BP). If accumulation rates were continuous, this suggests Unit 7b formed over a period of ~3,000 years which is considerably longer than at VC074.

- 5.5.6 The date from the base of the sequence (UB-36849) is much older than other dates acquired from Unit 7b. This date was produced using the only identifiable macrofossils present in the sample, *Potamogeton* sp. (pondweed) seeds, (**Table 8**) which are submerged aquatics and therefore not ideal for radiocarbon dating due to a possible uptake of dissolved organic carbon from the bedrock in hardwater areas (Olsson 2009). This effect can produce ages hundreds of years older than the true age and could be used to explain why the date at the base of VC074 is considerably older (UB-36849). However, results from the pollen assessment show a typical Late Glacial assemblage at the base of VC074 (**Figure 11**) which agrees with the radiocarbon date despite potential uncertainty around the plant macrofossils dated.
- 5.5.7 Two dates from Unit 7b in VC085 are inverted and therefore were not modelled. The date from the base of Unit 7b in VC085 is 8856 ± 48 BP (UB-36851; 10170-9740 cal. BP) which is comparable to the dates from the top of the Unit 7b in VC076, and to Unit 7b in VC074 (**Table 8**), and therefore considered reliable.
- 5.5.8 The date from the top of Unit 7b VC085 (UB-36850; 12100-11700 cal. BP) is older than one below (UB-36851; 10170-9740 cal. BP). Given the sub-sample was taken very close to the boundary with overlying intertidal mudflat deposit (Unit 7a) which appears to be erosional, older material may have been washed in from elsewhere as the peat flooded. This date is considered unreliable.
- 5.5.9 Of the eight radiocarbon dates submitted, five are considered reliable ages (UB-36846, UB-36847, UB-36848, UB-36849 and UB-36851) given the considerations discussed above. Four radiocarbon dates are Early Holocene in age and one dates to the Late Devensian. This possibly suggests two phases of peat formation across the site, which is supported by chronological modelling (**Figure 12c**).

**Table 8** AMS radiocarbon dates

Stage Laboratory No	Material dated	Depth mbsf (mLAT)	Age BP	Modern F14C	Age range cal. BP (95.4%)	Modelled range cal. BP (95.4%)
<b>VC074</b>						
UB-36846 *	Seeds ( <i>Nuphar lutea</i> 2x, <i>Nymphaea alba</i> 2x, <i>Juncus</i> sp. 1x, Cyperaceae 1/2x) + leaves ( <i>Sphagnum</i> sp. 25x)	0.90 (-39.40)	8955 ± 46	0.328 ± 0.0019	10230-9910	10230-9920
UBA-39469	Cyperaceae, <i>Solanum</i> sp. and <i>Alisma</i> sp. seeds, Poaceae husks	1.18 (-39.68)	9696 ± 44	0.2991 ± 0.0016	11230-10810	10290-10060
UBA-39470	<i>Juncus</i> sp., <i>Betula</i> sp., Caryophyllaceae, <i>Alisma</i> sp., Chenopodiaceae and <i>Carex</i> sp. seeds	1.45 (-39.95)	9613 ± 39	0.3022 ± 0.0015	11170-10770	10380-10170
UB-36847 *	Seeds ( <i>Betula</i> sp. 3x, <i>Solanum</i> sp. 2x, <i>Chenopodium</i> sp. 1x, Caryophyllaceae 1x, <i>Betula</i> sp. 5x, <i>Lycopus europaeus</i> 1x, <i>Potamogeton</i> sp. 1x,	1.56 (-40.06)	9122 ± 49	0.3212 ± 0.002	10420- 10190	10420-10190



Stage Laboratory No	Material dated	Depth mbsf (mLAT)	Age BP	Modern F14C	Age range cal. BP (95.4%)	Modelled range cal. BP (95.4%)
	<i>Nymphaea alba</i> 1x, Cyperaceae 15x), <i>Betula</i> sp. 1x catkin scale					
<b>VC076</b>						
UB-36848 *	Seeds: <i>Lycopus europaeus</i> 1x, <i>Juncus</i> sp 2x, Asteraceae 1x, <i>Carex</i> sp 2x, <i>Ranunculus</i> sp. 0.5	3.61-3.63 (-37.61- -37.63)	8936 ± 47	0.3288 ± 0.0019	10220-9910	10220-9910
UB-36849 *	Seeds: <i>Potamogeton</i> sp. 5x	3.91-3.93 (-37.91- -37.93)	11863 ± 55	0.2284 ± 0.0016	13790-13550	13790-13540
<b>VC085</b>						
UB-36850 *	Seeds: <i>Ceratophyllum</i> sp. 1x, <i>Menyanthes trifoliata</i> 2x	1.75-1.77 (-37.15- -37.17)	10192 ± 47	0.2812 ± 0.0016	12100-11700	-
UB-36851 *	Seeds: <i>Menyanthes trifoliata</i> 2x	2.07-2.09 (-37.47- -37.49)	8856 ± 48	0.3321 ± 0.002	10170-9740	-
* Indicates radiocarbon dates acquired during Stage 3						

## 5.6 Optical stimulated luminescence dating

- 5.6.1 Two sub-samples were taken for OSL dating from Unit 5 in VC074 (3.70-4.00 mbsf) and VC107 (4.65-5.00 mbsf), to supplement existing OSL dates acquired during Stage 3 assessment (WA 2018) (5.6.1).
- 5.6.2 Diagnostics were used to estimate the influence of laboratory and environmental factors on the results as a means of testing the analytical validity of the OSL age (5.6.1).
- 5.6.3 When considered alongside the OSL results from the Stage 3 assessment (WA 2018), a total of eight OSL dates from Unit 5 were acquired. Of these, four have been accepted without caveats (GL17076, GL17077, GL17081 and GL18024), two show evidence of feldspar contamination (GL17078 and GL18023) and are therefore considered minimum age estimates, and two are accepted tentatively as they did not fully meet the criteria of the SAR protocol (GL17079 and GL17080) (Table 9). Full details on the limitations of the OSL dating are presented in Appendix 5.
- 5.6.4 In VC074, the sub-sample at 3.70-4.00 mbsf returned an age of  $58.9 \pm 6.7$  ka (GL17081). However, this date should be interpreted as a minimum age estimate as the sub-sample shows evidence of feldspar contamination which can lead to an underestimation of the age (Appendix 5). Feldspar contamination is rarely related to sample handling or preparation, but instead results from inclusions of feldspar within quartz that cannot be accounted for during sample selection. Despite this analytical uncertainty, the date is in sequence given the sub-sample below at 5.00-5.36 mbsf gave an age of  $82.4 \pm 8.5$  ka (GL180230) (5.6.1).
- 5.6.5 Both OSL dates from VC079 are accepted tentatively due to analytical uncertainty. Sub-sample GL17079 gave an age of  $57.6 \pm 5.9$  ka but shows overdispersion of the regenerated signal which implies the effectiveness of sensitivity correction, a key part of the laboratory protocol, may be problematic. This is a function of the individual sample's response to the SAR protocol and is not related to sample handling, storage or preparation. Despite analytical uncertainty, the age is broadly the same as GL17081 from VC074 ( $58.9 \pm 6.7$  ka) which has been accepted without caveats.

- 5.6.6 The overlying sub-sample (GL17080) in VC079 gave an age of  $66.8 \pm 7.1$  ka and showed evidence of Uranium disequilibrium which can create temporal instability in the decay of radionuclides. This may influence the calculation of Dose Rate, a key part of equation used to calculate the OSL age. Therefore, where there is evidence of this phenomena, ages are accepted tentatively.
- 5.6.7 OSL dates from VC079 are unconformable but despite analytical uncertainty, they still lie within the range of other accepted OSL dates.
- 5.6.8 The two OSL dates from VC085 have been accepted with no caveats suggesting deposition between  $57.2 \pm 6.4$  ka (GL17076) and  $69.5 \pm 7.7$  ka (GL17077). The ages are unconformable but overlap within error margins (**Table 9**).
- 5.6.9 A sub-sample taken from VC107 at a depth of 4.65-5.00 mbsf returned an age of  $73.6 \pm 5.7$  ka (GL18024). This sub-sample passed analytical diagnostic tests and the age has been accepted. The OSL date from a sub-sample within the same core at a depth of 1.00-1.25 mbsf gave a minimum age of  $59.8 \pm 6.2$  ka (GL17078) due to feldspar contamination. These dates are in sequence and considered reliable estimates of burial age.

*Questions regarding partial bleaching*

- 5.6.10 The methodological approach to sub-sampling for OSL involved maximising the use of vibrocores recovered in transparent liners where the outer surface had been exposed to light (see section 4.6). Measures were taken to reduce the risk of exposed grains from the outer surface of the cores becoming incorporated in the OSL sample that was taken from the centre of the core under controlled light conditions (see section 4.6). If recently exposed, fully or partially bleached grains were included in the aliquots measured, this would lead to an underestimation of the burial age.
- 5.6.11 There are a number of tests to detect for partial bleaching. Within this study, signal analysis was used to quantify the change in  $D_e$  value with respect to optical stimulation time for multi-grain aliquots (**Figures 4** in **Appendix 5**). A statistically significant increase in natural  $D_e$  with time is indicative of partial bleaching, but this assumes certain laboratory conditions are met (see **Appendix 5**). The results from signal analysis from each of the sub-samples do not show an increase in natural  $D_e$  with time suggesting there is no evidence of partial bleaching, although interestingly, GL18023 and GL17078 which both show evidence of feldspar contamination, do not show a decline in  $D_e$  with time as observed in all other sub-samples. However, it is noted that the utility of signal analysis is strongly dependent upon a sample's pre-burial experience of sunlight's spectrum and its residual to post-burial signal ratio, and that all laboratory conditions are met.
- 5.6.12 Inter-aliquot  $D_e$  distributions studies may be used to test for partial bleaching. At present, it is contended that asymmetric inter-grain  $D_e$  distributions are symptomatic of partial bleaching (Murray et al. 1995; Olley et al. 1999; 2004 and Bateman et al. 2003). Samples GL17079, GL17080 and GL18023 exhibit asymmetric distributions which may be indicative of partial bleaching (**Figures 3** in **Appendix 3**). However, distinguishing between partial bleaching caused by the sampling process and that which occurred naturally during deposition is problematic, especially in water lain sediments such as Upper Brown Bank where partial bleaching is prolific (Murray et al. 1995). Single-grain analysis could be used to detect for statistical differences in  $D_e$  distribution but again, determining if this was caused by sample handling or depositional processes would remain problematic.
- 5.6.13 Based on the accepted OSL ages, deposition of Upper Brown Bank occurred between  $82.4 \pm 8.5$  and  $57.2 \pm 6.4$  ka, which correlates to the period between MIS 5b and MIS 3 (including

error bars) (**Figure 14**). Given that the dates acquired here are broadly comparable to OSL dates acquired using vibrocores collected in opaque liners (Limpenney et al. 2011; Tizzard et al. 2015), we therefore conclude that the likelihood of the results been affected by the sampling methodology are small, and that the dates can be considered reliable.

**Table 9** Dose Rate ( $D_r$ ) and Equivalent Dose ( $D_e$ ) and resulting OSL age estimates. Age estimates expressed in ka relative to year of sampling. Uncertainties in age are quoted at  $1\sigma$  confidence and include combined systematic and experimental variability.

Stage	Laboratory id	Depth mbsf (mLAT)	Total $D_r$ ( $Gy.k_a^{-1}$ )	$D_e$ (Gy)	Age (ka)	Considerations and analytical validity
<b>VC074</b>						
4	GL18023	3.70-4.00 (-42.20 - -42.50)	$1.70 \pm 0.16$	$100.1 \pm 6.2$	$58.9 \pm 6.7$	Significant feldspar contamination, accept as minimum age estimate
3	GL17081	5.00-5.36 (-43.50 - -44.00)	$1.75 \pm 0.16$	$144.3 \pm 7.3$	$82.4 \pm 8.5$	None, accept age
<b>VC079</b>						
3	GL17080	0.75-1.00 (-41.55 - -41.80)	$1.96 \pm 0.18$	$131.2 \pm 7.4$	$66.8 \pm 7.1$	Potentially significant U disequilibrium, accept tentatively
3	GL17079	4.15-4.35 (-44.95 - -45.15)	$2.42 \pm 0.22$	$139.1 \pm 6.3$	$57.6 \pm 5.9$	Overdispersion in the interpolated to applied regenerative-dose ratio, accept tentatively
<b>VC085</b>						
3	GL17077	4.60-4.80 (-40.00 - -40.20)	$2.19 \pm 0.21$	$152.0 \pm 8.7$	$69.5 \pm 7.7$	None, accept age
3	GL17076	5.10-5.30 (-40.50 - -40.70)	$2.43 \pm 0.22$	$139.0 \pm 8.7$	$57.2 \pm 6.4$	None, accept age
<b>VC107</b>						
3	GL17078	1.00-1.25 (-37.70 - -37.95)	$2.37 \pm 0.22$	$141.7 \pm 6.6$	$59.8 \pm 6.2$	Significant feldspar contamination, accept as minimum age estimate
4	GL18024	4.65-5.00 (-41.35 - -41.70)	$3.24 \pm 0.19$	$238.3 \pm 12.0$	$73.6 \pm 5.7$	None, accept age

## 5.7 Palaeogeographic reconstructions

5.7.1 Palaeogeographic reconstructions were compiled for two sea-level scenarios (see section 4.7 for selection criteria).

5.7.2 Scenario A corresponds to MIS 5d (115-105 ka) which is the earliest sub-stage (stadial) in the Early Devensian. During MIS 5d, sea level started to fall as climate cooled and ice sheets grew. According to global sea-level reconstructions (Waelbroeck et al. 2002), sea level reached a maximum low of -50 m during MIS 5d, before it started to rise again. The palaeogeography of NV West at the lowest sea level (-50 m) during MIS 5d (~110 ka) is presented in (**Figure 13**).



- 5.7.3 The results show a large proportion of NV West would have been sub-aerially exposed during sea-level scenario A (**Figure 13**). A shoreline runs broadly NW-SE with shallow water to the west and land to the east. Higher ground is located in the northern parts of the site. There appears to be localised isolated basins within the landscape that may have ponded water.
- 5.7.4 Scenario B corresponds to MIS 5b (92-84 ka) which is also a stadial (cool period) within the Early Devensian. At its lowest point, sea-level during this sub-stage reached -45 m (~88 ka) (Waelbroeck et al. 2002). The palaeogeography of NV West under this sea-level scenario is presented in **Figure 13**.
- 5.7.5 The results show NV West is largely submerged but water depths are expected to be shallow (<10 m). There are some areas in the northern part of the site that are sub-aerially exposed. The most striking feature is linear bank that runs the length of the site from NW to SE. This bank feature has similar morphology of a coastal barrier or spit, separating what appears to be open coast (to the east) from a restricted lagoon/embayment (to the west).

## 6 DISCUSSION

### 6.1 Introduction

- 6.1.1 The palaeoenvironmental and dating results are considered collectively with reference to the aims and objectives outlined in **Section 2**, and to the regional research agenda (Medlycott 2011) and the national maritime research framework (Ransley et al. 2013).
- 6.1.2 The results are discussed according to key geological and archaeological periods as follows:

### 6.2 Middle to Upper Palaeolithic (Early-Mid Devensian) [MIS 5e – MIS 3]

#### *Chronology*

- 6.2.1 The age of Upper Brown Bank (Unit 5) is of archaeological interest as it has implications for our understanding of the palaeogeographic development of the southern North Sea during a period of hiatus in the British archaeological record (MIS 6-4) (Lewis et al. 2011).
- 6.2.2 Cameron et al. (1992) defined Brown Bank Formation (equivalent to Unit 5) as a shallow, restricted, brackish lagoon that resulted from sea-level fall during the Early Devensian. In the UK sector, Brown Bank Formation is characterised by a series of north-south trending channels in the west, and a broad basin in the east that extends into the Dutch sector (Hiljma et al. 2012).
- 6.2.3 Brown Bank Formation has been previously dated using OSL (WA 2008; Limpenny et al. 2011; Tizzard et al. 2014; 2015) and ages fall into two broad ranges:
- $116.7 \pm 11.2$  ka to  $96 \pm 11$  ka (MIS 5d-5c) (WA 2008; Tizzard et al. 2014; 2015), and;
  - $53.4 \pm 5.4$  ka to  $30.4 \pm 6.9$  ka (MIS 3) (Limpenny et al. 2011).
- 6.2.4 Based on previous evidence it was not clear if Unit 5 was deposited gradually over the duration of the Early Devensian, or periodically, possibly punctuated by periods of hiatus and subaerial exposure (Tizzard et al. 2015).
- 6.2.5 The OSL dating results from Unit 5 deposits in the Norfolk Vanguard site suggest deposition occurred between  $82.4 \pm 8.5$  and  $57.2 \pm 6.4$  ka which extends from MIS 5b through to MIS

3 (**Figure 14**). When combined with dates from previous studies (Limpenny et al. 2011; Tizzard et al. 2015), these results suggest Brown Bank Formation was deposited gradually over the duration of the Early Devensian, a period of overall cooling and climatic instability characterised by stadial (cold) and interstadial (warm) sub-periods (**Figure 2**).

- 6.2.6 If there were periods of hiatus during deposition of Unit 5, it is unlikely these would be detected using OSL as the error margins (up to  $\pm 8.5$  ka) are greater than the length of the stadial to interstadial sub-periods (~5-14 ka).

*Palaeoenvironmental and palaeogeographic evolution*

- 6.2.7 The depositional history of Upper Brown Bank (Unit 5) is of archaeological interest as early studies proposed it was deposited in shallow lagoon (Cameron et al. 1992), and assessments of geophysical data identified shallow gas, possibly indicating organic material, and internal surfaces that may represent hiatuses resulting from sub-aerial exposure (WA 2017b).
- 6.2.8 The results from foraminifera and ostracod assessments of three vibrocores in the NV West site suggest Unit 5 was laid down in a shallow near-marine embayment, henceforth referred to as the Brown Bank embayment (**Figure 6, 8 and 9**). The dominant assemblage is marine, but several brackish taxa are present indicating slightly lower salinity than would be expected for a fully marine setting. In VC107, located ~30 km to the east in the NV East site, the foraminifera and ostracod assemblage is dominated by brackish taxa indicative of an outer estuarine environment (**Figure 10**).
- 6.2.9 Given the dates from Unit 5 in the NV East site (~74-60 ka) and the NV West site (~82-57 ka) are broadly contemporaneous, the embayment and outer estuary are likely part of the same landscape, suggesting Unit 5 becomes increasingly marine-marginal towards the east. If this is the case, Unit 5 may be a distal component of the Rhine-Meuse delta system prograding into the North Sea from the east (Hijma et al. 2012).
- 6.2.10 Foraminifera and ostracod assemblages from Unit 5 at both the NV West and NV East sites are dominated by species indicative of cool/cold environments (**Appendix 2**; WA 2018). In VC074 and VC085 (NV West), large, ornate *Ammonia batavus* are also observed which are more typical of warm interglacial climates. The presence of both warm and cool/cold climate indicators within Unit 5 may reflect climatic instability during the Early Devensian, with the “warm” species flourishing during interstadials and “cold” species during stadials. The results from the microfossil assessment therefore support an Early Devensian age for Unit 5, as indicated by OSL dates.
- 6.2.11 By comparing the elevation of the Brown Bank deposits to past sea-level and climate data, the palaeogeographic evolution of the NV West site can be reconstructed (**Table 10**). At a broad-scale, this provides information on when the site is likely to have been submerged and sub-aerially exposed (**Figure 14**), as summarised in **Table 10**.
- 6.2.12 The model suggests the NV West site was been submerged for the majority of the Early Devensian until MIS 4 when sea-levels fell to a low of -90 m (Siddall et al. 2003). There are two time-periods (MIS 5d and MIS 5c) when sea levels fell below the elevation of Unit 5, thus potentially subaerially exposing the NV West site (**Figure 13**). Palaeogeographic reconstructions for these time periods show that even when sea levels were low, the site was never fully exposed, but instead a more marine-marginal environment with a complex coastal configuration characterised by isolated basins, barrier islands/spits and lagoons.

- 6.2.13 The presence of coastal landscapes is of archaeological interest due to their potential to have been the focus of past human activity (Bailey and Parkington 1988). While the preservation of coastal deposits is typically poor due to reworking during sea-level rise, increasingly more examples of submerged and buried barrier coastlines are being uncovered (Mellett and Plater 2017). While there is no direct evidence of coastal deposits in the vibrocores assessed from the Norfolk Vanguard site, there are more sandy components of Unit 5 (e.g. VC078; **Figure 8**) which may reflect coastal settings. Furthermore, the geophysical assessment identified a series of buried dunes (**Figure 3b**) (WA 2017b). It is not known if these dunes formed in a terrestrial or sub-aqueous setting, but their exceptional preservation highlights the potential for preserving palaeolandscape features.
- 6.2.14 The palaeogeographic reconstructions can be tested with the palaeoenvironmental and dating results, which imply that Unit 5 was deposited in a near-marine embayment to open estuarine setting between  $82.4 \pm 8.5$  ka and  $57.6 \pm 5.9$  ka (MIS 5b to MIS 3). The results presented here suggest shallow marine conditions prevailed in the southern North Sea through MIS 4, which is an entire Marine Isotope Stage longer than predicted using global sea-level reconstructions. It also doesn't agree with terrestrial records that suggest MIS 4 in NW Europe was a period of intensive fluvial erosion and reworking driven by a fall in sea level (Busschers et al. 2007; Hijma et al. 2012).
- 6.2.15 The contradiction between records is not surprising given the large error bars on both sea-level reconstructions (up to 30 m) (Siddall et al. 2003) and OSL dates (up to 8 ka). Furthermore, the palaeogeographic reconstructions do not account for past land-level (crustal) changes and assume the elevation of Unit 5 in the present-day is the same as in the past, which is unlikely given isostatic effects associated with the last glaciation (Shennan et al. 2013) and possible reactivation of older tectonic structures (Arfaï et al. 2018).
- 6.2.16 After MIS 4, sea levels continued to fall in MIS 3 reaching a low of ~120 m below present day during the Last Glacial Maximum (35-21 ka) (Chiverrell and Thomas 2010). During this time, both the NV West and NV East sites would have been subaerially exposed. However, no deposits from this period are preserved within the Norfolk Vanguard site.

**Table 10** Palaeogeography of the NV West site during Early to Mid-Devensian

MIS <sup>1</sup> (Age)	Sea-level <sup>2</sup>	Climate	Palaeogeography
MIS 3 (~45 ka)	-70 m (low)	Pleniglacial (cold)	Entire site subaerially exposed
MIS 3-4 (~57 ka)	-60 m	Pleniglacial (cold)	Site largely sub-aerially exposed but may have been periodically submerged
MIS 4 (~60 ka)	-50 m (high)	Pleniglacial (cold)	Entire site subaerially exposed
MIS 4 (~65 ka)	-85 m (low)	Pleniglacial (cold)	Entire site subaerially exposed
MIS 5a (~80 ka)	-20 m (high)	Interstadial (warming)	Site submerged, water depths <20 m, but site may have become sub-aerially exposed after ~85 ka
MIS 5b (~88 ka)	-50 m (low)	Stadial (cooling)	Parts of the site potentially sub-aerially exposed for a short time (<5 ka)
MIS 5c (~100 ka)	-20 m (high)	Interstadial (warming)	Site submerged, water depths <20 m
MIS 5d (~110 ka)	-45 m (low)	Stadial (cooling)	Parts of the site potentially sub-aerially exposed for a short time (<3 ka)
MIS 5e (130-117 ka)	Highstand	Last Interglacial (warm)	Site submerged, 40-60 m water depth

<sup>1</sup>MIS stratigraphy from Lisiecki and Raymo (2005)  
<sup>2</sup>Sea level relative to today from Waelbroeck et al. (2002)  
 Shaded rows = palaeogeographic models for these periods presented in Figure 13

### *Archaeological significance*

- 6.2.17 The results indicate there was a shallow marine embayment (the Brown Bank embayment) at the Norfolk Vanguard site from the start of the Early Devensian (MIS 5b) through to the MIS 4/3 transition. The age of this embayment correlates to a period of hiatus in the British archaeological record (MIS 6-4) (Lewis et al. 2011). Therefore, it could be argued that the presence of this embayment created a significant geographic barrier to migration pathways through the southern North Sea during the Middle Palaeolithic.
- 6.2.18 The Brown Bank embayment appears to have been a persistent feature in the landscape, but there is potential for the NV West site to have been partially exposed during periods of lower sea level associated with cold stadial periods. The configuration of the coast during this time would have been complex, dynamic and highly irregular. These landscapes would have been a challenging environment for hominin exploitation.
- 6.2.19 The earliest evidence of reoccupation after the MIS 6-4 hiatus occurred at ~60 ka (Boismier et al. 2012). At this time, the southern North Sea is expected to have emerged creating a terrestrial landscape that may have supported migration pathways from continental Europe into Britain. At the Norfolk Vanguard site, the Upper Palaeolithic is characterised by a hiatus in the geological record of ~40,000 thousand years. Our understanding of palaeolandscape development within the context of the already sparse Upper Palaeolithic record from Britain (Pettitt and White 2012) is therefore limited and the potential for preservation of archaeological material from this period is considered low (**Table 11**).
- 6.2.20 However, there is a need to understand the palaeogeographic evolution of the Brown Bank embayment within the context of the wider North Sea and English Channel, to fully explore its role in influencing migration pathways through the southern North Sea during the Middle to Upper Palaeolithic.

## **6.3 Late Upper Palaeolithic to Mesolithic (Late Devensian to Holocene) [MIS 2-1]**

### *Chronology*

- 6.3.1 Late Devensian to Early Holocene deposits are characterised by Unit 7 which has been subdivided into three sub-units (**Table 4**).
- 6.3.2 Peat deposits (Unit 7b) preserved in the NV West site are of archaeological interest as they contain palaeoenvironmental material that can be used to reconstruct landscape history. Establishing the age of these deposits is important to provide a chronological framework for environmental change, but also to constrain the timing of inundation of the now-submerged landscape.
- 6.3.3 Of the eight radiocarbon dates from Unit 7b (VC074, VC079 and VC085), five are considered to be reliable estimates of age based on chronological modelling (see section **5.5**).
- 6.3.4 Four of these dates lie between  $9122 \pm 49$  BP (UB-36847; 10420- 10190 cal. BP) and  $8856 \pm 48$  BP (UB-36846; 10170-9740 cal. BP) and suggest the major phase of peat formation at the NV West site was during the Early Holocene. One date from the base of Unit 7b in VC076 (UB-36849; 13780-13550 cal. BP) suggests peat started to form at this location in the Late Devensian during a relative warm period known as the Windermere Interstadial in Britain (Roberts et al. 1998).
- 6.3.5 The dating and chronological modelling results suggest there are possibly two periods of peat formation recorded at the NV West site, one during the Windermere Interstadial in the

Late Devensian, and one during the Early Holocene, although the chronology would need to be refined to test this.

- 6.3.6 The dates from the NV West site are broadly comparable with dates from peat and organic sequences recovered elsewhere in the southern North Sea (Hazell 2008; Brown et al. 2017; Geary et al. 2017).
- 6.3.7 Unit 7a is the oldest of the deposits stratigraphically. While the unit has not been dated due to a lack of suitable material for radiocarbon or OSL dating, radiocarbon dates from overlying Unit 7b provide limiting dates which suggest Unit 7a was deposited during the Late Devensian, or earlier.
- 6.3.8 Similarly, Unit 7c has not been dated, but limiting dates from Unit 7b suggest Unit 7a was deposited later than 10230-9910 cal. BP.

*Palaeoenvironmental and palaeogeographic evolution*

- 6.3.9 Unit 7b preserved in VC074, VC076 and VC085 likely represents deposition during the Late Devensian (MIS 2). In VC074, diatoms indicate deposition occurred in a freshwater environment and the presence of reworked foraminifera and ostracods from underlying Unit 5 suggests a high-energy setting. The results imply deposition in an active freshwater channel which is supported by results from the geophysical assessment (WA 2017b) that identified a palaeochannel at this location (**Figure 6**). Similarly, in VC085, diatoms and ostracod assemblages indicate a freshwater environment, although a finer-grained deposit and absence of reworked foraminifera may suggest a lower energy setting such as floodplain.
- 6.3.10 Foraminifera, ostracods and diatoms are absent from Unit 7a in VC076 possibly suggesting a different depositional setting. Particle size distribution analysis on sub-samples from VC076 (WA 2018) showed unimodal distributions which can be typical of wind-blown or fluvial transport mechanisms. However, an assessment of grains under a microscope showed they were transparent and well-rounded which is more typical of water-lain sediment suggesting Unit 7a is in fact a fluvial deposit.
- 6.3.11 BGS have mapped Twente Formation (Unit 6), a wind-blown sand, within the NV West site (Cameron et al. 1992). However, Unit 6 was not definitively identified during the geophysical assessment (WA 2017b). While Unit 7a shows similar characteristics to Twente Formation, the results presented here suggest Unit 7a is fluvial in origin, and therefore part of the Elbow Formation (**Table 4**). Unit 6 is considered absent from the site.
- 6.3.12 In VC076, diatoms, foraminifera and ostracods were not preserved in Unit 7a making it difficult to determine palaeoenvironment, but Unit 7a in this vibrocore appears to differ in depositional history when compared to VC074 and VC085.
- 6.3.13 Unit 7a is interpreted to represent a period of active fluvial processes across the NV West site during the Late Devensian. At its maximum southerly limit, the North Sea Lobe of the British-Irish Ice Sheet (BIIS) would have been located ~20 km to the north of the NV West site (**Figure 4**) and the site may have been influenced by ice-marginal glaciofluvial processes (e.g Dove et al. 2017) resulting in the deposition of Unit 7a. However, geophysical data indicates palaeochannels within the NV West site are sinuous (**Figure 3** and **Figure 16**) which is a characteristic of mature channels that have developed over long periods of time (>1000 yrs), with vegetated margins. Deposits associated with these palaeochannels (e.g. VC074 and VC085) are therefore more likely to have formed in a fluvial setting, as appose to a highly erosive glaciofluvial environment.



- 6.3.14 The morphology of the palaeochannel network preserved at the NV West site is visible in both multibeam bathymetry and seismic data (**Figure 16**). A highly sinuous channel is present at seabed and can be traced for ~3 km until it disappears under a sand bank (**Figure 16**). The channel re-emerges on the eastern side of the sand bank where it becomes more linear extending south for a further kilometre where it meets a second palaeochannel (**Figure 16**). A comparison between bathymetric and seismic data shows the palaeochannels observed on the seabed are part of a larger system mapped from seismic data (WA 2017b). In total, the channel system is ~15 km in length and is comparable in size to the lower reaches of river systems such as the River Yare in Norfolk. The potential for preservation of artefactual material within, or along the margins of this palaeochannel network is considered high.
- 6.3.15 Overlying Unit 7a are peat deposits (Unit 7b) that cover an area up to ~40 km<sup>2</sup> according to geophysical data (WA 2017b) (**Figure 3b**). Unit 7b is predominantly located in the north of the NV West site where it forms an extensive irregular sheet deposit (VC085 and VC076), possibly dissected by palaeochannels (**Figure 3b**). In the south, peat is locally more restricted and appears to infill, or form along the margins of, a large river system that is observed in seismic and bathymetry data (**Figure 16**).
- 6.3.16 Radiocarbon dating and chronological modelling suggests two possible phases of peat development are captured in VC076. This vibrocore does not appear to be associated with a palaeochannel and therefore may provide a more regional record of palaeoenvironmental change.
- 6.3.17 The first phase of peat development commenced at around 11863 ± 55 BP (UB-36849; 13781-13557 cal. BP) during a relative warm period known as the Windermere Interstadial in Britain (Roberts et al. 1998). Pollen assessment results suggest the landscape was an open woodland dominated by *Betula* (birch) at this time (**Figure 7**), likely with wetlands forming on low-lying, open ground.
- 6.3.18 Subsequently, the pollen assemblage is characterised by a decline in arboreal pollen (3.91 and 3.75 mbsf) (WA 2018) which is interpreted as a switch to a tall herb swamp environment. The timing of this change in palaeoenvironment is unknown, but based on radiocarbon dates above and below, it is expected to have occurred between ~13.5 and 10.2 ka which correlates to the Loch Lomond stadial in Britain, a period of climate deterioration and cooling. Of interest, many terrestrial pollen records show a decline in birch during the Loch Lomond stadial, as birch woodland becomes locally restricted and more open-habitat taxa, such as grasses, become dominant (Pennington 1977; Walker 1982; Mayle et al 1997; Simmons 2016). This trend is also documented in the pollen assemblage from VC076.
- 6.3.19 In VC076, after 3.75 mbsf, the pollen assemblage shows a return to woodland environment, but this time dominated by *Pinus* (pine) and *Corylus* (hazel). Given the date from the top of this peat is 8936 ± 47 BP (UB-36848; 10220-9910 cal. BP), this second phase of peat development may have commenced at the onset of the Early Holocene.
- 6.3.20 The pollen assemblages from VC085 and VC074 are characterised by *Pinus-Corylus* dominated woodland suggesting the peat in these vibrocores overlaps with the later phase of peat development recorded in VC076.
- 6.3.21 The most complete pollen sequence is from VC074, which is located within a palaeochannel (**Figure 6**) and provides a high-resolution record of the vegetation at a local-regional scale during the Early Holocene (see section 5.3). The pollen assemblage is dominated by

woodland taxa, initially *Pinus* (pine) and *Betula* (birch), and later *Corylus avellana*-type (hazel), with herbaceous plants growing on the woodland floor and stands of reeds and sedges in wetland environments, possibly along the margins of the palaeochannels. The assemblage suggests peat formed in a freshwater wetland environment.

- 6.3.22 The pollen sequence from VC074 is comparable to other pollen studies from palaeochannels in the North Sea, although Unit 7b within VC074 is perhaps 1000 years older than deposits studied by Gearey et al. (2017), where the base of the peat infilling a channel was dated to  $8090 \pm 50$  BP (Beta-260805, 9242-8777 cal. BP), characterised by oak-hazel woodland preceded by pine-dominated woodland.
- 6.3.23 Several palaeoenvironmental studies were undertaken on thin peats infilling palaeochannels across the Humber REC area (Tappin et al. 2011), with dates covering ca. 10,000 to 8600 cal. BP, although in no individual case did peat formation last more than a few hundred years at most. These pollen studies show a consistent picture in which *Corylus* was the dominant canopy component, likewise apparent from a sequence at Borkum Riffgrund, 10 km of the north-west German coast, where *Corylus* succeeds a *Pinus-Betula* woodland at ca. 9500 cal. BP (Wolters et al 2010).
- 6.3.24 At the location of VC074, the radiocarbon dates suggest relatively short-lived formation of peat (~500 yrs), possibly reflecting local formation within a palaeochannel that may have become cut off from a main channel (e.g. meander cut-off or oxbow lake). This differs to VC076 which suggests more prolonged peat formation through the Late Devensian and Early Holocene, although it is not known if peat formation was continuous or punctuated by a hiatus during the Loch Lomond stadial. Assuming, peat formation was in part driven by ground water changes associated with post-glacial sea-level rise, a slow-down in the rate of rise is expected to have occurred during the Loch Lomond stadial (12.9-11.7 ka) (Lambeck et al. 2014) which may have influenced the rate of peat formation.
- 6.3.25 Overlying Unit 7b in VC085, lies Unit 7c which is a silty sandy clay deposit comprising marine diatoms, marine foraminifera and ostracods, brackish ostracods, and freshwater diatoms and ostracods (**Figure 9**). The mixed macrofaunal assemblage is interpreted to represent deposition in an intertidal environment and Unit 7c marks a shift from a freshwater, terrestrial environment, to a more coastal setting, most likely under the influence of rising sea levels.
- 6.3.26 It is expected that as sea-levels rose, former river channels would have flooded and with increasing tidal influence, the landscape would have been dominated by a network of tidal creeks and flats. Of interest, the extensive peat deposit mapped in the northern part of the NV West site, appears to be dissected (**Figure 3b**) creating a palaeogeography similar to what would be expected if the peatland was eroded by a series of tidal channels.
- 6.3.27 In VC074 and VC076, the upper surface of the peat is sharp, and deposits are overlain by marine sands that formed through recent seabed processes (**Figure 6 and 7**). At these locations, the transition to a marine environment was abrupt, and possibly even erosive. Dates from the top of Unit 7b in VC074 and VC076 provide limiting ages on the timing of landscape-inundation. The results suggest the NV West site became submerged after ~10,000 cal. BP, remarkably, the dates from both cores are almost identical (UB-36846; 10230-9910 cal. BP and, UB-36848; 10220-9910 cal. BP).
- 6.3.28 Rates of relative sea-level rise at this time were rapid (ca. 12-13 mm/yr; Smith et al. 2011), which may explain the sharp shift in depositional environment recorded in vibrocores. There is no evidence of a transition from a freshwater wetland to saltmarsh environment in the

peat deposits, which would be expected if the landscape kept pace with rising sea-level. This also supports the hypothesis that inundation was rapid.

- 6.3.29 When compared alongside the latest sea-level reconstructions for the southern North Sea (Shennan et al. 2018), the sea-level limiting point from VC076 agrees with the model results (**Figure 17**). The date from VC074, although similar to VC076, is from a lower elevation (-39.40 mLAT) and is therefore expected to have flooded earlier, assuming relative sea-level rise was the only control on inundation. This suggests local topography (e.g. proximity to palaeochannels) may have influenced the timing of inundation, or that differential compaction has influenced the peat deposits.
- 6.3.30 At the time of inundation (~10,000 cal. BP), reconstructions from paleogeographic modelling of the southern North Sea (Sturt et al. 2013) suggest sea-level flooded the Norfolk Vanguard site from the south. If this is the case, the Dover Straits was open much earlier than previously predicted (Shennan et al. 2000; Gaffney et al. 2007). The timing of inundation at the NV West site lies within the range of dates recorded from other peat deposits preserved offshore (ca. 11.5-7.5 ka; WA 2013a)

#### *Archaeological significance*

- 6.3.31 An extensive and rich submerged palaeolandscape record is preserved within the NV West site which documents palaeoenvironmental change from the late Upper Palaeolithic through to the early Mesolithic.
- 6.3.32 After initial recolonisation of Britain during MIS 3 (Boismier et al. 2012), there is evidence of sporadic incursions of various hominin groups into the southern North Sea from ~15 ka to the start of the Holocene (Jacobi and Highman 2011). This period is represented by Unit 7a at the NV West site, which was deposited in fluvial environment providing evidence for the presence of active rivers the landscape which may have been exploited for resources, but also used as routeways to support migration. The potential for encountering in-situ or artefactual material within or along the margins of these channels is considered high (**Table 11**).
- 6.3.33 Extensive peat deposits (Unit 7b) (~40 km<sup>2</sup>) are preserved within the NV West site and they have high potential to contain palaeoenvironmental material which can be used to reconstruct landscape change. The discovery of submerged peat deposits is not novel and there are many examples of peats preserved locally within palaeochannels (WA 2008; Brown et al. 2017; Gaffney et al. 2017). However, uncovering a widespread “peatland”, along with peat-infilled and peat-fringed palaeochannels within a single site, is rare and unique within the context of submerged landscape studies undertaken to date.
- 6.3.34 The vegetation history of the NV West site is comparable to other records from the southern North Sea (Tappin et al. 2011; Gearey et al. 2017), but it has a role in bridging the gap between widely studied palaeoecological records from terrestrial settings on both sides of the North Sea.
- 6.3.35 The North Sea has been largely ignored in mapping of late glacial and Holocene pollen data (e.g. Birks 1989; Brewer et al 2017) due to a lack of data, and yet this area has a critical role to play in understanding the vegetation history of north-west Europe, including the migration history of key plant taxa (especially trees) into Britain. A greater spatial density in pollen studies would provide the basis for a more informed understanding of variability in vegetation habitats across the North Sea and their response to environmental factors. These data would in turn help to inform palaeogeographic models for the region and refine our understanding of the likely range of environmental contexts for human activity.



- 6.3.36 There is evidence in VC076 of repeated fire-events during the early Holocene, although charcoal particles may have been transported long distances; therefore, it is not known if these fires are local or regional. Evidence for fire is widespread in Mesolithic Britain, in both upland and lowland environments (e.g. Simmons 1996; Mellars and Dark 1998; Bell 2007), although there is debate as to whether these fires are natural or anthropogenically induced events (Brown 1997; Moore 2000; Innes and Blackford 2003). At the NV West site, it is not possible to determine the cause of the fire-events, especially in the absence of known Mesolithic archaeology.
- 6.3.37 The major phase of peat development across the NV West site was between  $9122 \pm 49$  BP (UB-36847; 10420-10190 cal. BP) to  $8955 \pm 46$  BP (UB-36846; 10230-9910 cal. BP) which is broadly contemporaneous with key early Mesolithic sites located along the North Sea coast (e.g. Star Carr, Low Hauxley and Howick) (Waddington et al. 2015). The fluvial and wetland landscapes characteristic of the NV West site may have provided a pathway for Mesolithic hominin groups moving into Britain, driven by rising sea levels and landscape inundation. The potential for preservation of archaeological sites within this landscape is considered high (**Table 11**).
- 6.3.38 Inundation of the NV West site during the Mesolithic occurred sometime after  $\sim 10,000$  cal. BP. The rate of landscape inundation is expected to have been rapid based on palaeogeographic modelling (Sturt et al. 2013) supported by evidence from vibrocores. The NV West site is located on the southern limb of what would have been the last land bridge between Britain and continental Europe (not including the Dogger Bank Island), before final inundation at  $\sim 8.5$  ka (Sturt et al. 2013). The response of coastal communities to rapid rates of sea level rise is difficult to perceive without archaeological evidence. Given the relatively short life-expectancy of Mesolithic people (Burger et al 2012), it is unlikely coastal change would have been observable within a single generation.
- 6.3.39 The sediment sequences preserved in the NV West site may provide rare and necessary sea-level index points for the Early Holocene period (Hazell 2008; WA 2013a). At the very least, the sequences can provide sea-level limiting points, such as those discussed above. This data can help refine understanding of the timing and nature of sea-level rise for a time period which is poorly represented in sediment sequences preserved onshore, it can also be used to constrain sea-level models.
- 6.3.40 The exceptional preservation of palaeolandscape features within the NV West site may in part be due to rapid inundation of the area during the early Holocene. When rates of sea-level rise outpace a coastlines ability to adjust, the landscape becomes submerged offshore and assuming limited reworking by waves, the former-landscapes have high preservation potential. Of note, in the NV West site the distribution of palaeolandscape features is strongly correlated to the location of sand banks formed through seabed hydrodynamic processes (**Figure 16**). Here, burial of palaeolandscapes appears to protect them and increase their preservation potential. These observations can be used to help predict where palaeolandscapes are most likely to be preserved, moving towards more targeted assessments at the human-scale.
- 6.3.41 On a final note, the NV West site overlaps with the area of seabed investigated as part of the North Sea Palaeolandscapes Project (Gaffney et al. 2007) and the palaeolandscape features identified at the NV West site, were not picked up during the previous works. This highlights the importance of integrated geophysical and geoarchaeological approaches to palaeolandscape assessments and emphasises the benefit of site-scale assessments.

**Table 11** Archaeological potential of deposits studied within the Norfolk Vanguard site

WA Unit	WA Unit Name Age (MIS)	Palaeoenvironment	Archaeological potential
8	Seabed sediments <i>Holocene post-transgression (MIS 1)</i>	Marine, active hydrodynamic processes.	Unlikely to comprise prehistoric archaeology. Has a role in protecting palaeolandscape features.
7c	Elbow Formation – intertidal <i>Early Holocene (MIS 1)</i>	Coastal, tidal creeks and flats deposited under influence of rapid rates of Early Holocene sea-level rise.	Potential to comprise Early Mesolithic artefactual archaeology.
7b	Elbow Formation – organic <i>Late Devensian to Early Holocene (MIS 2-1)</i>	Freshwater wetland forming within and along the margins of palaeochannels, or within topographic lows in the landscape, with woodland occupying dry ground. Possible hiatus in peat development associated with the Loch Lomond stadial.	High preservation of palaeoenvironmental material. Potential to comprise Upper Palaeolithic or Early Mesolithic artefactual archaeology.
7a	Elbow Formation – fluvial <i>Late Devensian to Early Holocene (MIS 2-1)</i>	Freshwater active fluvial channels. Palaeochannels can be highly sinuous indicating maturity of the river system.	Potential to comprise in-situ and reworked archaeology is high, both within channels and along their margins.
6	Twente Formation – <i>Late Devensian (MIS 2)</i>	Not present	
5	Upper Brown Bank <i>Early-Mid Devensian (MIS 5d-3)</i>	A cold-climate, shallow near-marine embayment that becomes more estuarine towards the east. Water depths shallowed during periods of lower sea-level creating an irregular, dynamic coastal environment fringed by isolated basins and lagoons.	Potential for preservation of archaeological material low. However, the Brown Bank embayment may have created a significant geographic barrier to migration pathways through the southern North Sea during the Middle Palaeolithic, correlating to a period of absence in the British archaeological record.
4	Lower Brown Bank/Eem Formation <i>Ipswichian to Early Devensian (MIS 5e-5d)</i>	Not identified in geotechnical data.	
3	Swarte Bank Formation <i>Anglian (MIS 12)</i>	Not identified in geotechnical data.	
2	Yarmouth Roads Formation <i>Early to Mid-Pleistocene (&gt;MIS 13)</i>	Not identified in geotechnical data.	
1	Westkapelle Ground Formation	Not identified in geotechnical data	

## 7 CONCLUSIONS

7.1.1 This report aims to assess the submerged palaeolandscape resource within the Norfolk Vanguard site by addressing a series of research questions posed in **Section 2**. The key conclusions in relation to these research questions, are outlined below.

### *Middle to Upper Palaeolithic*

- What is the age and depositional history of Brown Bank Formation?

7.1.2 Brown Bank Formation (Unit 5) was deposited between 82 and 57 ka (MIS 5b-4), in a shallow marine environment with lower than expected salinity during a period of climatic instability characterised by cool (stadial) and warm (interstadial) periods, in the Early Devensian.

- What is the palaeogeography of the area during deposition of Brown Bank Formation?

7.1.3 The paleogeography of the NV site was a shallow near-marine embayment fringed by open estuaries in the east. During periods of lower sea level associated with cool stadials, the Brown Bank embayment would have shallowed with some areas emerging to create an irregular coastal geography characterised by isolation basins, barriers/spits and lagoons.

- How do the findings relate to the presence or absence of hominins in Britain during the Middle Palaeolithic?

7.1.4 The results suggest the Brown Bank embayment was a prominent feature in the southern North Sea during the Early Devensian, corresponding to a period of hiatus in the British archaeological record. The presence of this embayment would have created a significant geographic barrier to migration pathways through the southern North Sea during the Middle Palaeolithic and may in part explain the absence of hominins from Britain between MIS 6 and MIS 4.

#### *Late Upper Palaeolithic to Mesolithic*

- What is the age and formation history of the preserved peat deposits?

7.1.5 An initial phase of peat formation commenced in the Late Devensian (13780-13550 cal. BP) during the Windemere Interstadial (warm climate), followed by a period of slow-down or hiatus during the Loch Lomond Stadial (cool climate). Peat continued to form in the Early Holocene (between 10420- 10190 cal. BP and 10170-9740 cal. BP) creating an extensive wetland environment associated with a large river system. Peat formation was relatively short-lived (~500 yrs) along palaeochannel margins, but may have formed more gradually, over longer periods of time within low-lying areas.

- What is the landscape and vegetation history?

7.1.6 The Late Devensian landscape was characterised by active river systems with open birch woodland occupying dry-ground, and wetlands forming in topographic lows. As climate warmed in the Early Holocene, woodland remained relatively open, but became dominated by pine, and later hazel, with grasses and herbs growing on the forest floor. River systems matured and meandered across the landscape with wetlands forming along the margins in slow moving or static water bodies. Under rising sea levels, the coastline encroached periodically flooding the freshwater peat, giving way to tidal flats and creeks before final inundation.

- Is there evidence for hominin activity?

7.1.7 The presence of charcoal within peat deposits is evidence of repeated fire-events during the Early Holocene, although it is not possible to establish if these were caused by human activity. Despite the absence of known archaeological material, the potential for human activity within the extensive fluvial and wetland landscapes preserved at the NV West site, is considered high.

- What is the timing and nature of landscape inundation?



- 7.1.8 Two sea-level limiting points indicate the NV West site became submerged shortly after ca. 10,000 cal. BP which agrees with sea-level and regional-palaeogeographic models. Rates of sea-level rise were rapid (12-12 mm/yr) leaving the landscape little time to adjust; the palaeolandscape features appear to have drowned in-situ, possibly leading to their exceptional preservation.

## **8 RECOMMENDATIONS**

- 8.1.1 It is recommended the final results from geoarchaeological and geophysical works undertaken in support of the Norfolk Vanguard project, are disseminated publicly through publication in a peer reviewed journal.
- 8.1.2 Typically, it is advised all results are published in a single manuscript. However, given similarities in the techniques employed and research objectives between the Norfolk Vanguard and the adjacent Norfolk Boreas sites, it is recommended the results are integrated for publication in two period specific manuscripts, as follows;
- Late Devensian to Early Holocene landscape development and inundation
  - A reappraisal of Brown Bank Formation - Implications for palaeogeography and hominin occupation
- 8.1.3 This approach will produce regional scale palaeolandscape reconstructions driven by period specific research questions, thus having a wider impact than more localised site-specific data driven reconstructions.
- 8.1.4 The results presented here, in combination with those from the adjacent Norfolk Boreas site, have the potential for significant impact beyond the academic community. A range of options are being discussed with the Client in order to maximise the public benefits arising from this work.

## REFERENCES

- Adamiec, G and Aitken, M J 1998 Dose-rate conversion factors: new data. *Ancient TL*, 16, 37-50
- Arfai, J, Franke, D, Lutz, R, Reinhardt, L, Kley, J and Gaedicke, C 2018 Rapid Quaternary subsidence in the northwestern German North Sea. *Scientific Reports* 8, 11524.
- Ashton, N, and Lewis, S 2002 Deserted Britain: Declining Populations in the British Late Middle Pleistocene. *Antiquity* 76, 388–396
- Ashton, N., Lewis, S.G., Parfitt, S.A., Penkman, K.E.H., Coope, G.R., 2008. New evidence for complex climate change in MIS 11 from Hoxne, Suffolk, UK: *Quaternary Science Reviews* 27, 652–668
- Athersuch, J., Horne, D.J. & Whittaker, J.E. 1989. Marine and brackish water ostracods. In: Kermack, D.M. and Barnes, R.S.K. (eds), *Synopsis of the British Fauna (New Series)*, no. 43. E.J. Brill, Leiden (for the Linnean Society of London and The Estuarine and Brackish-water Sciences Association), 359pp.
- Bailey, G and Parkington, J 1988 *The Archaeology of Prehistoric Coastlines*, Cambridge University Press
- Bateman, M D, Frederick, C D, Jaiswal, M K, Singhvi, A K (2003) Investigations into the potential effects of pedoturbation on luminescence dating. *Quaternary Science Reviews*, 22, 1169-1176
- Bell, M 2007 (ed.) *Prehistoric coastal communities: the archaeology of western Britain 6000-3000 cal BC*. York, Council for British Archaeology Research Report 149.
- Bennett, K.D. Whittington, G. and Edwards, K.J., 1994, Recent plant nomenclatural changes and pollen morphology in the British Isles. *Quaternary Newsletter*, 73, 1–6.
- Bicket, A and Tizzard, L 2015 A review of the submerged prehistory and palaeolandscapes of the British Isles. *Proc Geol Assoc* 126, 6, 642-663
- Birks, HJB 1989 Pollen isochrone maps and patterns of tree-spreading in the British Isles. *J. Biogeography* 16, 503-40.
- Boismier, W, Gamble, C, and Coward, F 2012 *Neanderthals among Mammoths: Excavations at Lynford Quarry, Norfolk, UK*. English Heritage
- Boomer, I., Waddington, C., Stevenson, T., and Hamilton, D. (2007). Holocene Coastal Change and Geoarchaeology at Howick, Northumberland, UK. *The Holocene*, 17(1), pp. 89–104.
- Brewer, S, Giesecke, T, Davis, B A S, Finsinger, W, Wolters, S, Binney, H, de Beaulieu, J-L, Fyfe, R, Gil-Romera, G, Kuhl, N, Kunes, P, Leydet, M and Bradshaw, R H 2017 Late glacial and Holocene European pollen data, *J Maps* 13, 921–928
- Bridgland, D R, Field, M H, Holmes, J A, McNabb, J, Preece, R C, Selby, I, Wymer, J J, Boreham, S, Irving, B G, Parfitt, S A and Stuart, A J 1999 Middle Pleistocene interglacial Thames–Medway deposits at Clacton-on-Sea, England: Reconsideration of the biostratigraphical and environmental context of the type Clactonian Palaeolithic industry. *Quat Sci Rev* 18, 109–146



- Bronk-Ramsay, C., 2009. *OxCal calibration programme version v4.10*. Radiocarbon accelerator Unit, University of Oxford.
- Bronk Ramsey, C and Lee, S 2013, Recent and planned development of the Program OxCal. *Radiocarbon* 55, (2-3), 720–730
- Brown, A G 1997 Clearances and clearings: deforestation in Mesolithic/Neolithic Britain. *Oxford J Archaeol* 16, 133-46
- Brown, A, Russel, J, Scaife, R, Tizzard, L, Whittaker, J and Wyles, S 2018 Lateglacial/early Holocene palaeoenvironments in the southern North Sea Basin: new data from the Dudgeon offshore wind farm *J Quat Sci*
- Burger, O. Baudisch, A. and Vaupel, J W. 2012 Human mortality improvement in evolutionary context. *Proc Nat Acad Sci USA* 109, 18210-18214.
- Busschers, F S. Kasse, C. van Balen, R T. Vandenberghe, J. Cohen, K M. Weerts, H J T. Wallinga, J. Johns, C. Cleveringa, P. Bunnik, F P M. 2007 Late Pleistocene evolution of the Rhine-Meuse system in the southern North Sea basin: imprints of climate change, sea-level oscillation and glacio-isostasy. *Quaternary Science Reviews*, 26(25-28), 3216-3248.
- Cameron, T D J, Crosby, A, Balson, P S, Jeffery, D H, Lott, G K, Bulat, J and Harrison, D J 1992 *The Geology of the Southern North Sea*. British Geological Survey United Kingdom Offshore Regional Report, London, HMSO
- Candy, I, Silva, B and Lee, J 2011 Climates of the Early Middle Pleistocene in Britain: Environments of the Earliest Humans in Northern Europe. In Ashton N, Lewis, S G, and Stringer, C (eds.) *The Ancient Human Occupation of Britain*. Vol. 14, 11–22, Amsterdam, Netherlands, Elsevier B.V.
- Chiverrell R C. and Thomas G S P. 2010 Extent and timing of the Last Glacial Maximum (LGM) in Britain and Ireland: a review. *J. Quaternary Sci.*, Vol. 25 pp. 535–549.
- Clark, R L 1982 Point count estimate of charcoal in pollen preparations and thin sections of sediment. *Pollen et Spores* 24, 523-535.
- Cohen, K M, MacDonald, K, Joordens, J C A, Roebroeks, W and Gibbard, P L 2012 The Earliest Occupation of North-West Europe: a Coastal Perspective. *Quat Intl* 271, 70-83
- Coles, B 1998 Doggerland: a speculative survey. *Proceedings of the Prehistoric Society* 64, 45-81
- Cushing, E J 1967 Evidence for differential pollen preservation in late Quaternary sediments in Minnesota. *Review of Palaeobotany and Palynology* 4, 87–101
- Dix, J and Sturt, F 2011 *The Relic Palaeo-landscapes of the Thames Estuary*. Southampton, University of Southampton for MALSF
- Dove, D. Evans, D J A. Lee, J R. Roberts, D H. Tappin, D R. Mellett, C L. Long, D. Callard, S L. 2017 Phased occupation and retreat of the last British–Irish Ice Sheet in the southern North Sea: geomorphic and seismostratigraphic evidence of a dynamic ice lobe. *Quaternary Science Reviews*, 163. 114-134.
- Emu Ltd. 2009 *Outer Thames Estuary Regional Environmental Characterisation*. MALSF, Crown Copyright 2009, ISBN 978-00907545-28-9





- Fugro Survey B.V., (2017). Report 1 of 3: Geophysical Investigation Report. Volume 2 of 3: Geophysical Site Survey. Norfolk Vanguard Offshore Wind Farm. Unpublished report, ref. GE050-R1.
- Funnell, B M 1989 Chapter 12. Quaternary, in Jenkins, D G and Murray, J W (eds) *Stratigraphical Atlas of Fossil Foraminifera. Second Edition* 563-569. British Micropalaeontological Society Series, London, John Wiley & Sons
- Gaffney, V, Thomson, K and Fitch, S 2007 mapping Doggerland: The Mesolithic Landscapes of the Southern North Sea. Oxford, Archaeopress
- Galbraith, R F, Roberts, R G, Laslett, G M, Yoshida, H and Olley, J M 1999 Optical dating of single and multiple grains of quartz from Jinmium rock shelter (northern Australia): Part I, Experimental design and statistical models. *Archaeometry*, 41, 339-364
- Gearey, B, Hopla, E, Griffiths, S, Boomer, I, Smith, D, Marshall, P, Fitch, S and Tappin, D 2017 Integrating multi-proxy palaeoecological and archaeological approaches to submerged landscapes: a case study from the southern North Sea in Williams, H, Hill, Boomer, I and Wilkinson, I (eds) *The Archaeological and Forensic Applications of Microfossils: A Deeper Understanding of Human History*, Geological Society Special Publication
- Giesecke, T, Bennett, K D, Birks, J B, Bjune, A E, Bozilova, E, Feurdean, A, Finsinger, W, Froyd, C, Pokorný, P, Rösch, M, Seppä, H, Tonkov, S, Valsecchi, V. and Wolters, S. 2011 The pace of Holocene vegetation change—testing for synchronous developments. *Quat. Sci. Rev.* 30, 19-20
- Godwin, H and Godwin, M E 1933 British Maglemose Harpoon Sites. *Antiquity* 7, 36–48
- Grimm, E.C., 2011. Tilia 1.7.16 Software. Illinois State Museum, Research and Collection Center, Springfield.
- Hazell Z. 2008 Offshore and intertidal peat deposits, England – a resource assessment and development of a database *Env Arch* 13 2 101-110
- Hijma, M P, Cohen, K M, Roebroeks, W, Westerhoff, W E, Busschers, F S. 2012. Pleistocene Rhine-Thames landscapes: Geological background for hominin occupation of the southern North Sea region. *Journal of Quaternary Science*, 27, 17-39.
- Housley, R A 1991 AMS Dates from the Late Glacial and Early Postglacial in North-West Europe: a Review in Barton, N, Roberts, A J, and Roe, D A (eds) *The Late Glacial in North-West Europe: Human Adaptation and Environmental Change at the End of the Pleistocene*. London, Council for British Archaeology, 25-36
- Hublin J-J, Weston D. and Gunz P. 2009 Out of the North Sea: the Zeeland Ridges Neandertal. *Journal of Human Evolution* 57: 777– 785.
- Innes, J B and Blackford, J J 2003 The ecology of Late Mesolithic woodland disturbances: model testing with fungal spore assemblage data. *J Archaeol Sci* 30, 185-94  
Jacobi, R, and Higham, T 2011 The Later Upper Palaeolithic Recolonisation of Britain: New Results from AMS Radiocarbon Dating. In Ashton N, Lewis, S G, and Stringer, C (eds.) *The Ancient Human Occupation of Britain*. Vol. 14, 223–247, Amsterdam, Netherlands, Elsevier B.V.

- Jones, R.W. and Whittaker, J.E. 2010. Palaeoenvironmental interpretation of the Pleistocene-Holocene of the British Isles, using proxy Recent benthonic foraminiferal distribution data. In: Whittaker, J.E. & Hart, M.B. *Micropalaeontology, Sedimentary Environments and Stratigraphy: A Tribute to Dennis Curry (1912-2001)*. The Micropalaeontological Society, Special Publications. The Geological Society, London, 261-279.
- Lambeck, K. Rouby, H. Purcell, A. Sun, Y. and Sambridge, M. 2014 Sea level and global ice volumes from the Last Glacial Maximum to the Holocene. *PNAS* 111(43), 15296-15303.
- Lewis S G, Ashton N and Jacobi, R 2011 Testing Human Presence during the Last Interglacial (MIS 5e): A Review of the British Evidence, in Ashton N, Lewis, S G, and Stringer, C (eds.) *The Ancient Human Occupation of Britain*. Vol.14, 125-247, Amsterdam, Netherlands, Elsevier
- Limpenny, S E, Barrio Froján, C, Cotterill, C, Foster-Smith, R L, Pearce, B, Tizzard, L, Limpenny, D L, Long, D, Walmsley, S, Kirby, S, Baker, K, Meadows, W J, Rees, J, Hill, J, Wilson, C, Leivers, M, Churchley, S, Russell, J, Birchenough, A C, Green, S L and Law, R J 2011 *The East Coast Regional Environmental Characterisation*. MEPF
- Lisiecki, L. E., and M. E. Raymo (2005), A Pliocene-Pleistocene stack of 57 globally distributed benthic  $\delta^{18}O$  records, *Paleoceanography*, 20, PA1003
- Mayle, F E. Lowe, J J. and Sheldrick, C. 1997 The Late Devensian Lateglacial palaeoenvironmental record from Whitrig Bog, SE Scotland. 1. Lithostratigraphy, geochemistry and palaeobotany. *Boreas* 26, 279-295
- Medlycott, M 2011 Research and archaeology revisited: a revised framework for the East of England. *East Anglian Archaeology* 24
- Meisch, C 2000 Freshwater Ostracoda of Western and Central Europe in Schwoerbel, J. & Zwick, P. (eds) *Süßwasserfauna von Mitteleuropa, Band 8/3*. Spektrum Akademischer Verlag, Heidelberg and Berlin
- Mejdahl, V 1979 Thermoluminescence dating: beta-dose attenuation in quartz grains. *Archaeometry*, 21, 61-72
- Mellars, P A and Dark, S P (eds.) 1998 *Star Carr in context*. Cambridge, MacDonald Institute for Archaeological Research.
- Mellet, C L. and Plater, A. J. 2017. Drowned barriers as archives of coastal-response to rapid sea-level rise. In: Moore, L. and Murray, B. (Eds) *Barrier dynamics and response to changing climate*, Springer
- Momber, G, Tomalin, D, Scaife, R, Satchell, J and Gillespie, J 2011 *Mesolithic Occupation at Bouldner Cliff and the Submerged Prehistory Landscapes of the Solent*. CBA Report 164, Council for British Archaeology
- Moore, J 2000 Forest fire and human interaction in the early Holocene woodlands of Britain. *Palaeogeog, Palaeoclim, Palaeoecol* 164, 125-37
- Moore, P D, Webb, J A. and Collinson, M E 1991 *Pollen analysis*. Oxford, Blackwell
- Murray, A S, Olley, J M and Caitcheon, G G 1995 Measurement of equivalent doses in quartz from contemporary water-lain sediments using optically stimulated luminescence. *Quaternary Science Reviews*, 14, 365-371



- Murray, A.S. and Wintle, A.G. (2000) Luminescence dating of quartz using an improved single-aliquot regenerative-dose protocol. *Radiation Measurements*, 32, 57-73.
- Murray, A.S. and Wintle, A.G. (2003) The single aliquot regenerative dose protocol: potential for improvements in reliability. *Radiation Measurements*, 37, 377-381.
- Murray, J W 2006 *Ecology and Applications of Benthic Foraminifera*. Cambridge University
- Murray, J.W. 2006. *Ecology and Applications of Benthic Foraminifera*. Cambridge University
- Olley, J M, Caitcheon, G G and Roberts R G 1999 The origin of dose distributions in fluvial sediments, and the prospect of dating single grains from fluvial deposits using -optically stimulated luminescence. *Radiation Measurements*, 30, 207-217
- Olley, J M, Pietsch, T and Roberts, R G 2004 Optical dating of Holocene sediments from a variety of geomorphic settings using single grains of quartz. *Geomorphology*, 60, 337-358
- Olsson, I. U. (2009), 'Radiocarbon Dating History: Early Days, Questions, and Problems Met', *Radiocarbon* 51(1), 1-43
- Parfitt, S A, Ashton, N M, Lewis, S G, Abel, R L, Coope, G R., Field, M H, Gale, R, Hoare, P G, Larkin, N R, Lewis, M D, Karloukovski, V, Maher, B A, Peglar, S M, Preece, R C, Whittaker, J E, and Stringer, C B, 2010 Early Pleistocene human occupation at the edge of the boreal zone in northwest Europe. *Nature*, 466 (7303), 229–33
- Parfitt, S A, Barendregt, R W, Breda, M, Candy, I, Collins, M J, Coope, G R, Durbidge, P, Field, M H, Lee, J R, Lister, A M, Mutch, R, Penkman, K E H, Preece, R C, Rose, J, Stringer, C B, Symmons, R, Whittaker, J E, Wymer J, and Stuart, A J 2005 The earliest record of human activity in northern Europe, *Nature* 438, 1008–1012.
- Pennington, W. Tutin, T G. and Bertie, D M. 1977 The Late Devensian Flora and Vegetation of Britain. *Phil Transactions of the Royal Society of London. Series B, Biological Sciences* 280, 972
- Pettitt, P, and White, M J 2012 *The British Palaeolithic: Human Societies at the Edge of the Pleistocene World*. Abingdon, Routledge
- Prescott, J R and Hutton, J T 1994 Cosmic ray contributions to dose rates for luminescence and ESR dating: large depths and long-term time variations. *Radiation Measurements*, 23, 497-500
- Ramsey, C B. 2009. Dealing with Outliers and Offsets in Radiocarbon Dating. *Radiocarbon* 51, 1023-1045.
- Ransley, J, Sturt, F, Dix, J, Adams, J and Blue, L, 2013 *People and the sea: a maritime archaeological research agenda for England*. York, Council for British Archaeology Research Report 171
- Reid, C 1913 *Submerged Forests*. London, Cambridge University Press
- Reimer, P. J., Bard, E., Bayliss, A., Beck, J. W., Blackwell, P. G., Bronk Ramsey, C., Grootes, P. M., Guilderson, T. P., Hafliðason, H., Hajdas, I., HattĹ, C., Heaton, T. J., Hoffmann, D. L., Hogg, A. G., Hughen, K. A., Kaiser, K. F., Kromer, B., Manning, S. W., Niu, M., Reimer, R. W., Richards, D. A., Scott, E. M., Southon, J. R., Staff, R. A., Turney, C. S. M. and van der



- Plicht, J. (2013). IntCal13 and Marine13 Radiocarbon Age Calibration Curves 0-50,000 Years cal BP. *Radiocarbon*, 55(4), 1869–1887.
- Roberts, N. 1998 *The Holocene, An Environmental History*. Oxford, Uk, Blackwell Publishing
- Scott, B, and Ashton, N 2011 The Early Middle Palaeolithic: The European Context in Ashton, N, Lewis, S G, and Stringer, C (eds) *The Ancient Human Occupation of Britain. Volume 14*, 91–112, Amsterdam, Netherlands, Elsevier B.V.
- Scott, B, Ashton, N, Lewis, S G, Parfitt, S, and White, M, 2011 Technology and Landscape Use in the Early Middle Palaeolithic of the Thames Valley, in Ashton N, Lewis, S G, and Stringer, C (eds.) *The Ancient Human Occupation of Britain. Volume 14*, 67-89, Amsterdam, Netherlands, Elsevier B.V.
- Shennan et al. 2018, I. Bradley, S. and Edwards, R. 2018. Relative sea-level changes and crustal movements in Britain and Ireland since the Last Glacial Maximum. *Quaternary Science Reviews* 188 143-159
- Shennan, I. Lambeck, K. Flather, R. Horton, B. McArthur, J. Innes, J. Lloyd, J. Rutherford, M. Wingfield, R. 2000 Modelling western North Sea palaeogeographies and tidal changes during the Holocene. In: Shennan, I. Andrews, J E. (Eds.) *Holocene Land-ocean Interaction and Environmental Change Around the Western North Sea, vol. 166*. Geological Society Special Publication, pp. 299-319.
- M. Siddall, M. Rohling, E J. Almogi-Labin, A. Hemleben, C. Meischner, D. Schmelzer, I. and Smeed, D A. 2003 Sea-level fluctuations during the last glacial cycle. *Nature* 423
- Simmons, I G 1996 *The Environmental impact of later Mesolithic Cultures*. Edinburgh, Edinburgh University Press
- Simmons, M 2016. Examining the relationship between environmental change and human activities at the dryland-wetland interface during the late Upper Palaeolithic and Mesolithic in Southeast England. Unpublished PhD thesis, University of Reading.
- Stace, C, 1997, *New flora of the British Isles* (2nd edition), Cambridge, Cambridge University Press.
- Stoker, M S, Balson, P S, Long, D, Tappin, D R 2011 An overview of the lithostratigraphical framework for the Quaternary deposits on the United Kingdom continental shelf, British Geological Survey Research Report RR/11/03
- Sturt, F, Garrow, D and Bradley, S, 2013 New models of North West European Holocene palaeogeography and inundation. *Journal of Archaeological Science*, 40 3963-3976
- Sumbler, M G 1996 *British Regional Geology; London and the Thames Valley* London: HMSO
- Tappin, D R, Pearce, B, Fitch, S, Dove, D, Gearey, B, Hill, J M, Chambers, C, Bates, R, Pinnion, J, Diaz Doce, D, Green, M, Gallyot, J, Georgiou, L, Brutto, D, Marzioletti, S, Hopla, E, Ramsay, E, and Fielding, H 2011 *The Humber Regional Environmental Characterisation*. British Geological Survey Open Report OR/10/54
- Tizzard, L, Bicket, A R, Benjamin, J, and De Loecker, D 2014 A Middle Palaeolithic Site in the Southern North Sea: Investigating the Archaeology and Palaeogeography of Area 240. *J Quat. Sci* 29, 698–710



- Tizzard, L, Bicket, A. R, Benjamin, J and De Loecker, D 2015 *A Middle Palaeolithic Site in the Southern North Sea: Investigating the Archaeology and Palaeogeography of Area 240*. Salisbury, Wessex Archaeology Monograph no 35
- Waddington C. 2015 Mesolithic re-colonisation of Britain following on the drowning of North Sea landscapes in *No Stone Unturned. Papers in Honour of Roger Jacobi*, Ashton N, Harris C (eds) Lithic Studies Society: London; 221-232
- Waelbroeck, C. Labeyrie, L. Michel, E. Duplessy, J.C. McManus, J.F. Lambeck, K. Balbon, E. Labracherie, M. 2002. Sea-level and deep water temperature changes derived from benthic foraminifera isotopic records. *Quaternary Science Reviews*, 21(1–3), 295-305.
- Walker, M J C. 1982, The late glacial and early Flandrian deposits at Traeth Mawr, Brecon Beacons, South Wales. *New Phytologist* 90, 1, 177-194
- Wessex Archaeology 2008 Seabed Prehistory: Gauging the Effects of Marine Aggregate Dredging. Round 2 Final Report, Volume II: Arun. Wessex Archaeology, Salisbury 57422.32
- Wessex Archaeology 2011 Seabed Prehistory: Site Evaluation Techniques (Area 240). Salisbury, unpubl report, ref: 70754.04
- Wessex Archaeology 2013a Audit of Current State of Knowledge of Submerged Palaeolandscapes and Sites. Salisbury, unpubl report, ref: 84570.01
- Wessex Archaeology 2013b Palaeo-Yare Catchment Assessment. Salisbury, unpubl report, ref: 83740.04
- Wessex Archaeology 2018a. Norfolk Vanguard Offshore Windfarm: Stage 2 Geoarchaeological Recording. Unpublished client report ref: 112380.03.
- Wessex Archaeology 2018b. Norfolk Vanguard Offshore Windfarm: Stage 3 Palaeoenvironmental Assessment. Unpublished client report ref: 112380.03.
- Wessex Archaeology 2018c Norfolk Boreas Offshore Wind Farm: Archaeological assessment of geophysical data. Salisbury, unpublished report ref 114843.03
- Wessex Archaeology 2018d Norfolk Boreas Offshore Wind Farm: Stage 1 Geoarchaeological Report, Salisbury, unpublished report ref 117120.01
- Wessex Archaeology 2018e Norfolk Boreas Offshore Wind Farm: Stage 2 Geoarchaeological Review, Salisbury, unpublished report ref 117120.02
- Wessex Archaeology 2018f Norfolk Boreas Offshore Wind Farm: Stage 3 Palaeoenvironmental Assessment, Salisbury, unpublished report ref 117122.02
- Wessex Archaeology 2017a *Vanguard Offshore Wind Farm, Stage 1 geoarchaeological review*. Unpublished client report, ref: 11480.01.
- Wessex Archaeology 2017b. *Norfolk Vanguard Offshore Wind Farm, marine archaeological technical report*. Unpublished client report, ref: 112380.02.
- White, M 2006 Things to Do in Doggerland when you're Dead: Surviving OIS3 at the Northwestern-Most Fringe of Middle Palaeolithic Europe. *World Archaeology* 44(April), 0–28



- White, M J, Ashton, N. 2003 Lower Paleolithic Core Technology and the Origins of the Levallois Method in North-Western Europe. *Current Anthropology* 44 (4), 598-609.
- White, M I, Jacobi, R. 2002 Two sides to every story: bout coupe handaxes revisited. *Oxford Journal of Archaeology* 21, 109-133
- Wolters S, Zeller M, Burgenstock F 2010 Early Holocene environmental history of sunken landscapes: pollen, plant macrofossil and geochemical analyses from the Borkum Riffgrund, southern North Sea. *International J Earth Sci* 99, 1707-1719
- Wymer, J J 1999 *The Lower Palaeolithic Occupation of Britain*. Wessex Archaeology and English Heritage
- Zimmerman, D W 1971 Thermoluminescent dating using fine grains from pottery. *Archaeometry*, 13, 29-52





## APPENDICES

### Appendix 1 – list of sub-samples

VC074 (NV West)				
Depth (m down core)		Depth (m LAT)		Technique
From	To	From	To	
<b>Stage 3</b>				
0.80		-39.30		Foraminifera, ostracod and diatom
0.85		-39.35		Foraminifera, ostracod and diatom
0.88		-39.38		Pollen assessment
0.90		-39.40		Radiocarbon and plant macrofossils
0.98		-39.48		Pollen assessment
1.08		-39.58		Pollen assessment
1.18		-39.68		Pollen assessment
1.24		-39.74		Foraminifera, ostracod and diatom
1.28		-39.78		Pollen assessment
1.30		-39.80		Foraminifera, ostracod and diatom
1.38		-39.88		Pollen assessment
1.40		-39.90		Foraminifera, ostracod and diatom
1.46		-39.96		Pollen assessment
1.50		-40.00		Foraminifera, ostracod and diatom
1.56		-40.06		Radiocarbon and plant macrofossils
1.58		-40.08		Pollen assessment
1.61		-40.11		Foraminifera, ostracod and diatom
1.76		-40.26		Foraminifera, ostracod and diatom
5.00	5.50	-43.50	-44.00	OSL
<b>Stage 4</b>				
1.18		-39.68		Radiocarbon and plant macrofossils
1.45		-39.95		Radiocarbon and plant macrofossils
0.88		-39.38		Pollen analysis
0.93		-39.43		Pollen analysis
0.98		-39.48		Pollen analysis
1.03		-39.53		Pollen analysis
1.08		-39.58		Pollen analysis
1.13		-39.63		Pollen analysis
1.18		-39.68		Pollen analysis
1.23		-39.73		Pollen analysis
1.28		-39.78		Pollen analysis
1.32		-39.82		Pollen analysis
1.38		-39.88		Pollen analysis
1.42		-39.92		Pollen analysis
1.46		-39.96		Pollen analysis
1.48		-39.98		Pollen analysis



<b>VC074 (NV West)</b>				
<b>Depth (m down core)</b>		<b>Depth (m LAT)</b>		
<b>From</b>	<b>To</b>	<b>From</b>	<b>To</b>	<b>Technique</b>
1.54		-40.04		Pollen analysis
1.58		-40.08		Pollen analysis
3.70	4.00	-42.20	-42.50	OSL
1.90		-40.40		Foraminifera and ostracod
2.80		-41.30		Foraminifera and ostracod
3.60		-42.10		Foraminifera and ostracod
4.60		-43.10		Foraminifera and ostracod



VC076 (NV West)				
Depth (m down core)		Depth (m LAT)		
From	To	From	To	Technique
<b>Stage 3</b>				
3.40		-37.40		Foraminifera, ostracod and diatom
3.50		-37.50		Foraminifera, ostracod and diatom
3.60		-37.60		Pollen assessment
3.61	3.63	-37.61	-37.63	Radiocarbon and plant macrofossils
3.70		-37.70		Pollen assessment
3.80		-37.80		Pollen assessment
3.87		-37.87		Pollen assessment
3.91	3.93	-37.91	-37.93	Radiocarbon and plant macrofossils
3.95		-37.95		Pollen assessment
3.98		-37.98		Foraminifera, ostracod and diatom
4.08		-38.08		Foraminifera, ostracod and diatom
3.99	4.01	-37.99	-38.01	Particle size analysis
4.13	4.15	-38.13	-38.15	Particle size analysis
4.20	4.24	-38.20	-38.24	Particle size analysis



VC079 (NV West)				
Depth (m down core)		Depth (m LAT)		
From	To	From	To	Assessment
<b>Stage 3</b>				
0.40		-41.20		Foraminifera, ostracod and diatom
0.70		-41.50		Foraminifera, ostracod and diatom
0.75	1.00	-41.55	-41.80	OSL
1.40		-42.20		Foraminifera, ostracod and diatom
1.90		-42.70		Foraminifera, ostracod and diatom
2.10		-42.90		Foraminifera, ostracod and diatom
2.90		-43.70		Foraminifera, ostracod and diatom
3.40		-44.20		Foraminifera, ostracod and diatom
3.90		-44.70		Foraminifera, ostracod and diatom
4.15	4.35	-44.95	-45.15	OSL
4.40		-45.20		Foraminifera, ostracod and diatom
4.90		-45.70		Foraminifera, ostracod and diatom
2.80		-41.30		Foraminifera and ostracod
3.60		-42.10		Foraminifera and ostracod
4.60		-43.10		Foraminifera and ostracod



VC085 (NV West)				
Depth (m down core)		Depth (m LAT)		
From	To	From	To	Assessment
<b>Stage 3</b>				
1.58		-36.98		Foraminifera, ostracod and diatom
1.70		-37.10		Foraminifera, ostracod and diatom
1.75	1.77	-37.15	-37.17	Radiocarbon and plant macrofossils
1.76		-37.16		Pollen assessment
1.86		-37.26		Pollen assessment
1.96		-37.36		Pollen assessment
2.06		-37.46		Pollen assessment
2.07	2.09	-37.47	-37.49	Radiocarbon and plant macrofossils
2.14		-37.54		Foraminifera, ostracod and diatom
2.16		-37.56		Pollen assessment
2.26		-37.66		Foraminifera, ostracod and diatom
2.38		-37.78		Foraminifera, ostracod and diatom
2.50		-37.90		Foraminifera, ostracod and diatom
4.60	4.80	-40.00	-40.20	OSL
5.10	5.30	-40.50	-40.70	OSL
<b>Stage 4</b>				
3.50		-38.90		Foraminifera and ostracod
4.40		-39.80		Foraminifera and ostracod
5.60		-41.00		Foraminifera and ostracod



<b>VC107 (NV East)</b>				
<b>Depth (m down core)</b>		<b>Depth (m LAT)</b>		
<b>From</b>	<b>To</b>	<b>From</b>	<b>To</b>	<b>Assessment</b>
<b>Stage 3</b>				
1.00	1.25	-37.70	-37.95	OSL
1.33		-38.03		Foraminifera and ostracod
1.80		-38.50		Foraminifera and ostracod
2.10		-38.80		Foraminifera and ostracod
2.50		-39.20		Foraminifera and ostracod
3.05		-39.75		Foraminifera and ostracod
3.50		-40.20		Foraminifera and ostracod
4.05		-40.75		Foraminifera and ostracod
4.50		-41.20		Foraminifera and ostracod
5.05		-41.75		Foraminifera and ostracod
5.50		-42.20		Foraminifera and ostracod
<b>Stage 4</b>				
4.65	5.00	-41.35	-41.70	OSL





## Appendix 2 – Foraminifera and ostracod results

DEPTH IN CORE		0.80m	0.85m	1.24m	1.30m	1.40m	1.50m	1.61m	1.76m	1.90m	2.80m	3.60m	4.60m	
VC074	<b>MARINE FORAMINIFERA</b>													
	<i>Ammonia batavus</i> *	x	x	x	xx					x		xx	xx	
	milolids	x									xxx	xxx	xxx	
	<i>Elphidium excavatum</i>		o											
	<i>Elphidium bartletti</i>										xx	x	x	
	<i>Elphidium clavatum</i>										x	x	x	
	<i>Pseudopolymorphina novangliae</i>										x	x	x	
	<b>FRESHWATER OSTRACODS</b>													
	<i>Candona neglecta</i>	x									o			
	<i>Limnocythere inopinata</i>		o											
	<i>Darwinula stevensoni</i>		o											
	<i>Limnocytherina sanctipatricii</i>				o									
	<b>MARINE OSTRACODS</b>													
	<i>Sarsicytheridea bradli</i>				o									
	<i>Elofsonella concinna</i>									x	xxx	xxx	xxx	
	<i>Leptocythere tenera</i>											x	x	x
	<i>Sclerochilus</i> sp.											x	x	x
	<i>Hemicytherura clathrata</i>											x	x	x
	<i>Cytheropteron</i> spp.											x	x	x
	<i>Semicytherura</i> spp.											x	x	
<i>Hemicythere villosa</i>											x	o	x	
<i>Hirschmannia viridis</i>											x	x		
<i>Cythere lutea</i>												o	x	
<i>Pontocythere elongata</i>												o		
<i>Finmarchinella angulata</i>												o		
<i>Robertsonites tuberculatus</i>													o	
<b>BRACKISH FORAMINIFERA</b>														
<i>Elphidium williamsoni</i>											xxx	xxx	xxx	
<b>BRACKISH OSTRACODS</b>														
<i>Leptocythere psammophila</i>											xx	xx	xx	
<i>Leptocythere lacertosa</i>											x	x		

Contained material is listed on a presence(x)/absence basis; wf – worn and/or fragmentary; j – juveniles

Ostracods and foraminifera are listed: o- one specimen; x – several specimens; xx- common

Freshwater ostracod: cool/cold indicator

Marine ostracod not part of the British fauna but living today further north in Europe

Cold indicator foraminifera

Marine ostracods restricted to northern Britain today and further north

\* Large & highly ornate form – warm indicator



		DEPTH IN CORE	0.80m	0.85m	1.24m	1.30m	1.40m	1.50m	1.61m	1.76m	
VC074	<b>MARINE FORAMINIFERA</b>										
		<i>Ammonia batavus</i>	x	x	x	xx					
		miliolids	x								
		<i>Elphidium excavatum</i>		o							
	<b>FRESHWATER OSTRACODS</b>										
		<i>Candona neglecta</i>	x								
		<i>Limnocythere inopinata</i>		o							
		<i>Darwinula stevensoni</i>		o							
		<i>Limnocytherina sanctipatricii</i>				o					
	<b>MARINE OSTRACODS</b>										
		<i>Sarsicytheridea bradii</i>				o					

cool/cold indicator

cool/cold indicator

		DEPTH IN CORE	3.40m	3.50m	3.98m	4.08m
VC076	<b>MARINE FORAMINIFERA</b>					
		miliolids	x	x		
		<i>Ammonia batavus</i>	x	x		
	<b>MARINE OSTRACODS</b>					
		<i>Sarsicytheridea bradii</i>	o			

cool/cold indicator



DEPTH IN CORE		0.40m	0.70m	1.40m	1.90m	2.10m	2.90m	3.40m	3.90m	4.40m	4.90m
VC079	<b>MARINE &amp; OUTER ESTUARINE FORAMINIFERA</b>										
	<i>Ammonia batavus</i>	xxx	xxx	xxx	xxx	xxx	xxx			xx	xxx
	miliolids	xx	xx	x	xx	x	xx	x	x		x
	<i>Elphidium williamsoni</i>	x	xx	xx	x	x	x	x		o	
	<i>Elphidium exavatum</i>	x	x	x		x	xx	x	x	x	
	<i>Elphidium margaritaceum</i>	x			o			o			
	<i>Haynesina germanica</i>	x		x	x			x	x		
	<i>Elphidium macellum</i>	o				o					x
	lagenids		x	o			o		o		
	discorbids							o	x	o	
	<b>MARINE &amp; OUTER ESTUARINE OSTRACODS</b>										
	<i>Elofonella concinna</i>	xxx	xx	x	x	xx	xxx			o	o
	<i>Letocythere pellucida</i>	x				o	x	o		x	
	<i>Pontocythere elongata</i>	x		o	o		x				
	<i>Leptocythere psammophila</i>	x	xx	xx	x	x	o				
	<i>Sclerochilus</i> spp.	x	x	x	x		o			o	
	<i>Cytheropteron latissimum</i>	x		o		o		o			
	<i>Cythere lutea</i>	x	x				o	o		x	
	<i>Hemicytherura clathrata</i>	x		x	x		x	x	x		o
	<i>Eucythere argus</i>	x				o		o	o		
<i>Semicytherura undata</i>	x	o	x								
<i>Semicytherura</i> spp.	x	x	x	x	x	x	x				
<i>Hirschmannia viridis</i>	x	x	o	x	o	x					
<i>Paradoxostomas</i> sp.	o	x	o	o							
<i>Hemicythere villosa</i>	o		o	x	o	x	x	x	x	x	
<i>Leptocythere tenera</i>		x	x	x	x	o		x			
<i>Finmarchinella angulata</i>					o						
<i>Leptocythere lacertosa</i>						o		o			
<i>Robertsonites tuberculatus</i>						x			x	o	
<i>Sarsicytheridea bradii</i>						o		o	x	x	
<b>FRESHWATER OSTRACODS</b>											
<i>Cytherissa lacustris</i>							o				

Contained material is listed on a presence(x)/absence basis

Ostracods and foraminifera are listed: o- one specimen; x – several specimens; xx- common; xxx – abundant/superabundant

cool/cold indicators

cold indicator, extinct in Britain since Early Holocene



DEPTH IN CORE		1.58m	1.70m	2.14m	2.26m	2.38m	2.50m
VC085	<b>MARINE FORMANIFERA</b>						
	<i>Ammonia batavus</i>	xx	xx				
	miliolids	xx	xx				
	<i>Elphidium macellum</i>	x	x				
	<b>MARINE OSTRACODS</b>						
	<i>Pontocythere elongata</i>	xx	xx				
	<i>Leptocythere pellucida</i>	x	x				
	<i>Elofsonella concinna</i>	x	o				
	<i>Heterocythereis albomaculata</i>	x	o				
	<i>Hemicythere villosa</i>	x	o				
	<i>Cythere lutea</i>	o					
	<i>Semicytherura undata</i>		o				
	<b>BRACKISH OSTRACODS</b>						
	<i>Cyprideis torosa</i>	x	x				
	<b>FRESHWATER OSTRACODS</b>						
	<i>Ilyocypris bradyi</i>	x	x			xx	xx
	<i>Herpetocypris reptans</i>					xx	xx
	<i>Candona neglecta</i>					xx	xx
	<i>Limnocythere inopinata</i>					xx	xx
	<i>Cyclocypris ovum</i>					x	x
	<i>Candona candida</i>					x	
	<i>Potamocypris zschokkei</i>						x
<i>Eucypris pigra</i>						x	
	<b>northern cool/cold indicators</b>						



DEPTH IN CORE		1.58m	1.70m	2.14m	2.26m	2.38m	2.50m	3.50m	4.40m	5.60m	
VC085	<b>MARINE FORAMINIFERA</b>										
	<i>Ammonia batavus</i> *	xx	xx					xxx	xxx		
	miliolids	xx	xx					x	x	x	
	<i>Elphidium macellum</i>	x	x								
	<i>Elphidium bartletti</i>							xx	xx	x	
	<i>Elphidium clavatum</i>							x	x		
	<i>Elphidium margaritaceum</i>							x			
	lagenids							x			
	<i>Pseudopolymorphina novangliae</i>							o	x	o	
	<i>Elphidium albiumbilicatum</i>									o	
	<b>MARINE OSTRACODS</b>										
	<i>Pontocythere elongata</i>	xx	xx						o		
<i>Leptocythere pellucida</i>	x	x						x	xx		
<i>Elofsonella concinna</i>	x	o						xxx	xxx		
<i>Heterocythereis albomaculata</i>	x	o							o		
<i>Hemicythere villosa</i>	x	o							o		
<i>Cythere lutea</i>	o							o	x		
<i>Semicytherura undata</i>		o							o		
<i>Robertsonites tuberculatus</i>								xx	xxx	o	
<i>Cytheropteron</i> spp.								x	x		
<i>Eucythere argus</i>								x	x	o	
<i>Hirschmannia viridis</i>								x			
<i>Finmarchinella angulata</i>								x	o		
<i>Hemicytherura clathrata</i>								x	x	o	
<i>Finmarchinella finmarchica</i>								o			
<i>Sarsicytheridea punctillata</i>									x		
<i>Sarsicytheridea bradii</i>									x	x	
<b>BRACKISH OSTRACODS</b>											
<i>Cyprideis torosa</i>	x	x									
<i>Leptocythere psammophila</i>								x			
<b>FRESHWATER OSTRACODS</b>											
<i>Ilyocypris bradyi</i>	x	x				xx	xx				
<i>Herpetocypris reptans</i>						xx	xx				
<i>Candona neglecta</i>						xx	xx				
<i>Limnocythere inopinata</i>						xx	xx				
<i>Cyclocypris ovum</i>						x	x				
<i>Candona candida</i>						x					
<i>Potamocypris zschokkei</i>							x				
<i>Eucypris pigra</i>							x				
<b>BRACKISH FORAMINIFERA</b>											
<i>Elphidium williamsoni</i>								xx	x		

Contained material is listed on a presence(x)/absence basis; f – fragments  
 Ostracods and foraminifera are listed: o- one specimen; x – several specimens; xx- common

Ostracods not part of the British fauna but living today further north in Europe  
 Ostracods restricted to northern Britain today and further north

Cold indicator foraminifera  
 \* Large & highly ornate form – warm indicator



DEPTH IN CORE		1.33m	1.80m	2.10m	2.50m	3.05m	3.50m	4.05m	4.50m	5.05m	5.50m
VC-107	<b>BRACKISH/OUTER ESTUARINE FORAMINIFERA</b>										
	<i>Haynesina germanica</i>	x	xx	x	x	x	xx	x	o	x	x
	<i>Elphidium williamsoni</i>	x	x	o		x	o	x			x
	<i>Elphidium excavatum/clavatum*</i>	x	x		x	x	x	x	x	x	x
	<i>Ammoniasp. (small)</i>	o	o								
	miliolids			o	o	o		xx	x	x	x
	<i>Pseudopolymorphina novangliae*</i>				x	o	o	o			
	<i>Ammonia batavus</i>								o		
	<i>Elphidium macellum</i>									o	
	<b>BRACKISH/OUTER ESTUARINE OSTRACODS</b>										
	<i>Ssmicytherura nigrescens</i>	x									
	<i>Hirschmannia viridis</i>	x	x								
	<i>Leptocythere psammophila</i>	x				x					
	<i>Hemicythere villosa</i>	x						o			
	<i>Cytheropteronsp.</i>			x							
	<i>Finmarchinella angulata*</i>				o						
	<i>Eucythere argus</i>					o					
	<i>Leptocythere pellucida</i>							o			
	<i>Sclerochilus</i> sp.							o			
	<i>Sarsicytheridea bradlii*</i>							o	o		o
	<b>FRESHWATER OSTRACODS</b>										
	<i>Limnocythere inopinata</i>							o			

Contained material is listed on a presence(x)/absence basis  
 Ostracods and foraminifera are listed: o- one specimen; x – several specimens; xx- common \* - cool/cold indicator



### Appendix 3 – raw pollen data VC074

Depth (mbsf)	0.88	0.93	0.98	1.03	1.08	1.13	1.18	1.23
Sample volume (ml)	1	1	1	1	1	1	1	1
<i>Lycopodium</i> tablets	1	1	1	1	1	1	1	1
Exotic	42	76	41	44	37	46	45	295
Charcoal hits	614	298	1274	539	70	181	340	124
<i>Betula</i>	31	32	31	33	36	38	28	42
<i>Pinus sylvestris</i>	185	171	204	196	189	199	172	246
<i>Corylus avellana</i> type	169	174	110	131	136	136	158	108
<i>Ulmus</i>	18	8	18	11	7	22	11	7
<i>Quercus</i>	17	17	21	16	17	18	19	5
<i>Tilia</i>	0	0	0	0	0	0	0	0
<i>Alnus glutinosa</i>	1	0	0	0	1	0	0	0
<i>Acer</i>	0	0	0	0	0	0	0	1
<i>Salix</i>	13	3	6	8	3	6	16	12
<i>Cornus</i>	0	0	0	0	1	0	0	0
<i>Ilex aquifolium</i>	0	0	0	0	0	0	0	2
<i>Hedera helix</i>	0	0	0	0	0	1	0	0
Ericaceae	0	0	0	0	0	1	0	0
<i>Calluna vulgaris</i>	0	0	0	0	0	0	0	0
Poaceae	65	71	84	92	97	69	89	63
Cyperaceae	7	18	14	6	10	7	5	12
Ranunculaceae	0	0	0	0	0	0	0	0
<i>Thalictrum</i>	0	0	0	0	0	0	0	1
Caryophyllaceae	0	0	0	1	0	0	0	0
<i>Silene</i> type	0	0	0	0	1	0	0	0
Chenopodiaceae	0	0	2	0	0	0	1	0
Brassicaceae	1	0	1	0	0	0	0	1
<i>Artemisia</i> type	0	0	0	0	2	0	0	1
<i>Rumex acetosa</i>	0	0	0	0	0	0	0	1
<i>Rumex obtusifolius</i>	0	0	0	0	0	0	0	0
Rosaceae	4	2	0	1	0	1	5	0
<i>Filipendula</i>	1	0	2	2	0	0	2	4
<i>Potentilla</i>	1	0	0	1	0	0	1	0
Fabaceae	0	0	0	0	0	0	0	0
<i>Trifolium</i> type	1	2	1	0	0	0	0	0
<i>Lythrum salicaria</i> type	0	0	0	0	0	0	0	0
Apiaceae	0	0	3	0	1	0	0	1
<i>Apium nodiflorum</i>	0	0	1	0	0	0	0	1
Rubiaceae	1	0	1	1	1	0	0	0
<i>Cirsium</i>	0	1	0	0	0	0	0	0





Depth (mbsf)	0.88	0.93	0.98	1.03	1.08	1.13	1.18	1.23
Astertype	1	2	1	1	0	2	2	0
Anthemis	0	0	0	1	0	0	0	0
Pteropsida undiff.	123	78	77	71	78	74	59	117
<i>Pteridium aquilinum</i>	0	0	2	1	0	1	0	0
<i>Dryopteris filix-mas</i>	1	6	10	4	9	9	1	2
<i>Thelypteris palustris</i>	17	52	21	17	28	18	21	2
<i>Polypodium vulgare</i>	1	0	0	0	0	0	1	0
<i>Myriophyllum spicatum</i>	0	1	0	0	1	0	0	1
<i>Potamogeton natans</i> type	14	41	35	36	42	23	48	33
<i>Sparganium emersum</i> type	5	3	8	3	5	4	2	5
<i>Typha latifolia</i>	10	9	8	6	6	6	5	7
<i>Nuphar</i>	0	1	0	0	0	0	0	0
<i>Sphagnum</i>	1	1	2	2	0	3	2	3
Indeterminables	<b>9</b>	<b>2</b>	<b>6</b>	<b>4</b>	<b>5</b>	<b>4</b>	<b>3</b>	<b>5</b>
<b>TLP</b>	<b>516</b>	<b>501</b>	<b>500</b>	<b>501</b>	<b>502</b>	<b>500</b>	<b>509</b>	<b>508</b>
Charcoal	614	298	1274	539	70	181	340	124
Points	202	202	202	202	202	202	202	202
Charcoal/points	3.04	1.48	6.31	2.67	0.35	0.90	1.68	0.61
Field of view	0.00238	0.00238	0.00238	0.00238	0.00238	0.00238	0.00238	0.00238
No <i>Lycopodium</i> spores	20848	20848	20848	20848	20848	20848	20848	20848
<i>Lycopodium</i> spores counted	50	50	50	50	50	50	50	50
Total spores/total counted	416.96	416.96	416.96	416.96	416.96	416.96	416.96	416.96
Total	3.01	1.46	6.25	2.64	0.34	0.89	1.67	0.61



Depth (mbsf)	1.28	1.32	1.38	1.42	1.46	1.48	1.54	1.58
Sample volume (ml)	1	1	1	1	1	1	1	1
<i>Lycopodium</i> tablets	1	1	1	1	1	1	1	1
Exotic	175	89	98	57	87	86	103	249
Charcoal hits	145	1077	716	1540	449	557	751	84
<i>Betula</i>	41	45	31	52	53	80	62	70
<i>Pinus sylvestris</i>	233	279	297	264	265	230	215	98
<i>Corylus avellana</i> type	98	89	63	94	106	108	88	28
<i>Ulmus</i>	11	4	11	6	7	10	8	2
<i>Quercus</i>	15	9	20	5	5	5	2	4
<i>Tilia</i>	0	0	0	0	0	0	0	0
<i>Alnus glutinosa</i>	0	0	0	0	0	0	0	0
<i>Acer</i>	0	0	0	0	0	0	0	0
<i>Salix</i>	15	14	3	9	6	8	13	9
<i>Cornus</i>	0	0	0	0	0	0	0	0
<i>Ilex aquifolium</i>	1	0	1	0	0	2	0	0
<i>Hedera helix</i>	0	0	0	0	0	0	0	0
Ericaceae	0	0	0	0	0	0	0	0
<i>Calluna vulgaris</i>	0	0	0	1	0	0	0	0
Poaceae	68	51	57	65	60	50	93	69
Cyperaceae	10	12	8	8	12	7	13	10
Ranunculaceae	0	0	1	0	0	0	0	0
<i>Thalictrum</i>	0	0	0	0	0	0	0	0
Caryophyllaceae	0	0	2	0	0	0	1	0
<i>Silene</i> type	0	0	0	1	0	0	0	0
Chenopodiaceae	0	0	0	0	0	1	1	4
Brassicaceae	0	2	0	1	1	0	1	1
<i>Artemisia</i> type	0	1	0	0	0	0	1	1
<i>Rumex acetosa</i>	0	0	0	0	0	0	0	2
<i>Rumex obtusifolius</i>	0	1	0	1	0	0	0	0
Rosaceae	1	0	2	3	0	2	2	0
<i>Filipendula</i>	1	0	0	2	1	1	0	2
<i>Potentilla</i>	0	0	1	0	0	0	0	0
Fabaceae	0	0	0	1	0	0	0	0
<i>Trifolium</i> type	1	0	0	1	0	0	0	0
<i>Lythrum salicaria</i> type	0	0	0	1	0	0	0	0
Apiaceae	3	3	0	2	1	1	4	3
<i>Apium nodiflorum</i>	1	1	0	0	0	0	0	0
Rubiaceae	0	0	0	0	0	0	1	1
<i>Cirsium</i>	0	0	0	0	0	0	0	0
<i>Aster</i> type	1	0	3	2	0	0	3	0



Depth (mbsf)	1.28	1.32	1.38	1.42	1.46	1.48	1.54	1.58
<i>Anthemis</i>	0	0	0	0	0	0	0	0
Pteropsida undiff.	44	105	61	106	57	100	141	7
<i>Pteridium aquilinum</i>	0	1	0	0	0	0	0	0
<i>Dryopteris filix-mas</i>	6	0	0	2	7	4	7	2
<i>Thelypteris palustris</i>	19	4	4	5	12	10	15	5
<i>Polypodium vulgare</i>	0	0	0	0	0	0	0	0
<i>Myriophyllum spicatum</i>	1	1	0	0	0	0	0	0
<i>Potamogeton natans</i> type	44	44	61	46	35	33	36	11
<i>Sparganium emersum</i> type	6	7	6	7	5	2	7	8
<i>Typha latifolia</i>	7	1	0	6	5	2	4	5
<i>Nuphar</i>	0	0	0	0	0	0	1	0
<i>Sphagnum</i>	0	1	0	1	1	0	0	1
<b>Indeterminables</b>	<b>8</b>	<b>3</b>	<b>10</b>	<b>1</b>	<b>1</b>	<b>0</b>	<b>0</b>	<b>0</b>
<b>TLP</b>	<b>500</b>	<b>511</b>	<b>500</b>	<b>519</b>	<b>517</b>	<b>505</b>	<b>508</b>	<b>304</b>
Charcoal	145	1077	716	1540	449	557	751	84
Points	202	202	202	202	202	202	202	202
Charcoal/points	0.72	5.33	3.54	7.62	2.22	2.76	3.72	0.42
Field of view	0.00238	0.00238	0.00238	0.00238	0.00238	0.00238	0.00238	0.00238
No <i>Lycopodium</i> spores	20848	20848	20848	20848	20848	20848	20848	20848
<i>Lycopodium</i> spores counted	50	50	50	50	50	50	50	50
Total spores/total counted	416.96	416.96	416.96	416.96	416.96	416.96	416.96	416.96
Total	0.71	5.28	3.51	7.55	2.20	2.73	3.68	0.41



## Appendix 4 – radiocarbon reports

UBANo	Sample ID	Material Type	<sup>14</sup> C Age	±	F14C	±
UBA-39469	114844_VC074_1.18m	Cyperaceae, Solanum sp. and Alisma sp. seeds, Poaceae husks	9696	44	0.2991	0.0016
UBA-39470	114844_VC075_1.45m	Juncus sp., Betula sp., Caryophyllaceae, Alisma sp., Chenopodiaceae and Carex sp. seeds	9613	39	0.3022	0.0015
UBA-39471	117122_VC039_2.96m	Menyanthes trifoliata seed	8510	58	0.3467	0.0025
UBA-39472	117122_VC039_3.13m	Menyanthes trifoliata, Betula sp., Characeae oospores, Typha sp.	10435	66	0.2728	0.0022
UBA-39473	117122_VC032_3.61m	Organic material with Sphagnum sp. leaves	9124	77	0.3212	0.0031
UBA-39474	117122_VC032_3.95m	Lamiaceae, Ranunculus sp., Menyanthes trifoliata seeds	8894	78	0.3305	0.0032
UBA-39475	117122_VC028_2.5m	Failed	Failed	Failed	Failed	Failed

Inez Lopez-Doriga  
Wessex Archaeology  
Portway House  
Old Sarum Park  
Salisbury, Wiltshire  
SP4 6EB  
England  
Customer No.  
2144166



<sup>14</sup>CHRONO Centre  
Queens University  
Belfast  
42 Fitzwilliam  
Street  
Belfast BT9 6AX  
Northern Ireland

## Radiocarbon Date Certificate

Laboratory Identification: UBA-39469  
Date of Measurement: 2018-12-12  
Site: Vanguard  
Sample ID: 114844\_VC074\_1.18m  
Material Dated: plant macrofossil  
Pretreatment: Acid Only  
Submitted by: Ines Lopez Doriga

Conventional	9696±44
<sup>14</sup> C Age:	BP
	using
Fraction	AMS
corrected	δ <sup>13</sup> C

Inez Lopez-Doriga  
Wessex Archaeology  
Portway House  
Old Sarum Park  
Salisbury, Wiltshire  
SP4 6EB  
England  
Customer No.  
2144166



<sup>14</sup>CHRONO Centre  
Queens University  
Belfast  
42 Fitzwilliam  
Street  
Belfast BT9 6AX  
Northern Ireland

## Radiocarbon Date Certificate

Laboratory Identification: UBA-39470  
Date of Measurement: 2018-12-12  
Site: Vanguard  
Sample ID: 114844\_VC075\_1.45m  
Material Dated: plant macrofossil  
Pretreatment: Acid Only  
Submitted by: Ines Lopez Doriga

Conventional	9613±39
<sup>14</sup> C Age:	BP
	using
Fraction	AMS
corrected	δ <sup>13</sup> C



Inez Lopez-Doriga  
Wessex Archaeology  
Portway House  
Old Sarum Park  
Salisbury, Wiltshire  
SP4 6EB  
England  
Customer No.  
2144166



<sup>14</sup>CHRONO Centre  
Queens University  
Belfast  
42 Fitzwilliam  
Street  
Belfast BT9 6AX  
Northern Ireland

## Radiocarbon Date Certificate

Laboratory Identification: UBA-39471  
Date of Measurement: 2018-12-12  
Site: Boreas  
Sample ID: 117122\_VC039\_2.96m  
Material Dated: plant macrofossil  
Pretreatment: Acid Only  
Submitted by: Ines Lopez Doriga

Conventional	8510±58
<sup>14</sup> C Age:	BP
	using
Fraction	AMS
corrected	δ <sup>13</sup> C

Inez Lopez-Doriga  
Wessex Archaeology  
Portway House  
Old Sarum Park  
Salisbury, Wiltshire  
SP4 6EB  
England  
Customer No.  
2144166



<sup>14</sup>CHRONO Centre  
Queens University  
Belfast  
42 Fitzwilliam  
Street  
Belfast BT9 6AX  
Northern Ireland

## Radiocarbon Date Certificate

Laboratory Identification: UBA-39472  
Date of Measurement: 2018-12-12  
Site: Boreas  
Sample ID: 117122\_VC039\_3.13m  
Material Dated: plant macrofossil  
Pretreatment: Acid Only  
Submitted by: Ines Lopez Doriga

Conventional	10435±66
<sup>14</sup> C Age:	BP
	using
Fraction	AMS
corrected	δ <sup>13</sup> C

Inez Lopez-Doriga  
Wessex Archaeology  
Portway House  
Old Sarum Park  
Salisbury, Wiltshire  
SP4 6EB  
England  
Customer No.  
2144166



<sup>14</sup>CHRONO Centre  
Queens University  
Belfast  
42 Fitzwilliam  
Street  
Belfast BT9 6AX  
Northern Ireland

## Radiocarbon Date Certificate

Laboratory Identification: UBA-39473  
Date of Measurement: 2018-12-12  
Site: Boreas  
Sample ID: 117122\_VC032\_3.61m  
Material Dated: plant macrofossil  
Pretreatment: Acid Only  
Submitted by: Ines Lopez Doriga

Conventional	9124±77
<sup>14</sup> C Age:	BP
	using
Fraction	AMS
corrected	δ <sup>13</sup> C

Inez Lopez-Doriga  
Wessex Archaeology  
Portway House  
Old Sarum Park  
Salisbury, Wiltshire  
SP4 6EB  
England  
Customer No.  
2144166



<sup>14</sup>CHRONO Centre  
Queens University  
Belfast  
42 Fitzwilliam  
Street  
Belfast BT9 6AX  
Northern Ireland

## Radiocarbon Date Certificate

Laboratory Identification: UBA-39474  
Date of Measurement: 2018-12-12  
Site: Boreas  
Sample ID: 117122\_VC032\_3.95m  
Material Dated: plant macrofossil  
Pretreatment: Acid Only  
Submitted by: Ines Lopez Doriga

Conventional	8894±78
<sup>14</sup> C Age:	BP
	using
Fraction	AMS
corrected	δ <sup>13</sup> C

## Information about radiocarbon calibration

RADIOCARBON CALIBRATION PROGRAM\*

CALIB REV7.0.0

Copyright 1986-2013 M Stuiver and PJ Reimer

\*To be used in conjunction with:

Stuiver, M., and Reimer, P.J., 1993, Radiocarbon, 35, 215-230.

Annotated results (text) - -

Export file - c14res.csv

39469

UBA-39469

Radiocarbon Age BP 9696 +/- 44

Calibration data set: intcal13.14c

% area enclosed cal AD age ranges

68.3 (1 sigma) cal BC 9252- 9151

95.4 (2 sigma) cal BC 9276- 9121

9002- 8918

8890- 8864

# Reimer et al. 2013  
relative area under  
probability distribution

1.000

0.819

0.164

0.016

39470

UBA-39470

Radiocarbon Age BP 9613 +/- 39

Calibration data set: intcal13.14c

% area enclosed cal AD age ranges

68.3 (1 sigma) cal BC 9174- 9118

9068- 9060

9009- 8913

8902- 8848

95.4 (2 sigma) cal BC 9215- 9101

9089- 8827

# Reimer et al. 2013  
relative area under  
probability distribution

0.249

0.033

0.488

0.230

0.278

0.722

39471

UBA-39471

Radiocarbon Age BP 8510 +/- 58

Calibration data set: intcal13.14c

% area enclosed cal AD age ranges

68.3 (1 sigma) cal BC 7587- 7533

95.4 (2 sigma) cal BC 7606- 7479

# Reimer et al. 2013  
relative area under  
probability distribution

1.000

1.000

39472

UBA-39472

Radiocarbon Age BP 10435 +/- 66

Calibration data set: intcal13.14c

% area enclosed cal AD age ranges

68.3 (1 sigma) cal BC 10572- 10526

10479- 10418

10407- 10280

10261- 10213

95.4 (2 sigma) cal BC 10601- 10131

# Reimer et al. 2013  
relative area under  
probability distribution

0.150

0.234

0.459

0.156

1.000

39473

UBA-39473

Radiocarbon Age BP 9124 +/- 77

Calibration data set: intcal13.14c

% area enclosed cal AD age ranges

68.3 (1 sigma) cal BC 8446- 8362

# Reimer et al. 2013  
relative area under  
probability distribution

0.428

	8356- 8271	0.572
95.4 (2 sigma)	cal BC 8554- 8230	1.000
39474		
UBA-39474		
Radiocarbon Age BP	8894 +/- 78	
Calibration data set: intcal13.14c		# Reimer et al. 2013
% area enclosed	cal AD age ranges	relative area under probability distribution
68.3 (1 sigma)	cal BC 8227- 7957	1.000
95.4 (2 sigma)	cal BC 8263- 7784	0.992
	7769- 7758	0.008

References for calibration datasets:

Reimer PJ, Bard E, Bayliss A, Beck JW, Blackwell PG, Bronk Ramsey C, Buck CE, Cheng H, Edwards RL, Friedrich M, Grootes PM, Guilderson TP, Hafliðason H, Hajdas I, Hattā C, Heaton TJ, Hogg AG, Hughen KA, Kaiser KF, Kromer B, Manning SW, Niu M, Reimer RW, Richards DA, Scott EM, Southon JR, Turney CSM, van der Plicht J.

IntCal13 and MARINE13 radiocarbon age calibration curves 0-50000 years calBP Radiocarbon 55(4). DOI: 10.2458/azu\_js\_rc.55.16947

Comments:

\* This standard deviation (error) includes a lab error multiplier.  
 \*\* 1 sigma = square root of (sample std. dev.^2 + curve std. dev.^2)  
 \*\* 2 sigma = 2 x square root of (sample std. dev.^2 + curve std. dev.^2)  
 where ^2 = quantity squared.  
 [ ] = calibrated range impinges on end of calibration data set  
 0\* represents a "negative" age BP  
 1955\* or 1960\* denote influence of nuclear testing C-14

NOTE: Cal ages and ranges are rounded to the nearest year which may be too precise in many instances. Users are advised to round results to the nearest 10 yr for samples with standard deviation in the radiocarbon age greater than 50 yr.

<>

UBANo	Sample ID	Material Type	<sup>14</sup> C Age	±	F14C	±
UBA-36846	114843_VC074_0.9	Seeds (Nuphar lutea 2x, Nymphaea alba 2x, Juncus sp. 1x, Cyperaceae 1/2x) + leaves (Sphagnum sp. 25x)	8955	46	0.3280	0.0019
UBA-36847	114843_VC074_1.56	Seeds (Betula sp. 3x, Solanum sp. 2x, Chenopodium sp. 1x, Caryophyllaceae 1x, Betula sp. 5x, Lycopus europaeus 1x, Potamogeton)	9122	49	0.3212	0.0020
UBA-36848	114843_VC076_3.61-3.63	Seeds (Lycopus europaeus 1x, Juncus sp. 2x, Asteraceae 1x, Carex sp. 2x, Ranunculus sp. 1/2, indet. 2x)	8936	47	0.3288	0.0019
UBA-36849	114843_VC076_3.91-3.93	Seeds (Potamogeton sp. 5x)	11863	55	0.2284	0.0016
UBA-36850	114843_VC085_1.75-1.77	Seeds (Ceratophyllum sp. 1x and Menyanthes trifoliata 2x)	10192	47	0.2812	0.0016
UBA-36851	114843_VC085_2.07-2.09	Seeds (Menyanthes trifoliata 2x)	8856	48	0.3321	0.0020



Inez Lopez-Doriga  
Wessex Archaeology  
Portway House  
Old Sarum Park  
Salisbury, Wiltshire SP4  
6EB  
England  
Customer No. 2144166



<sup>14</sup>CHRONO Centre  
Queens University  
Belfast  
42 Fitzwilliam Street  
Belfast BT9 6AX  
Northern Ireland

## Radiocarbon Date Certificate

Laboratory Identification: UBA-36846  
Date of Measurement: 2018-03-12  
Site: Vanguard  
Sample ID: 114843\_VC074\_0.9  
Material Dated: plant macrofossil  
Pretreatment: Acid Only  
Submitted by: Ines Lopez Doriga

Conventional <sup>14</sup> C
Age: 8955±46 BP
using AMS
Fraction corrected δ <sup>13</sup> C

Inez Lopez-Doriga  
Wessex Archaeology  
Portway House  
Old Sarum Park  
Salisbury, Wiltshire SP4  
6EB  
England  
Customer No. 2144166



<sup>14</sup>CHRONO Centre  
Queens University  
Belfast  
42 Fitzwilliam Street  
Belfast BT9 6AX  
Northern Ireland

## Radiocarbon Date Certificate

Laboratory Identification: UBA-36847  
Date of Measurement: 2018-03-09  
Site: Vanguard  
Sample ID: 114843\_VC074\_1.56  
Material Dated: plant macrofossil  
Pretreatment: Acid Only  
Submitted by: Ines Lopez Doriga

Conventional <sup>14</sup> C Age: 9122±49 BP using AMS Fraction corrected δ <sup>13</sup> C
--

Inez Lopez-Doriga  
Wessex Archaeology  
Portway House  
Old Sarum Park  
Salisbury, Wiltshire SP4  
6EB  
England  
Customer No. 2144166



<sup>14</sup>CHRONO Centre  
Queens University  
Belfast  
42 Fitzwilliam Street  
Belfast BT9 6AX  
Northern Ireland

## Radiocarbon Date Certificate

Laboratory Identification: UBA-36848  
Date of Measurement: 2018-03-09  
Site: Vanguard  
Sample ID: 114843\_VC076\_3.61-3.63  
Material Dated: plant macrofossil  
Pretreatment: Acid Only  
Submitted by: Ines Lopez Doriga

Conventional <sup>14</sup> C Age: 8936±47 BP using AMS Fraction corrected δ <sup>13</sup> C
--

Inez Lopez-Doriga  
Wessex Archaeology  
Portway House  
Old Sarum Park  
Salisbury, Wiltshire SP4  
6EB  
England  
Customer No. 2144166



<sup>14</sup>CHRONO Centre  
Queens University  
Belfast  
42 Fitzwilliam Street  
Belfast BT9 6AX  
Northern Ireland

## Radiocarbon Date Certificate

Laboratory Identification: UBA-36849  
Date of Measurement: 2018-03-09  
Site: Vanguard  
Sample ID: 114843\_VC076\_3.91-3.93  
Material Dated: plant macrofossil  
Pretreatment: Acid Only  
Submitted by: Ines Lopez Doriga

Conventional <sup>14</sup> C	11863±55
Age:	BP
Fraction	using AMS
corrected	δ <sup>13</sup> C

Inez Lopez-Doriga  
Wessex Archaeology  
Portway House  
Old Sarum Park  
Salisbury, Wiltshire SP4  
6EB  
England  
Customer No. 2144166



<sup>14</sup>CHRONO Centre  
Queens University  
Belfast  
42 Fitzwilliam Street  
Belfast BT9 6AX  
Northern Ireland

## Radiocarbon Date Certificate

Laboratory Identification: UBA-36850  
Date of Measurement: 2018-03-09  
Site: Vanguard  
Sample ID: 114843\_VC085\_1.75-1.77  
Material Dated: plant macrofossil  
Pretreatment: Acid Only  
Submitted by: Ines Lopez Doriga

Conventional <sup>14</sup> C	10192±47
Age:	BP
Fraction	using AMS
corrected	δ <sup>13</sup> C

Inez Lopez-Doriga  
Wessex Archaeology  
Portway House  
Old Sarum Park  
Salisbury, Wiltshire SP4  
6EB  
England  
Customer No. 2144166



<sup>14</sup>CHRONO Centre  
Queens University  
Belfast  
42 Fitzwilliam Street  
Belfast BT9 6AX  
Northern Ireland

## Radiocarbon Date Certificate

Laboratory Identification: UBA-36851  
Date of Measurement: 2018-03-09  
Site: Vanguard  
Sample ID: 114843\_VC085\_2.07-2.09  
Material Dated: plant macrofossil  
Pretreatment: Acid Only  
Submitted by: Ines Lopez Doriga

Conventional <sup>14</sup> C
Age: 8856±48 BP
using AMS
Fraction corrected δ <sup>13</sup> C



## Information about radiocarbon calibration

RADIOCARBON CALIBRATION PROGRAM\*  
CALIB REV7.0.0

Copyright 1986–2013 M Stuiver and PJ Reimer

\*To be used in conjunction with:

Stuiver, M., and Reimer, P.J., 1993, Radiocarbon, 35, 215–230.

Annotated results (text) - -

Export file - c14res.csv

36846

UBA-36846

Radiocarbon Age BP 8955 +/- 46

Calibration data set: intcal13.14c

% area enclosed cal AD age ranges

68.3 (1 sigma) cal BC 8255– 8184

8112– 8088

8077– 8062

8041– 7996

95.4 (2 sigma) cal BC 8276– 8164

8141– 7968

# Reimer et al. 2013

relative area under  
probability distribution

0.525

0.126

0.075

0.274

0.470

0.530

36847

UBA-36847

Radiocarbon Age BP 9122 +/- 49

Calibration data set: intcal13.14c

% area enclosed cal AD age ranges

68.3 (1 sigma) cal BC 8423– 8405

8391– 8378

8349– 8275

95.4 (2 sigma) cal BC 8465– 8250

# Reimer et al. 2013

relative area under  
probability distribution

0.102

0.071

0.827

1.000

36848

UBA-36848

Radiocarbon Age BP 8936 +/- 47

Calibration data set: intcal13.14c

% area enclosed cal AD age ranges

68.3 (1 sigma) cal BC 8242– 8178

8113– 8059

8044– 7991

95.4 (2 sigma) cal BC 8257– 7962

# Reimer et al. 2013

relative area under  
probability distribution

0.391

0.297

0.311

1.000

36849

UBA-36849

Radiocarbon Age BP 11863 +/- 55

Calibration data set: intcal13.14c

% area enclosed cal AD age ranges

68.3 (1 sigma) cal BC 11791– 11660

95.4 (2 sigma) cal BC 11831– 11607

# Reimer et al. 2013

relative area under  
probability distribution

1.000

1.000

36850

UBA-36850

Radiocarbon Age BP 10192 +/- 47

Calibration data set: intcal13.14c

% area enclosed cal AD age ranges

# Reimer et al. 2013

relative area under  
probability distribution

68.3 (1 sigma)	cal BC 10042- 9852	0.973
	9833- 9825	0.027
95.4 (2 sigma)	cal BC 10141- 9757	0.999
	9707- 9706	0.001

36851

UBA-36851

Radiocarbon Age BP 8856 +/- 48

Calibration data set: intcal13.14c

# Reimer et al. 2013

% area enclosed cal AD age ranges

relative area under  
probability distribution

68.3 (1 sigma)	cal BC 8204- 8035	0.681
	8016- 7938	0.302
	7922- 7921	0.003
	7889- 7883	0.014
95.4 (2 sigma)	cal BC 8219- 7811	0.988
	7806- 7795	0.012

## References for calibration datasets:

Reimer PJ, Bard E, Bayliss A, Beck JW, Blackwell PG, Bronk Ramsey C, Buck CE, Cheng H, Edwards RL, Friedrich M, Grootes PM, Guilderson TP, Haflidason H, Hajdas I, Hattä C, Heaton TJ, Hogg AG, Hughen KA, Kaiser KF, Kromer B, Manning SW, Niu M, Reimer RW, Richards DA, Scott EM, Southon JR, Turney CSM, van der Plicht J.

IntCal13 and MARINE13 radiocarbon age calibration curves 0-50000 years calBP  
Radiocarbon 55(4). DOI: 10.2458/azu\_js\_rc.55.16947

## Comments:

\* This standard deviation (error) includes a lab error multiplier.

\*\* 1 sigma = square root of (sample std. dev.^2 + curve std. dev.^2)

\*\* 2 sigma = 2 x square root of (sample std. dev.^2 + curve std. dev.^2)

where ^2 = quantity squared.

[ ] = calibrated range impinges on end of calibration data set

0\* represents a "negative" age BP

1955\* or 1960\* denote influence of nuclear testing C-14

NOTE: Cal ages and ranges are rounded to the nearest year which may be too precise in many instances. Users are advised to round results to the nearest 10 yr for samples with standard deviation in the radiocarbon age greater than 50 yr.

&lt;&gt;

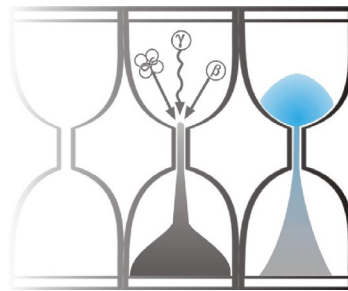


## Appendix 5 – OSL report



University of Gloucestershire

Luminescence dating laboratory



**Optical dating of sediments: Vanguard Offshore Windfarm**

to

**Dr C. Mellett**

**Wessex Archaeology**

**Analysis & Reporting, Prof. P.S. Toms**

**Sample Preparation & Measurement, Mr J.C. Wood**

**16 March 2018**

**Updated 14 December 2018 (to include samples GL18023 & GL18024)**

# Contents

Section		Page
	Table 1 $D_r$ , $D_e$ and Age data of submitted samples	3
	Table 2 Analytical validity of sample suite ages	4
1.0	Mechanisms and Principles	5
2.0	Sample Preparation	5
3.0	Acquisition and accuracy of $D_e$ value	6
	3.1 Laboratory Factors	6
	3.1.1 Feldspar Contamination	6
	3.1.2 Preheating	7
	3.1.3 Irradiation	7
	3.1.4 Internal Consistency	7
	3.2 Environmental Factors	7
	3.2.1 Incomplete Zeroing	7
	3.2.2 Turbation	8
4.0	Acquisition and accuracy of $D_r$ value	8
5.0	Estimation of age	9
6.0	Analytical Uncertainty	9
	Sample diagnostics, luminescence and age data	12
	References	20

## Scope of Report

This is a standard report of the Luminescence dating laboratory, University of Gloucestershire. In large part, the document summarises the processes, diagnostics and data drawn upon to deliver Table 1. A conclusion on the analytical validity of each sample's optical age estimate is expressed in Table 2; where there are caveats, the reader is directed to the relevant section of the report that explains the issue further in general terms.

## Copyright Notice

Permission must be sought from Prof. P.S. Toms of the University of Gloucestershire Luminescence dating laboratory in using the content of this report, in part or whole, for the purpose of publication.

Field Code	Lab Code	Overburden (m)	Grain size (µm)	Moisture content (%)	Nal γ-spectrometry ( <i>in situ</i> )			γ D <sub>r</sub> (Gy.ka <sup>-1</sup> )	Ge γ-spectrometry ( <i>ex situ</i> )			α D <sub>r</sub> (Gy.ka <sup>-1</sup> )	β D <sub>r</sub> (Gy.ka <sup>-1</sup> )	Cosmic D <sub>r</sub> (Gy.ka <sup>-1</sup> )	Preheat (°C for 10s)	Low Dose Repeat Ratio	Interpolated:Applied Low Regenerative-dose D <sub>e</sub>	High Dose Repeat Ratio	Interpolated:Applied High Regenerative-dose D <sub>e</sub>	Post-IR OSL Ratio
					K (%)	Th (ppm)	U (ppm)		K (%)	Th (ppm)	U (ppm)									
VC85 (5.10-5.30)	GL17076	5.20	125-180	19 ± 5	-	-	-	0.87 ± 0.12	1.96 ± 0.12	8.70 ± 0.54	1.91 ± 0.14	-	1.46 ± 0.17	0.09 ± 0.01	260	1.04 ± 0.02	1.06 ± 0.03	1.02 ± 0.02	1.08 ± 0.04	0.98 ± 0.02
VC85 (4.60-4.80)	GL17077	4.70	125-180	20 ± 5	-	-	-	0.78 ± 0.11	1.76 ± 0.11	7.80 ± 0.52	1.83 ± 0.14	-	1.31 ± 0.16	0.10 ± 0.01	240	1.02 ± 0.03	1.04 ± 0.03	1.01 ± 0.02	1.05 ± 0.04	0.94 ± 0.02
VC107 (1.00-1.25)	GL17078	1.08	90-125	20 ± 5	-	-	-	0.84 ± 0.12	1.75 ± 0.11	8.82 ± 0.56	2.06 ± 0.14	-	1.36 ± 0.17	0.17 ± 0.02	260	1.01 ± 0.03	1.03 ± 0.03	0.99 ± 0.03	1.02 ± 0.05	0.73 ± 0.02
VC79 (4.15-4.35)	GL17079	4.25	90-125	19 ± 5	-	-	-	0.87 ± 0.12	1.86 ± 0.12	9.14 ± 0.57	1.89 ± 0.14	-	1.44 ± 0.17	0.10 ± 0.01	240	1.05 ± 0.02	1.09 ± 0.03	1.03 ± 0.02	1.17 ± 0.07	0.99 ± 0.02
VC79 (0.75-1.00)	GL17080	0.90	90-125	19 ± 5	-	-	-	0.65 ± 0.10	1.49 ± 0.10	5.91 ± 0.46	1.56 ± 0.13	-	1.14 ± 0.14	0.18 ± 0.02	240	1.02 ± 0.02	1.04 ± 0.02	1.03 ± 0.02	1.07 ± 0.04	1.01 ± 0.02
VC74 (5.00-5.36)	GL17081	5.25	125-180	18 ± 4	-	-	-	0.62 ± 0.09	1.35 ± 0.09	5.64 ± 0.45	1.54 ± 0.13	-	1.04 ± 0.13	0.09 ± 0.01	240	1.01 ± 0.02	1.02 ± 0.02	1.01 ± 0.02	1.07 ± 0.04	0.99 ± 0.02
VC074 (3.70-4.00)	GL18023	3.85	90-125	19 ± 5	-	-	-	0.58 ± 0.09	1.33 ± 0.09	5.24 ± 0.43	1.42 ± 0.12	-	1.01 ± 0.13	0.11 ± 0.01	280	1.01 ± 0.01	1.01 ± 0.02	1.02 ± 0.01	1.04 ± 0.02	0.79 ± 0.01
VC107 (4.65-5.00)	GL18024	4.82	5-15	18 ± 4	-	-	-	1.00 ± 0.08	1.98 ± 0.12	10.30 ± 0.61	2.37 ± 0.15	0.43 ± 0.05	1.71 ± 0.16	0.10 ± 0.01	280	0.98 ± 0.02	0.98 ± 0.03	1.02 ± 0.02	1.09 ± 0.06	0.97 ± 0.02

Field Code	Lab Code	Total D <sub>r</sub> (Gy.ka <sup>-1</sup> )	D <sub>e</sub> (Gy)	Age (ka)
VC85 (5.10-5.30)	GL17076	2.43 ± 0.22	139.0 ± 8.7	57.2 ± 6.4 (5.7)
VC85 (4.60-4.80)	GL17077	2.19 ± 0.21	152.0 ± 8.7	69.5 ± 7.7 (6.9)
VC107 (1.00-1.25)	GL17078	2.37 ± 0.22	141.7 ± 6.6	59.8 ± 6.2 (5.5)
VC79 (4.15-4.35)	GL17079	2.42 ± 0.22	139.1 ± 6.3	57.6 ± 5.9 (5.1)
VC79 (0.75-1.00)	GL17080	1.96 ± 0.18	131.2 ± 7.4	66.8 ± 7.1 (6.3)
VC74 (5.00-5.36)	GL17081	1.75 ± 0.16	144.3 ± 7.3	82.4 ± 8.5 (7.5)
VC074 (3.70-4.00)	GL18023	1.70 ± 0.16	100.1 ± 6.2	58.9 ± 6.7 (6.0)
VC107 (4.65-5.00)	GL18024	3.24 ± 0.19	238.3 ± 12.0	73.6 ± 5.7 (4.8)

**Table 1** D<sub>r</sub>, D<sub>e</sub> and Age data of submitted samples located at c. 53°N, 2°E. Age estimates expressed relative to year of sampling. Uncertainties in age are quoted at 1σ confidence, are based on analytical errors and reflect combined systematic and experimental variability and (in parenthesis) experimental variability alone (see 6.0). **Blue** indicates samples with accepted age estimates, **red**, age estimates with caveats (see Table 2).

Generic considerations	Field Code	Lab Code	Sample specific considerations
Absence of <i>in situ</i> $\gamma$ spectrometry data (see section 4.0)	VC85 (5.10-5.30)	GL17076	None
	VC85 (4.60-4.80)	GL17077	None
	VC107 (1.00-1.25)	GL17078	Significant feldspar contamination (see section 3.1.1, Table 1 & Fig. 1) Accept as minimum age estimate
	VC79 (4.15-4.35)	GL17079	Overdispersed interpolated to applied regenerative-dose ratio (see section 3.1.4 and Table 1) Accept tentatively
	VC79 (0.75-1.00)	GL17080	Potentially significant U disequilibrium (see section 4.0 & Fig. 5) Accept tentatively
	VC74 (5.00-5.36)	GL17081	None
	VC074 (3.70-4.00)	GL18023	Significant feldspar contamination (see section 3.1.1, Table 1 & Fig. 1) Accept as minimum age estimate
	VC107 (4.65-5.00)	GL18024	None

**Table 2** Analytical validity of sample suite age estimates and caveats for consideration



## 1.0 Mechanisms and principles

Upon exposure to ionising radiation, electrons within the crystal lattice of insulating minerals are displaced from their atomic orbits. Whilst this dislocation is momentary for most electrons, a portion of charge is redistributed to meta-stable sites (traps) within the crystal lattice. In the absence of significant optical and thermal stimuli, this charge can be stored for extensive periods. The quantity of charge relocation and storage relates to the magnitude and period of irradiation. When the lattice is optically or thermally stimulated, charge is evicted from traps and may return to a vacant orbit position (hole). Upon recombination with a hole, an electron's energy can be dissipated in the form of light generating crystal luminescence providing a measure of dose absorption.

Herein, quartz is segregated for dating. The utility of this minerogenic dosimeter lies in the stability of its datable signal over the mid to late Quaternary period, predicted through isothermal decay studies (e.g. Smith *et al.*, 1990; retention lifetime 630 Ma at 20°C) and evidenced by optical age estimates concordant with independent chronological controls (e.g. Murray and Olley, 2002). This stability is in contrast to the anomalous fading of comparable signals commonly observed for other ubiquitous sedimentary minerals such as feldspar and zircon (Wintle, 1973; Templer, 1985; Spooner, 1993)

Optical age estimates of sedimentation (Huntley *et al.*, 1985) are premised upon reduction of the minerogenic time dependent signal (Optically Stimulated Luminescence, OSL) to zero through exposure to sunlight and, once buried, signal reformulation by absorption of litho- and cosmogenic radiation. The signal accumulated post burial acts as a dosimeter recording total dose absorption, converting to a chronometer by estimating the rate of dose absorption quantified through the assay of radioactivity in the surrounding lithology and streaming from the cosmos.

$$\text{Age} = \frac{\text{Mean Equivalent Dose (D}_e\text{, Gy)}}{\text{Mean Dose Rate (D}_r\text{, Gy.ka}^{-1}\text{)}}$$

Aitken (1998) and Bøtter-Jensen *et al.* (2003) offer a detailed review of optical dating.

## 2.0 Sample Preparation

Six sediment cores were submitted for Optical dating. To preclude optical erosion of the datable signal prior to measurement, all samples were opened and prepared under controlled laboratory illumination provided by Encapsulite RB-10 (red) filters. To isolate that material potentially exposed to daylight during sampling, sediment located within 10 mm of each core face was removed.

The remaining sample was dried and then sieved. The fine sand and fine silt fractions were segregated and subjected to acid and alkaline digestion (10% HCl, 15% H<sub>2</sub>O<sub>2</sub>) to attain removal of carbonate and organic components respectively.

For fine sand fractions, a further acid digestion in HF (40%, 60 mins) was used to etch the outer 10-15 µm layer affected by α radiation and degrade each samples' feldspar content. During HF treatment, continuous magnetic stirring was used to effect isotropic etching of grains. 10% HCl was then added to remove acid soluble fluorides. Each sample was dried, resieved and quartz isolated from the remaining heavy mineral fraction using a sodium polytungstate density separation at 2.68g.cm<sup>-3</sup>. Twelve 8 mm multi-grain aliquots (c. 3-6 mg) of quartz from each sample were then mounted on aluminium discs for determination of D<sub>e</sub> values.

Fine silt sized quartz, along with other mineral grains of varying density and size, was extracted by sample sedimentation in acetone (<15 µm in 2 min 20 s, >5 µm in 21 mins at 20°C). Feldspars and amorphous silica were then removed from

this fraction through acid digestion (35%  $\text{H}_2\text{SiF}_6$  for 2 weeks, Jackson *et al.*, 1976; Berger *et al.*, 1980). Following addition of 10% HCl to remove acid soluble fluorides, grains degraded to  $<5 \mu\text{m}$  as a result of acid treatment were removed by acetone sedimentation. Twelve multi-grain aliquots (ca. 1.5 mg) were then mounted on aluminium discs for  $D_e$  evaluation.

All drying was conducted at  $40^\circ\text{C}$  to prevent thermal erosion of the signal. All acids and alkalis were Analar grade. All dilutions (removing toxic-corrosive and non-minerogenic luminescence-bearing substances) were conducted with distilled water to prevent signal contamination by extraneous particles.

### 3.0 Acquisition and accuracy of $D_e$ value

All minerals naturally exhibit marked inter-sample variability in luminescence per unit dose (sensitivity). Therefore, the estimation of  $D_e$  acquired since burial requires calibration of the natural signal using known amounts of laboratory dose.  $D_e$  values were quantified using a single-aliquot regenerative-dose (SAR) protocol (Murray and Wintle 2000; 2003) facilitated by a Risø TL-DA-15 irradiation-stimulation-detection system (Markey *et al.*, 1997; Bøtter-Jensen *et al.*, 1999). Within this apparatus, optical signal stimulation is provided by an assembly of blue diodes (5 packs of 6 Nichia NSPB500S), filtered to  $470\pm 80 \text{ nm}$  conveying  $15 \text{ mW}\cdot\text{cm}^{-2}$  using a 3 mm Schott GG420 positioned in front of each diode pack. Infrared (IR) stimulation, provided by 6 IR diodes (Telefunken TSHA 6203) stimulating at  $875\pm 80 \text{ nm}$  delivering  $\sim 5 \text{ mW}\cdot\text{cm}^{-2}$ , was used to indicate the presence of contaminant feldspars (Hütt *et al.*, 1988). Stimulated photon emissions from quartz aliquots are in the ultraviolet (UV) range and were filtered from stimulating photons by 7.5 mm HOYA U-340 glass and detected by an EMI 9235QA photomultiplier fitted with a blue-green sensitive bialkali photocathode. Aliquot irradiation was conducted using a  $1.48 \text{ GBq } ^{90}\text{Sr}/^{90}\text{Y}$   $\beta$  source calibrated for multi-grain aliquots of  $5\text{-}15 \mu\text{m}$ ,  $90\text{-}125 \mu\text{m}$  and  $125\text{-}180 \mu\text{m}$  quartz against the 'Hotspot 800'  $^{60}\text{Co}$   $\gamma$  source located at the National Physical Laboratory (NPL), UK.

SAR by definition evaluates  $D_e$  through measuring the natural signal (Fig. 1) of a single aliquot and then regenerating that aliquot's signal by using known laboratory doses to enable calibration. For each aliquot, five different regenerative-doses were administered so as to image dose response.  $D_e$  values for each aliquot were then interpolated, and associated counting and fitting errors calculated, by way of exponential plus linear regression (Fig. 1). Weighted (geometric) mean  $D_e$  values were calculated from 12 aliquots using the central age model outlined by Galbraith *et al.* (1999) and are quoted at  $1\sigma$  confidence (Table 1). The accuracy with which  $D_e$  equates to total absorbed dose and that dose absorbed since burial was assessed. The former can be considered a function of laboratory factors, the latter, one of environmental issues. Diagnostics were deployed to estimate the influence of these factors and criteria instituted to optimise the accuracy of  $D_e$  values.

### 3.1 Laboratory Factors

#### 3.1.1 Feldspar contamination

The propensity of feldspar signals to fade and underestimate age, coupled with their higher sensitivity relative to quartz makes it imperative to quantify feldspar contamination. At room temperature, feldspars generate a signal (IRSL; Fig. 1) upon exposure to IR whereas quartz does not. The signal from feldspars contributing to OSL can be depleted by prior exposure to IR. For all aliquots the contribution of any remaining feldspars was estimated from the OSL IR depletion ratio (Duller, 2003). The influence of IR depletion on the OSL signal can be illustrated by comparing the regenerated post-IR OSL  $D_e$  with the applied regenerative-dose. If the addition to OSL by feldspars is insignificant, then the repeat dose ratio of OSL to post-IR OSL should be statistically consistent with unity (Table 1). If any aliquots do not fulfil this criterion, then the sample age estimate should be accepted tentatively. The source of feldspar contamination is rarely rooted in sample preparation; it predominantly results from the occurrence of feldspars as inclusions within quartz.

### 3.1.2 Preheating

Preheating aliquots between irradiation and optical stimulation is necessary to ensure comparability between natural and laboratory-induced signals. However, the multiple irradiation and preheating steps that are required to define single-aliquot regenerative-dose response leads to signal sensitisation, rendering calibration of the natural signal inaccurate. The SAR protocol (Murray and Wintle, 2000; 2003) enables this sensitisation to be monitored and corrected using a test dose, here set at 5 Gy preheated to 220°C for 10s, to track signal sensitivity between irradiation-preheat steps. However, the accuracy of sensitisation correction for both natural and laboratory signals can be preheat dependent.

The Dose Recovery test was used to assess the optimal preheat temperature for accurate correction and calibration of the time dependent signal. Dose Recovery (Fig. 2) attempts to quantify the combined effects of thermal transfer and sensitisation on the natural signal, using a precise lab dose to simulate natural dose. The ratio between the applied dose and recovered  $D_e$  value should be statistically concordant with unity. For this diagnostic, 6 aliquots were each assigned a 10 s preheat between 180°C and 280°C.

That preheat treatment fulfilling the criterion of accuracy within the Dose Recovery test was selected to generate the final  $D_e$  value from a further 12 aliquots. Further thermal treatments, prescribed by Murray and Wintle (2000; 2003), were applied to optimise accuracy and precision. Optical stimulation occurred at 125°C in order to minimise effects associated with photo-transferred thermoluminescence and maximise signal to noise ratios. Inter-cycle optical stimulation was conducted at 280°C to minimise recuperation.

### 3.1.3 Irradiation

For all samples having  $D_e$  values in excess of 100 Gy, matters of signal saturation and laboratory irradiation effects are of concern. With regards the former, the rate of signal accumulation generally adheres to a saturating exponential form and it is this that limits the precision and accuracy of  $D_e$  values for samples having absorbed large doses. For such samples, the functional range of  $D_e$  interpolation by SAR has been verified up to 600 Gy by Pawley *et al.* (2010). Age estimates based on  $D_e$  values exceeding this value should be accepted tentatively.

### 3.1.4 Internal consistency

Abanico plots (Dietze *et al.*, 2016) are used to illustrate inter-aliquot  $D_e$  variability (Fig. 3).  $D_e$  values are standardised relative to the central  $D_e$  value for natural signals and are described as overdispersed when >5% lie beyond  $\pm 2\sigma$  of the standardising value; resulting from a heterogeneous absorption of burial dose and/or response to the SAR protocol. For multi-grain aliquots, overdispersion of natural signals does not necessarily imply inaccuracy. However where overdispersion is observed for regenerated signals, the efficacy of sensitivity correction may be problematic. Murray and Wintle (2000; 2003) suggest repeat dose ratios (Table 1) offer a measure of SAR protocol success, whereby ratios ranging across 0.9-1.1 are acceptable. However, this variation of repeat dose ratios in the high-dose region can have a significant impact on  $D_e$  interpolation. The influence of this effect can be outlined by quantifying the ratio of interpolated to applied regenerative-dose ratio (Table 1). In this study, where both the repeat dose ratios and interpolated to applied regenerative-dose ratios range across 0.9-1.1, sensitivity-correction is considered effective.

## 3.2 Environmental factors

### 3.2.1 Incomplete zeroing

Post-burial OSL signals residual of pre-burial dose absorption can result where pre-burial sunlight exposure is limited in spectrum, intensity and/or period, leading to age overestimation. This effect is particularly acute for material eroded and redeposited sub-aqueously (Olley *et al.*, 1998, 1999; Wallinga, 2002) and exposed to a burial dose of <20 Gy (e.g. Olley *et al.*, 2004), has some influence in sub-aerial contexts but is rarely of consequence where aerial transport has occurred.

Within single-aliquot regenerative-dose optical dating there are two diagnostics of partial resetting (or bleaching); signal analysis (Agersnap-Larsen *et al.*, 2000; Bailey *et al.*, 2003) and inter-aliquot  $D_e$  distribution studies (Murray *et al.*, 1995).

Within this study, signal analysis was used to quantify the change in  $D_e$  value with respect to optical stimulation time for multi-grain aliquots. This exploits the existence of traps within minerogenic dosimeters that bleach with different efficiency for a given wavelength of light to verify partial bleaching.  $D_e(t)$  plots (Fig. 4; Bailey *et al.*, 2003) are constructed from separate integrals of signal decay as laboratory optical stimulation progresses. A statistically significant increase in natural  $D_e(t)$  is indicative of partial bleaching assuming three conditions are fulfilled. Firstly, that a statistically significant increase in  $D_e(t)$  is observed when partial bleaching is simulated within the laboratory. Secondly, that there is no significant rise in  $D_e(t)$  when full bleaching is simulated. Finally, there should be no significant augmentation in  $D_e(t)$  when zero dose is simulated. Where partial bleaching is detected, the age derived from the sample should be considered a maximum estimate only. However, the utility of signal analysis is strongly dependent upon a samples pre-burial experience of sunlight's spectrum and its residual to post-burial signal ratio. Given in the majority of cases, the spectral exposure history of a deposit is uncertain, the absence of an increase in natural  $D_e(t)$  does not necessarily testify to the absence of partial bleaching.

Where requested and feasible, the insensitivities of multi-grain single-aliquot signal analysis may be circumvented by inter-aliquot  $D_e$  distribution studies. This analysis uses aliquots of single sand grains to quantify inter-grain  $D_e$  distribution. At present, it is contended that asymmetric inter-grain  $D_e$  distributions are symptomatic of partial bleaching and/or pedoturbation (Murray *et al.*, 1995; Olley *et al.*, 1999; Olley *et al.*, 2004; Bateman *et al.*, 2003). For partial bleaching at least, it is further contended that the  $D_e$  acquired during burial is located in the minimum region of such ranges. The mean and breadth of this minimum region is the subject of current debate, as it is additionally influenced by heterogeneity in microdosimetry, variable inter-grain response to SAR and residual to post-burial signal ratios.

### 3.2.2 Turbation

As noted in section 3.1.1, the accuracy of sedimentation ages can further be controlled by post-burial trans-strata grain movements forced by pedo- or cryoturbation. Berger (2003) contends pedogenesis prompts a reduction in the apparent sedimentation age of parent material through bioturbation and illuviation of younger material from above and/or by biological recycling and resetting of the datable signal of surface material. Berger (2003) proposes that the chronological products of this remobilisation are A-horizon age estimates reflecting the cessation of pedogenic activity, Bc/C-horizon ages delimiting the maximum age for the initiation of pedogenesis with estimates obtained from Bt-horizons providing an intermediate age 'close to the age of cessation of soil development'. Singhvi *et al.* (2001), in contrast, suggest that B and C-horizons closely approximate the age of the parent material, the A-horizon, that of the 'soil forming episode'. Recent analyses of inter-aliquot  $D_e$  distributions have reinforced this complexity of interpreting burial age from pedoturbated deposits (Lombard *et al.*, 2011; Gliganic *et al.*, 2015; Jacobs *et al.*, 2008; Bateman *et al.*, 2007; Gliganic *et al.*, 2016). At present there is no definitive post-sampling mechanism for the direct detection of and correction for post-burial sediment remobilisation. However, intervals of palaeosol evolution can be delimited by a maximum age derived from parent material and a minimum age obtained from a unit overlying the palaeosol. Inaccuracy forced by cryoturbation may be bidirectional, heaving older material upwards or drawing younger material downwards into the level to be dated. Cryogenic deformation of matrix-supported material is, typically, visible; sampling of such cryogenically-disturbed sediments can be avoided.

## 4.0 Acquisition and accuracy of $D_r$ value

Lithogenic  $D_r$  values were defined through measurement of U, Th and K radionuclide concentration and conversion of these quantities into  $\alpha$ ,  $\beta$  and  $\gamma$   $D_r$  values (Table 1).  $\alpha$  and  $\beta$  contributions were estimated from sub-samples by

laboratory-based  $\gamma$  spectrometry using an Ortec GEM-S high purity Ge coaxial detector system, calibrated using certified reference materials supplied by CANMET.  $\gamma$  dose rates can be estimated from *in situ* NaI gamma spectrometry or, where direct measurements are unavailable as in the present case, from laboratory-based Ge  $\gamma$  spectrometry. *In situ* measurements reduce uncertainty relating to potential heterogeneity in the  $\gamma$  dose field surrounding each sample. The level of U disequilibrium was estimated by laboratory-based Ge  $\gamma$  spectrometry. Estimates of radionuclide concentration were converted into  $D_r$  values (Adamiec and Aitken, 1998), accounting for  $D_r$  modulation forced by grain size (Mejdahl, 1979), present moisture content (Zimmerman, 1971) and, where  $D_e$  values were generated from 5-15  $\mu\text{m}$  quartz, reduced signal sensitivity to  $\alpha$  radiation (a-value  $0.050 \pm 0.002$ ). Cosmogenic  $D_r$  values were calculated on the basis of sample depth, geographical position and matrix density (Prescott and Hutton, 1994).

The spatiotemporal validity of  $D_r$  values can be considered a function of five variables. Firstly, age estimates devoid of *in situ*  $\gamma$  spectrometry data should be accepted tentatively if the sampled unit is heterogeneous in texture or if the sample is located within 300 mm of strata consisting of differing texture and/or mineralogy. However, where samples are obtained throughout a vertical profile, consistent values of  $\gamma$   $D_r$  based solely on laboratory measurements may evidence the homogeneity of the  $\gamma$  field and hence accuracy of  $\gamma$   $D_r$  values. Secondly, disequilibrium can force temporal instability in U and Th emissions. The impact of this infrequent phenomenon (Olley *et al.*, 1996) upon age estimates is usually insignificant given their associated margins of error. However, for samples where this effect is pronounced (>50% disequilibrium between  $^{238}\text{U}$  and  $^{226}\text{Ra}$ ; Fig. 5), the resulting age estimates should be accepted tentatively. Thirdly, pedogenically-induced variations in matrix composition of B and C-horizons, such as radionuclide and/or mineral remobilisation, may alter the rate of energy emission and/or absorption. If  $D_r$  is invariant through a dated profile and samples encompass primary parent material, then element mobility is likely limited in effect. Fourthly, spatiotemporal detractors from present moisture content are difficult to assess directly, requiring knowledge of the magnitude and timing of differing contents. However, the maximum influence of moisture content variations can be delimited by recalculating  $D_r$  for minimum (zero) and maximum (saturation) content. Finally, temporal alteration in the thickness of overburden alters cosmic  $D_r$  values. Cosmic  $D_r$  often forms a negligible portion of total  $D_r$ . It is possible to quantify the maximum influence of overburden flux by recalculating  $D_r$  for minimum (zero) and maximum (surface sample) cosmic  $D_r$ .

## 5.0 Estimation of Age

Ages reported in Table 1 provide an estimate of sediment burial period based on mean  $D_e$  and  $D_r$  values and their associated analytical uncertainties. Uncertainty in age estimates is reported as a product of systematic and experimental errors, with the magnitude of experimental errors alone shown in parenthesis (Table 1). Cumulative frequency plots indicate the inter-aliquot variability in age (Fig. 6). The maximum influence of temporal variations in  $D_r$  forced by minima-maxima in moisture content and overburden thickness is also illustrated in Fig. 6. Where uncertainty in these parameters exists this age range may prove instructive, however the combined extremes represented should not be construed as preferred age estimates. The analytical validity of each sample is presented in Table 2.

## 6.0 Analytical uncertainty

All errors are based upon analytical uncertainty and quoted at  $1\sigma$  confidence. Error calculations account for the propagation of systematic and/or experimental (random) errors associated with  $D_e$  and  $D_r$  values.

For  $D_e$  values, systematic errors are confined to laboratory  $\beta$  source calibration. Uncertainty in this respect is that combined from the delivery of the calibrating  $\gamma$  dose (1.2%; NPL, pers. comm.), the conversion of this dose for  $\text{SiO}_2$  using the respective mass energy-absorption coefficient (2%; Hubbell, 1982) and experimental error, totalling 3.5%. Mass

attenuation and bremsstrahlung losses during  $\gamma$  dose delivery are considered negligible. Experimental errors relate to  $D_e$  interpolation using sensitisation corrected dose responses. Natural and regenerated sensitisation corrected dose points ( $S_i$ ) were quantified by,

$$S_i = (D_i - x.L_i) / (d_i - x.L_i) \quad \text{Eq.1}$$

where  $D_i$  = Natural or regenerated OSL, initial 0.2 s  
 $L_i$  = Background natural or regenerated OSL, final 5 s  
 $d_i$  = Test dose OSL, initial 0.2 s  
 $x$  = Scaling factor, 0.08

The error on each signal parameter is based on counting statistics, reflected by the square-root of measured values. The propagation of these errors within Eq. 1 generating  $\sigma S_i$  follows the general formula given in Eq. 2.  $\sigma S_i$  were then used to define fitting and interpolation errors within exponential plus linear regressions.

For  $D_r$  values, systematic errors accommodate uncertainty in radionuclide conversion factors (5%),  $\beta$  attenuation coefficients (5%),  $a$ -value (4%; derived from a systematic  $\alpha$  source uncertainty of 3.5% and experimental error), matrix density ( $0.20 \text{ g.cm}^{-3}$ ), vertical thickness of sampled section (specific to sample collection device), saturation moisture content (3%), moisture content attenuation (2%) and burial moisture content (25% relative, unless direct evidence exists of the magnitude and period of differing content). Experimental errors are associated with radionuclide quantification for each sample by Ge gamma spectrometry.

The propagation of these errors through to age calculation was quantified using the expression,

$$\sigma y (\delta y / \delta x) = (\sum ((\delta y / \delta x_n) \cdot \sigma x_n)^2)^{1/2} \quad \text{Eq. 2}$$

where  $y$  is a value equivalent to that function comprising terms  $x_n$  and where  $\sigma y$  and  $\sigma x_n$  are associated uncertainties.

Errors on age estimates are presented as combined systematic and experimental errors and experimental errors alone. The former (combined) error should be considered when comparing luminescence ages herein with independent chronometric controls. The latter assumes systematic errors are common to luminescence age estimates generated by means identical to those detailed herein and enable direct comparison with those estimates.

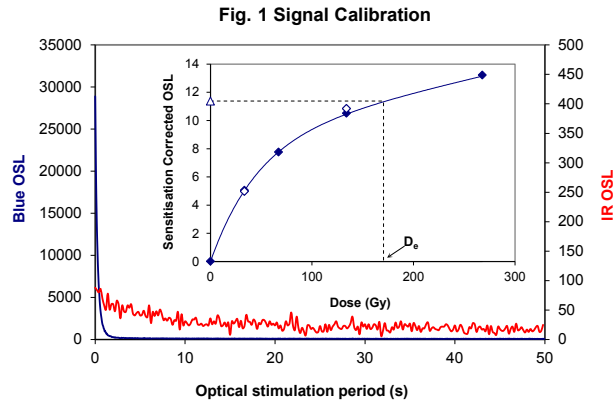


Fig. 1 Signal Calibration

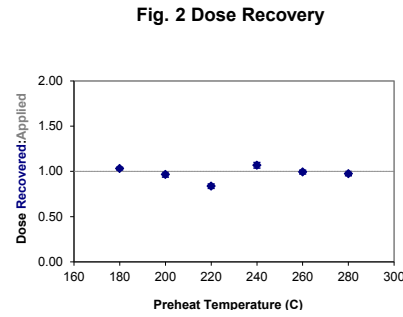


Fig. 2 Dose Recovery

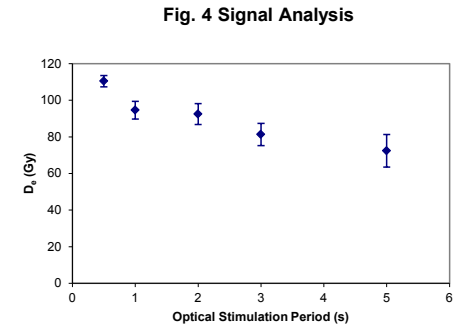
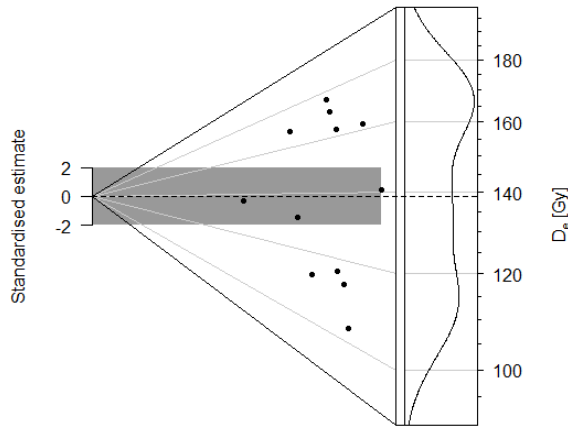


Fig. 4 Signal Analysis

Fig. 3 Inter-aliquot De distribution



**Fig. 1 Signal Calibration** Natural blue and laboratory-induced infrared (IR) OSL signals. Detectable IR signal decays are diagnostic of feldspar contamination. Inset, the natural blue OSL signal (open triangle) of each aliquot is calibrated against known laboratory doses to yield equivalent dose ( $D_e$ ) values. Repeats of low and high doses (open diamonds) illustrate the success of sensitivity correction.

**Fig. 2 Dose Recovery** The acquisition of  $D_e$  values is necessarily predicated upon thermal treatment of aliquots succeeding environmental and laboratory irradiation. The Dose Recovery test quantifies the combined effects of thermal transfer and sensitisation on the natural signal using a precise lab dose to simulate natural dose. Based on this an appropriate thermal treatment is selected to generate the final  $D_e$  value.

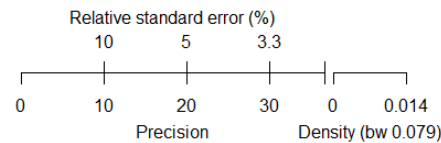
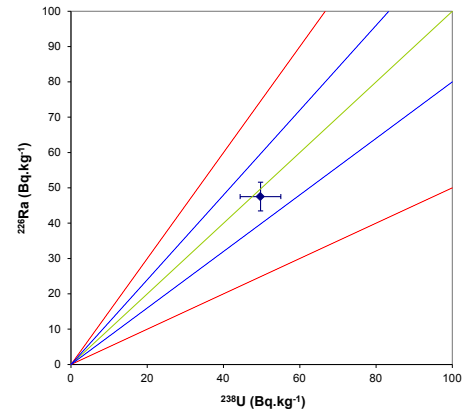
**Fig. 3 Inter-aliquot  $D_e$  distribution** Abanico plot of inter-aliquot statistical concordance in  $D_e$  values derived from natural irradiation. Discordant data (those points lying beyond  $\pm 2$  standardised ln  $D_e$ ) reflect heterogeneous dose absorption and/or inaccuracies in calibration.

**Fig. 4 Signal Analysis** Statistically significant increase in natural  $D_e$  value with signal stimulation period is indicative of a partially-bleached signal, provided a significant increase in  $D_e$  results from simulated partial bleaching followed by insignificant adjustment in  $D_e$  for simulated zero and full bleach conditions. Ages from such samples are considered maximum estimates. In the absence of a significant rise in  $D_e$  with stimulation time, simulated partial bleaching and zero/full bleach tests are not assessed.

**Fig. 5 U Activity** Statistical concordance (equilibrium) in the activities of the daughter radioisotope  $^{226}\text{Ra}$  with its parent  $^{238}\text{U}$  may signify the temporal stability of  $D_e$  emissions from these chains. Significant differences (disequilibrium;  $>50\%$ ) in activity indicate addition or removal of isotopes creating a time-dependent shift in  $D_e$  values and increased uncertainty in the accuracy of age estimates. A 20% disequilibrium marker is also shown.

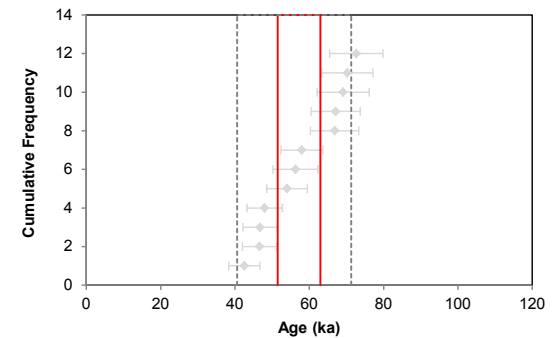
**Fig. 6 Age Range** The Cumulative frequency plot indicates the inter-aliquot variability in age. It also shows the mean age range: an estimate of sediment burial period based on mean  $D_e$  and  $D_e$  values with associated analytical uncertainties. The maximum influence of temporal variations in  $D_e$  forced by minima-maxima variation in moisture content and overburden thickness is outlined and may prove instructive where there is uncertainty in these parameters. However the combined extremes represented should not be construed as preferred age estimates.

Fig. 5 U Decay Activity



Sample: GL17076

Fig. 6 Age Range





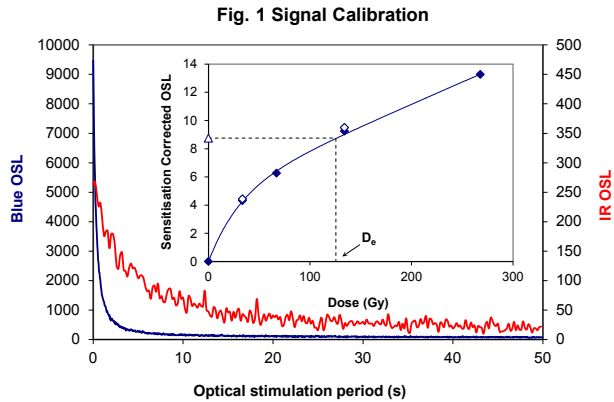


Fig. 1 Signal Calibration

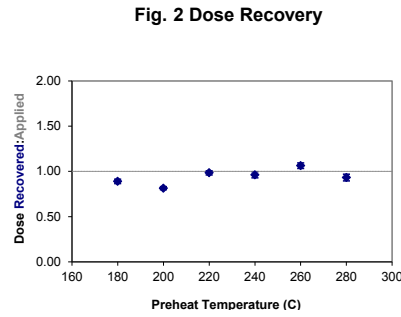
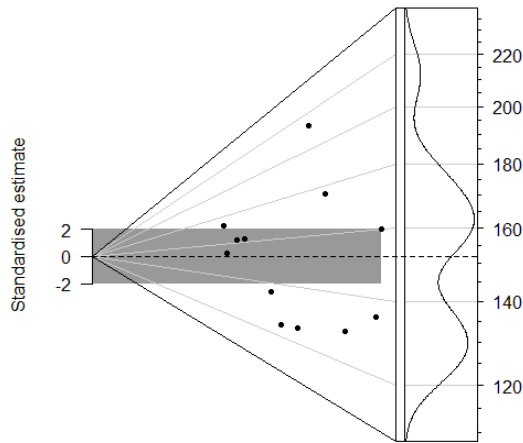


Fig. 2 Dose Recovery

Fig. 3 Inter-aliquot D<sub>0</sub> distribution



**Fig. 1 Signal Calibration** Natural blue and laboratory-induced infrared (IR) OSL signals. Detectable IR signal decays are diagnostic of feldspar contamination. Inset, the natural blue OSL signal (open triangle) of each aliquot is calibrated against known laboratory doses to yield equivalent dose ( $D_0$ ) values. Repeats of low and high doses (open diamonds) illustrate the success of sensitivity correction.

**Fig. 2 Dose Recovery** The acquisition of  $D_0$  values is necessarily predicated upon thermal treatment of aliquots succeeding environmental and laboratory irradiation. The Dose Recovery test quantifies the combined effects of thermal transfer and sensitisation on the natural signal using a precise lab dose to simulate natural dose. Based on this an appropriate thermal treatment is selected to generate the final  $D_0$  value.

**Fig. 3 Inter-aliquot  $D_0$  distribution** Abanico plot of inter-aliquot statistical concordance in  $D_0$  values derived from natural irradiation. Discordant data (those points lying beyond  $\pm 2$  standardised  $\ln D_0$ ) reflect heterogeneous dose absorption and/or inaccuracies in calibration.

**Fig. 4 Signal Analysis** Statistically significant increase in natural  $D_0$  value with signal stimulation period is indicative of a partially-bleached signal, provided a significant increase in  $D_0$  results from simulated partial bleaching followed by insignificant adjustment in  $D_0$  for simulated zero and full bleach conditions. Ages from such samples are considered maximum estimates. In the absence of a significant rise in  $D_0$  with stimulation time, simulated partial bleaching and zero/full bleach tests are not assessed.

**Fig. 5 U Activity** Statistical concordance (equilibrium) in the activities of the daughter radioisotope  $^{226}\text{Ra}$  with its parent  $^{238}\text{U}$  may signify the temporal stability of  $D_0$  emissions from these chains. Significant differences (disequilibrium;  $>50\%$ ) in activity indicate addition or removal of isotopes creating a time-dependent shift in  $D_0$  values and increased uncertainty in the accuracy of age estimates. A 20% disequilibrium marker is also shown.

**Fig. 6 Age Range** The Cumulative frequency plot indicates the inter-aliquot variability in age. It also shows the mean age range: an estimate of sediment burial period based on mean  $D_0$  and  $D_0$  values with associated analytical uncertainties. The maximum influence of temporal variations in  $D_0$  forced by minima-maxima variation in moisture content and overburden thickness is outlined and may prove instructive where there is uncertainty in these parameters. However the combined extremes represented should not be construed as preferred age estimates.

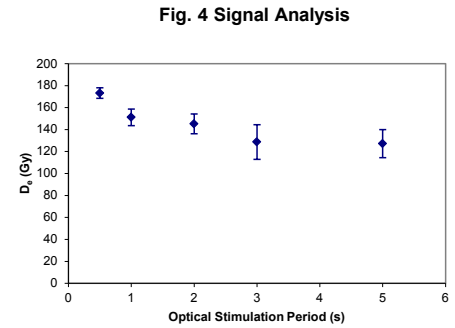


Fig. 4 Signal Analysis

Fig. 5 U Decay Activity

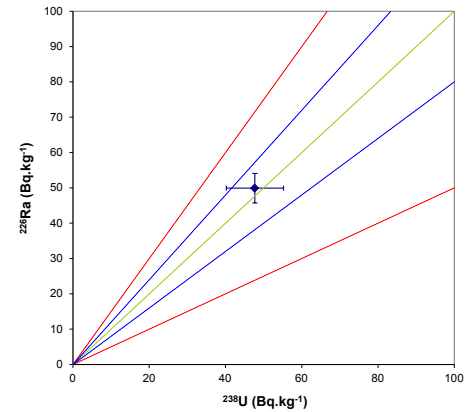
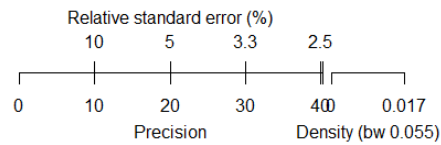
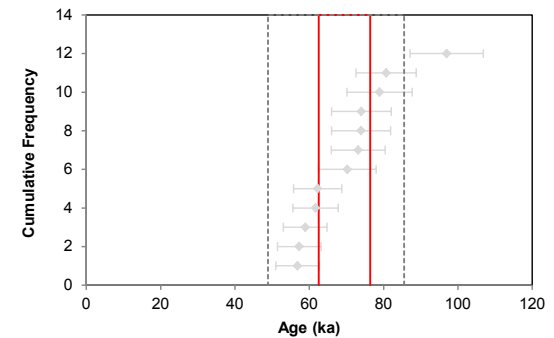
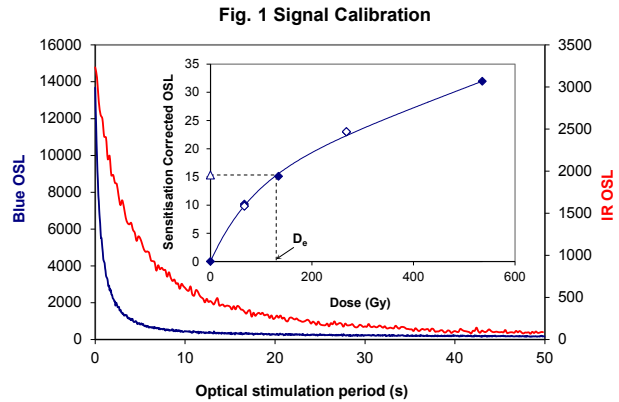


Fig. 6 Age Range



Sample: GL17077



**Fig. 1 Signal Calibration**

**Fig. 1 Signal Calibration** Natural blue and laboratory-induced infrared (IR) OSL signals. Detectable IR signal decays are diagnostic of feldspar contamination. Inset, the natural blue OSL signal (open triangle) of each aliquot is calibrated against known laboratory doses to yield equivalent dose ( $D_e$ ) values. Repeats of low and high doses (open diamonds) illustrate the success of sensitivity correction.

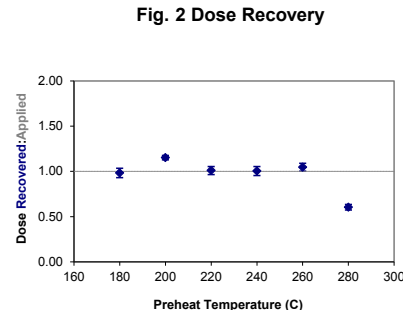


**Fig. 2 Dose Recovery**

**Fig. 2 Dose Recovery** The acquisition of  $D_e$  values is necessarily predicated upon thermal treatment of aliquots succeeding environmental and laboratory irradiation. The Dose Recovery test quantifies the combined effects of thermal transfer and sensitisation on the natural signal using a precise lab dose to simulate natural dose. Based on this an appropriate thermal treatment is selected to generate the final  $D_e$  value.

**Fig. 3 Inter-aliquot  $D_e$  distribution**

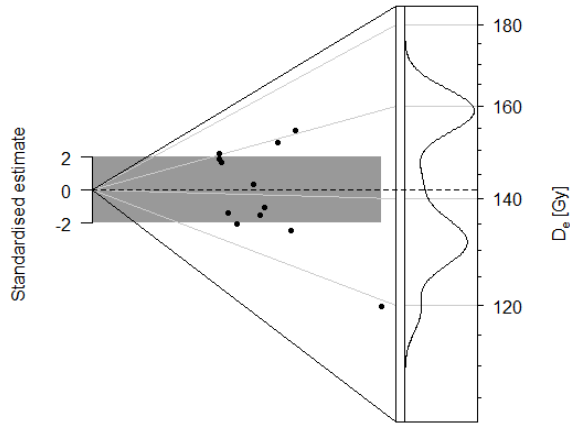


**Fig. 3 Inter-aliquot  $D_e$  distribution** Abanico plot of inter-aliquot statistical concordance in  $D_e$  values derived from natural irradiation. Discordant data (those points lying beyond  $\pm 2$  standardised  $\ln D_e$ ) reflect heterogeneous dose absorption and/or inaccuracies in calibration.

**Fig. 4 Signal Analysis** Statistically significant increase in natural  $D_e$  value with signal stimulation period is indicative of a partially-bleached signal, provided a significant increase in  $D_e$  results from simulated partial bleaching followed by insignificant adjustment in  $D_e$  for simulated zero and full bleach conditions. Ages from such samples are considered maximum estimates. In the absence of a significant rise in  $D_e$  with stimulation time, simulated partial bleaching and zero/full bleach tests are not assessed.

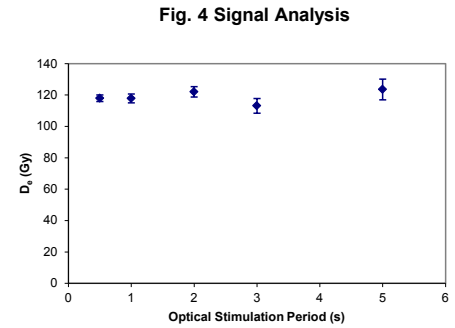


**Fig. 4 Signal Analysis**

**Fig. 5 U Activity** Statistical concordance (equilibrium) in the activities of the daughter radioisotope  $^{226}\text{Ra}$  with its parent  $^{238}\text{U}$  may signify the temporal stability of  $D_e$  emissions from these chains. Significant differences (disequilibrium;  $>50\%$ ) in activity indicate addition or removal of isotopes creating a time-dependent shift in  $D_e$  values and increased uncertainty in the accuracy of age estimates. A 20% disequilibrium marker is also shown.

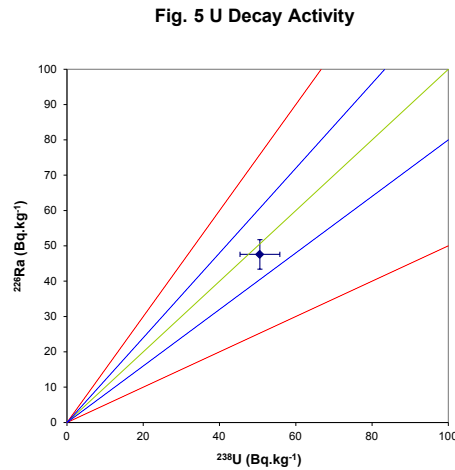
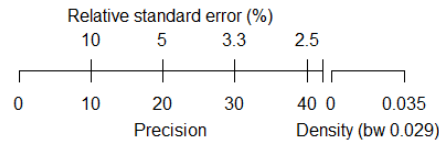


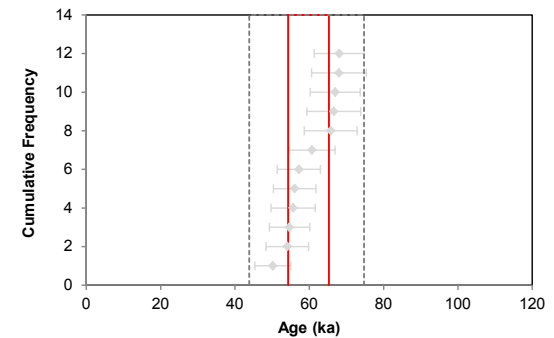
**Fig. 5 U Decay Activity**

**Fig. 6 Age Range** The Cumulative frequency plot indicates the inter-aliquot variability in age. It also shows the mean age range: an estimate of sediment burial period based on mean  $D_e$  and  $D_e$  values with associated analytical uncertainties. The maximum influence of temporal variations in  $D_e$  forced by minima-maxima variation in moisture content and overburden thickness is outlined and may prove instructive where there is uncertainty in these parameters. However the combined extremes represented should not be construed as preferred age estimates.



**Sample: GL17078**

**Fig. 6 Age Range**



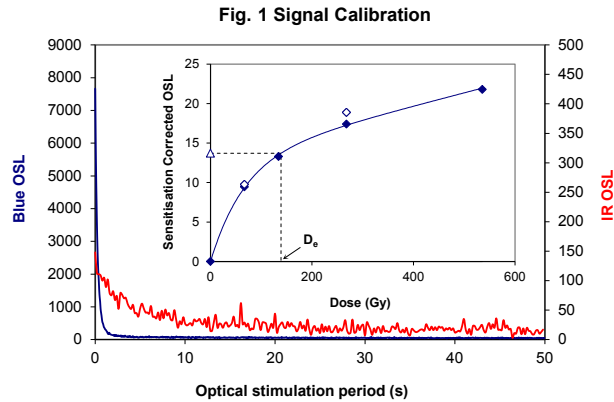


**Fig. 1 Signal Calibration** Natural blue and laboratory-induced infrared (IR) OSL signals. Detectable IR signal decays are diagnostic of feldspar contamination. Inset, the natural blue OSL signal (open triangle) of each aliquot is calibrated against known laboratory doses to yield equivalent dose ( $D_e$ ) values. Repeats of low and high doses (open diamonds) illustrate the success of sensitivity correction.

**Fig. 2 Dose Recovery** The acquisition of  $D_e$  values is necessarily predicated upon thermal treatment of aliquots succeeding environmental and laboratory irradiation. The Dose Recovery test quantifies the combined effects of thermal transfer and sensitisation on the natural signal using a precise lab dose to simulate natural dose. Based on this an appropriate thermal treatment is selected to generate the final  $D_e$  value.

**Fig. 3 Inter-aliquot  $D_e$  distribution** Abanico plot of inter-aliquot statistical concordance in  $D_e$  values derived from natural irradiation. Discordant data (those points lying beyond  $\pm 2$  standardised  $\ln D_e$ ) reflect heterogeneous dose absorption and/or inaccuracies in calibration.

**Fig. 4 Signal Analysis** Statistically significant increase in natural  $D_e$  value with signal stimulation period is indicative of a partially-bleached signal, provided a significant increase in  $D_e$  results from simulated partial bleaching followed by insignificant adjustment in  $D_e$  for simulated zero and full bleach conditions. Ages from such samples are considered maximum estimates. In the absence of a significant rise in  $D_e$  with stimulation time, simulated partial bleaching and zero/full bleach tests are not assessed.

**Fig. 5 U Activity** Statistical concordance (equilibrium) in the activities of the daughter radioisotope  $^{226}\text{Ra}$  with its parent  $^{238}\text{U}$  may signify the temporal stability of  $D_e$  emissions from these chains. Significant differences (disequilibrium;  $>50\%$ ) in activity indicate addition or removal of isotopes creating a time-dependent shift in  $D_e$  values and increased uncertainty in the accuracy of age estimates. A 20% disequilibrium marker is also shown.

**Fig. 6 Age Range** The Cumulative frequency plot indicates the inter-aliquot variability in age. It also shows the mean age range: an estimate of sediment burial period based on mean  $D_e$  and  $D_e$  values with associated analytical uncertainties. The maximum influence of temporal variations in  $D_e$  forced by minima-maxima variation in moisture content and overburden thickness is outlined and may prove instructive where there is uncertainty in these parameters. However the combined extremes represented should not be construed as preferred age estimates.

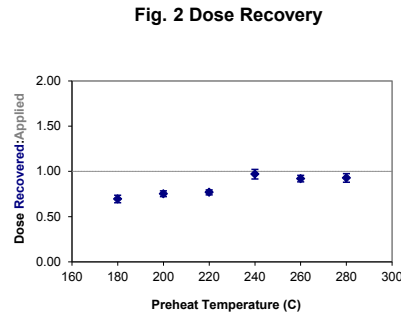
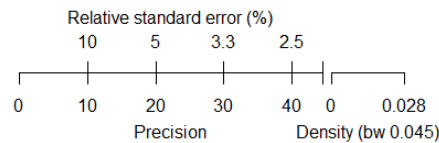
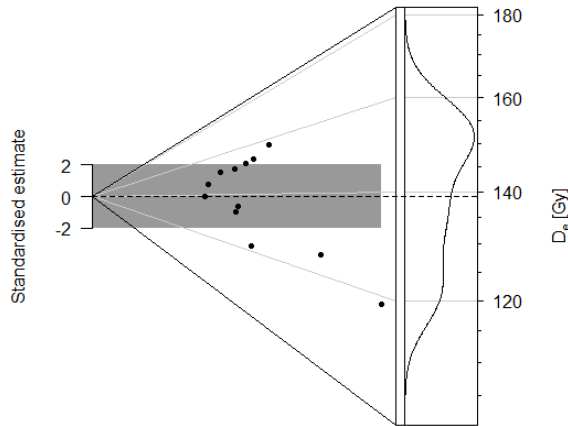
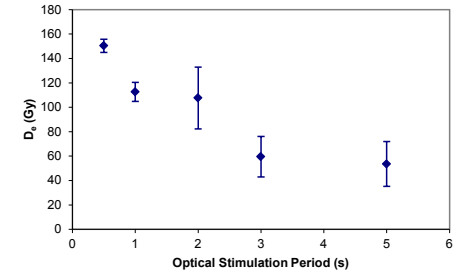


**Fig. 3 Inter-aliquot  $D_e$  distribution**

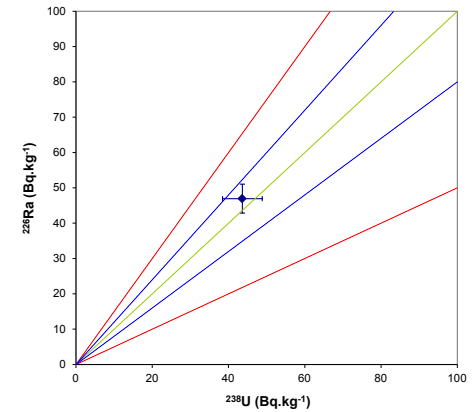


Sample: GL17079

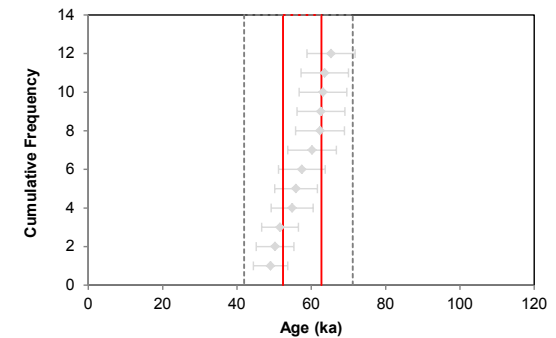
**Fig. 4 Signal Analysis**



**Fig. 5 U Decay Activity**



**Fig. 6 Age Range**



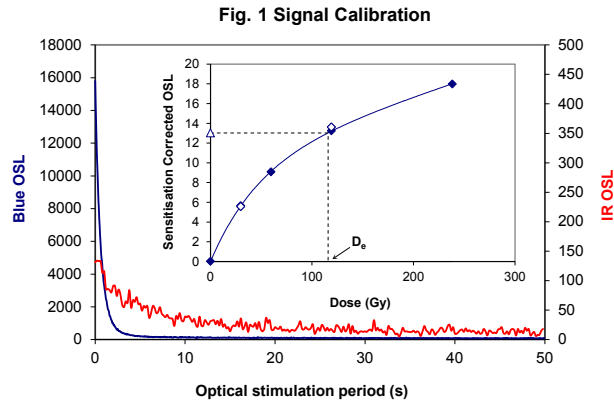


Fig. 1 Signal Calibration

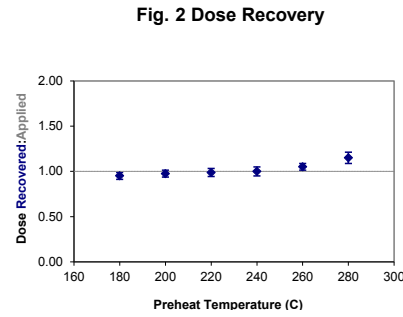


Fig. 2 Dose Recovery

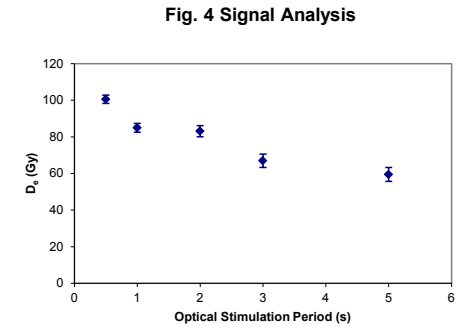


Fig. 4 Signal Analysis

Fig. 3 Inter-aliquot  $D_e$  distribution

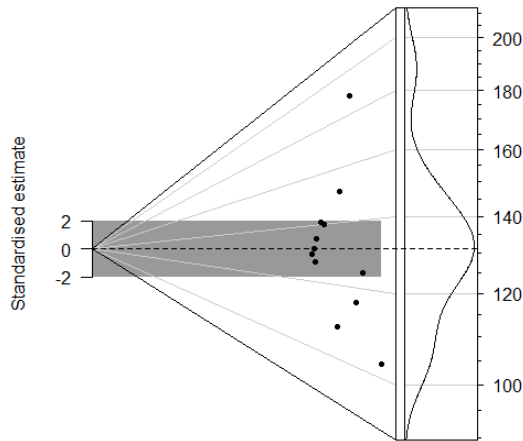


Fig. 1 Signal Calibration Natural blue and laboratory-induced infrared (IR) OSL signals. Detectable IR signal decays are diagnostic of feldspar contamination. Inset, the natural blue OSL signal (open triangle) of each aliquot is calibrated against known laboratory doses to yield equivalent dose ( $D_e$ ) values. Repeats of low and high doses (open diamonds) illustrate the success of sensitivity correction.

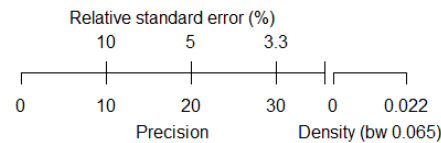
Fig. 2 Dose Recovery The acquisition of  $D_e$  values is necessarily predicated upon thermal treatment of aliquots succeeding environmental and laboratory irradiation. The Dose Recovery test quantifies the combined effects of thermal transfer and sensitisation on the natural signal using a precise lab dose to simulate natural dose. Based on this an appropriate thermal treatment is selected to generate the final  $D_e$  value.

Fig. 3 Inter-aliquot  $D_e$  distribution Abanico plot of inter-aliquot statistical concordance in  $D_e$  values derived from natural irradiation. Discordant data (those points lying beyond  $\pm 2$  standardised  $\ln D_e$ ) reflect heterogeneous dose absorption and/or inaccuracies in calibration.

Fig. 4 Signal Analysis Statistically significant increase in natural  $D_e$  value with signal stimulation period is indicative of a partially-bleached signal, provided a significant increase in  $D_e$  results from simulated partial bleaching followed by insignificant adjustment in  $D_e$  for simulated zero and full bleach conditions. Ages from such samples are considered maximum estimates. In the absence of a significant rise in  $D_e$  with stimulation time, simulated partial bleaching and zero/full bleach tests are not assessed.

Fig. 5 U Activity Statistical concordance (equilibrium) in the activities of the daughter radioisotope  $^{226}\text{Ra}$  with its parent  $^{238}\text{U}$  may signify the temporal stability of  $D_e$  emissions from these chains. Significant differences (disequilibrium;  $>50\%$ ) in activity indicate addition or removal of isotopes creating a time-dependent shift in  $D_e$  values and increased uncertainty in the accuracy of age estimates. A 20% disequilibrium marker is also shown.

Fig. 6 Age Range The Cumulative frequency plot indicates the inter-aliquot variability in age. It also shows the mean age range: an estimate of sediment burial period based on mean  $D_e$  and  $D_e$  values with associated analytical uncertainties. The maximum influence of temporal variations in  $D_e$  forced by minima-maxima variation in moisture content and overburden thickness is outlined and may prove instructive where there is uncertainty in these parameters. However the combined extremes represented should not be construed as preferred age estimates.



Sample: GL17080

Fig. 5 U Decay Activity

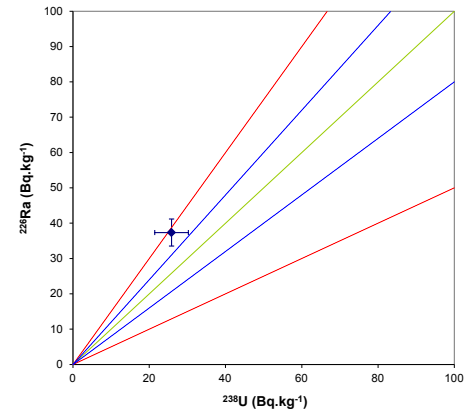
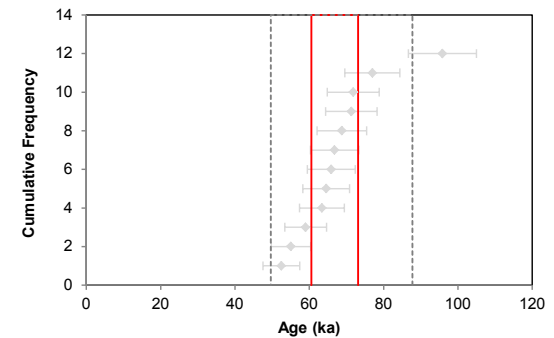


Fig. 6 Age Range



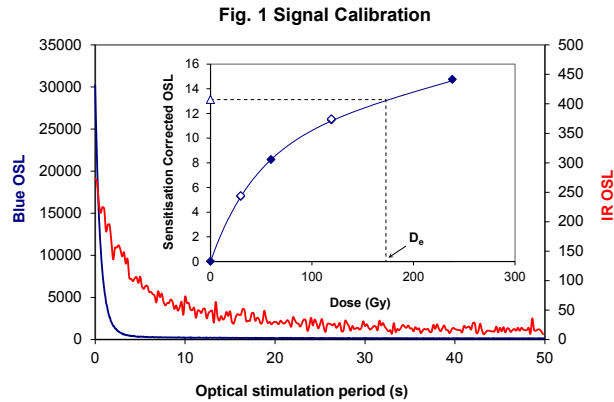


Fig. 1 Signal Calibration

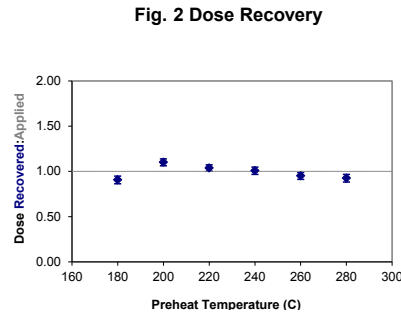


Fig. 2 Dose Recovery

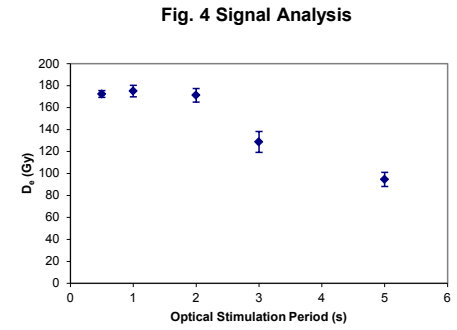
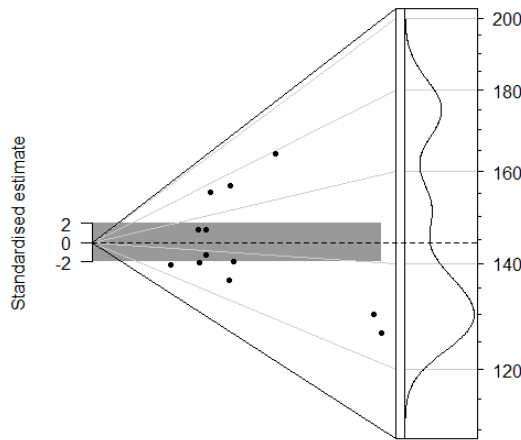


Fig. 4 Signal Analysis

Fig. 3 Inter-aliquot D0 distribution



**Fig. 1 Signal Calibration** Natural blue and laboratory-induced infrared (IR) OSL signals. Detectable IR signal decays are diagnostic of feldspar contamination. Inset, the natural blue OSL signal (open triangle) of each aliquot is calibrated against known laboratory doses to yield equivalent dose ( $D_0$ ) values. Repeats of low and high doses (open diamonds) illustrate the success of sensitivity correction.

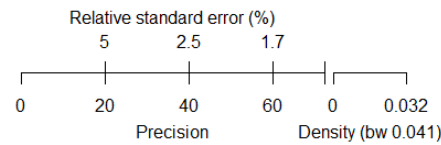
**Fig. 2 Dose Recovery** The acquisition of  $D_0$  values is necessarily predicated upon thermal treatment of aliquots succeeding environmental and laboratory irradiation. The Dose Recovery test quantifies the combined effects of thermal transfer and sensitisation on the natural signal using a precise lab dose to simulate natural dose. Based on this an appropriate thermal treatment is selected to generate the final  $D_0$  value.

**Fig. 3 Inter-aliquot  $D_0$  distribution** Abanico plot of inter-aliquot statistical concordance in  $D_0$  values derived from natural irradiation. Discordant data (those points lying beyond  $\pm 2$  standardised  $\ln D_0$ ) reflect heterogeneous dose absorption and/or inaccuracies in calibration.

**Fig. 4 Signal Analysis** Statistically significant increase in natural  $D_0$  value with signal stimulation period is indicative of a partially-bleached signal, provided a significant increase in  $D_0$  results from simulated partial bleaching followed by insignificant adjustment in  $D_0$  for simulated zero and full bleach conditions. Ages from such samples are considered maximum estimates. In the absence of a significant rise in  $D_0$  with stimulation time, simulated partial bleaching and zero/full bleach tests are not assessed.

**Fig. 5 U Activity** Statistical concordance (equilibrium) in the activities of the daughter radioisotope  $^{226}\text{Ra}$  with its parent  $^{238}\text{U}$  may signify the temporal stability of  $D_0$  emissions from these chains. Significant differences (disequilibrium;  $>50\%$ ) in activity indicate addition or removal of isotopes creating a time-dependent shift in  $D_0$  values and increased uncertainty in the accuracy of age estimates. A 20% disequilibrium marker is also shown.

**Fig. 6 Age Range** The Cumulative frequency plot indicates the inter-aliquot variability in age. It also shows the mean age range: an estimate of sediment burial period based on mean  $D_0$  and  $D_0$  values with associated analytical uncertainties. The maximum influence of temporal variations in  $D_0$  forced by minima-maxima variation in moisture content and overburden thickness is outlined and may prove instructive where there is uncertainty in these parameters. However the combined extremes represented should not be construed as preferred age estimates.



Sample: GL17081

Fig. 5 U Decay Activity

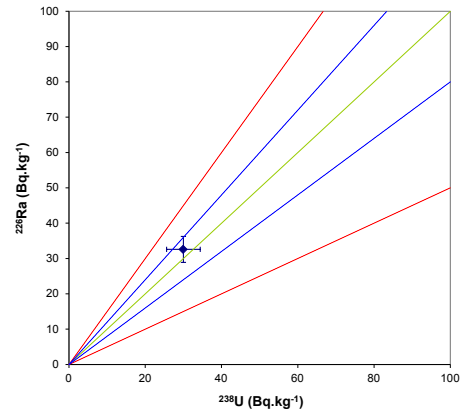
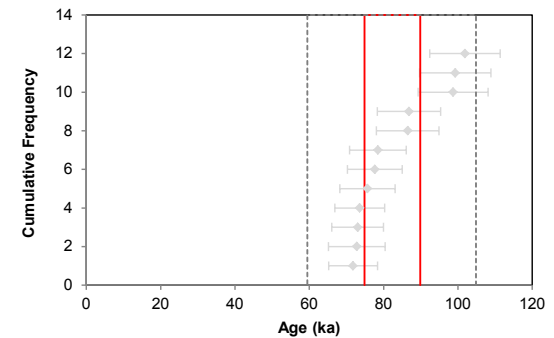


Fig. 6 Age Range



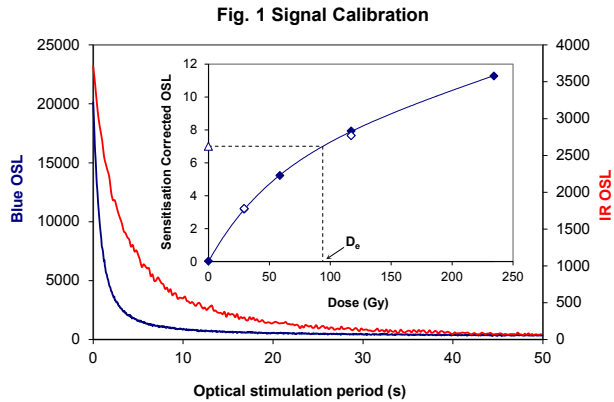


Fig. 1 Signal Calibration

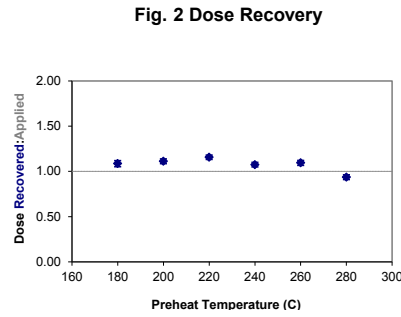


Fig. 2 Dose Recovery

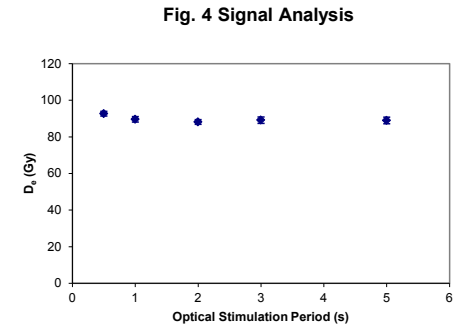
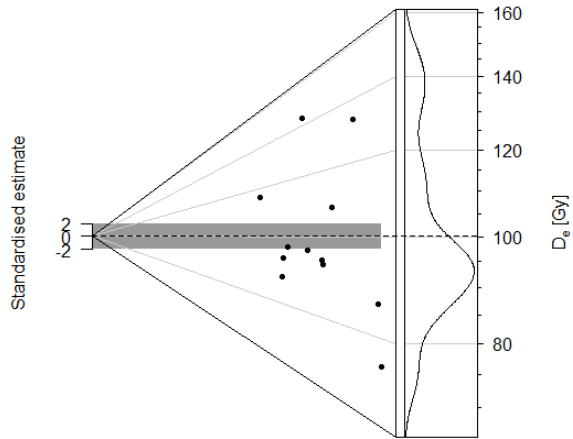


Fig. 4 Signal Analysis

Fig. 3 Inter-aliquot D<sub>e</sub> distribution



**Fig. 1 Signal Calibration** Natural blue and laboratory-induced infrared (IR) OSL signals. Detectable IR signal decays are diagnostic of feldspar contamination. Inset, the natural blue OSL signal (open triangle) of each aliquot is calibrated against known laboratory doses to yield equivalent dose ( $D_e$ ) values. Repeats of low and high doses (open diamonds) illustrate the success of sensitivity correction.

**Fig. 2 Dose Recovery** The acquisition of  $D_e$  values is necessarily predicated upon thermal treatment of aliquots succeeding environmental and laboratory irradiation. The Dose Recovery test quantifies the combined effects of thermal transfer and sensitisation on the natural signal using a precise lab dose to simulate natural dose. Based on this an appropriate thermal treatment is selected to generate the final  $D_e$  value.

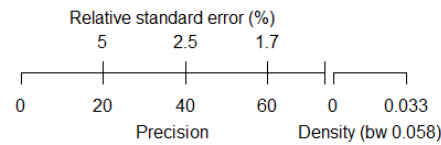
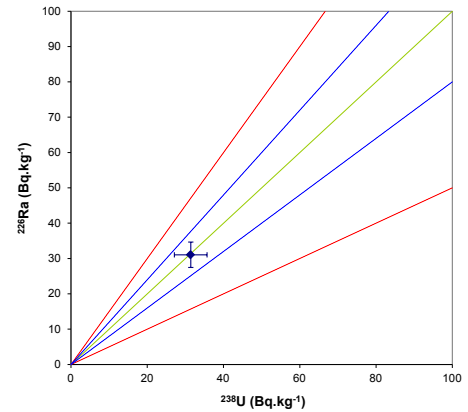
**Fig. 3 Inter-aliquot  $D_e$  distribution** Abanico plot of inter-aliquot statistical concordance in  $D_e$  values derived from natural irradiation. Discordant data (those points lying beyond  $\pm 2$  standardised  $\ln D_e$ ) reflect heterogeneous dose absorption and/or inaccuracies in calibration.

**Fig. 4 Signal Analysis** Statistically significant increase in natural  $D_e$  value with signal stimulation period is indicative of a partially-bleached signal, provided a significant increase in  $D_e$  results from simulated partial bleaching followed by insignificant adjustment in  $D_e$  for simulated zero and full bleach conditions. Ages from such samples are considered maximum estimates. In the absence of a significant rise in  $D_e$  with stimulation time, simulated partial bleaching and zero/full bleach tests are not assessed.

**Fig. 5 U Activity** Statistical concordance (equilibrium) in the activities of the daughter radioisotope  $^{226}\text{Ra}$  with its parent  $^{238}\text{U}$  may signify the temporal stability of  $D_e$  emissions from these chains. Significant differences (disequilibrium;  $>50\%$ ) in activity indicate addition or removal of isotopes creating a time-dependent shift in  $D_e$  values and increased uncertainty in the accuracy of age estimates. A 20% disequilibrium marker is also shown.

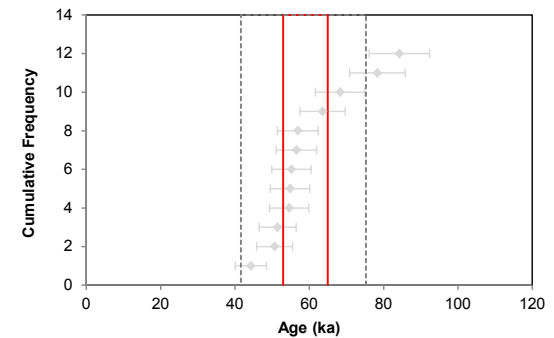
**Fig. 6 Age Range** The Cumulative frequency plot indicates the inter-aliquot variability in age. It also shows the mean age range: an estimate of sediment burial period based on mean  $D_e$  and  $D_e$  values with associated analytical uncertainties. The maximum influence of temporal variations in  $D_e$  forced by minima-maxima variation in moisture content and overburden thickness is outlined and may prove instructive where there is uncertainty in these parameters. However the combined extremes represented should not be construed as preferred age estimates.

Fig. 5 U Decay Activity



Sample: GL18023

Fig. 6 Age Range



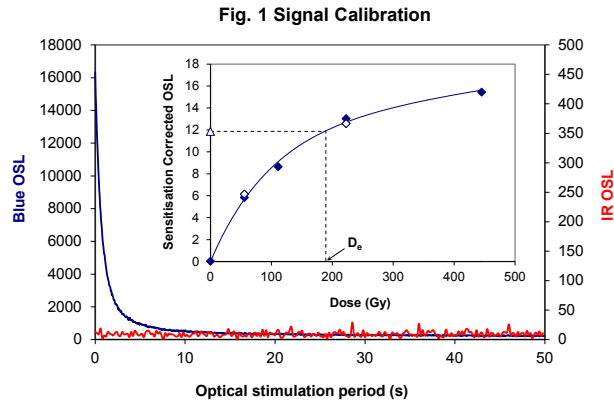


Fig. 1 Signal Calibration

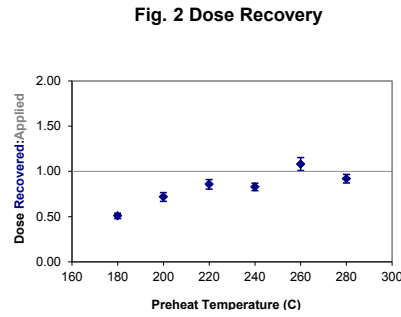


Fig. 2 Dose Recovery

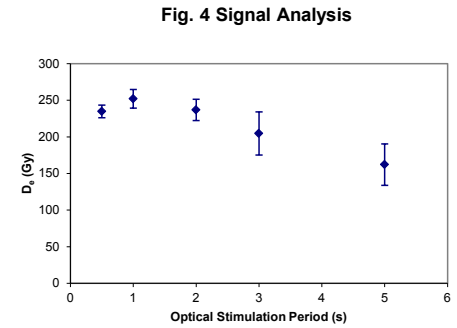


Fig. 4 Signal Analysis

Fig. 3 Inter-aliquot D0 distribution

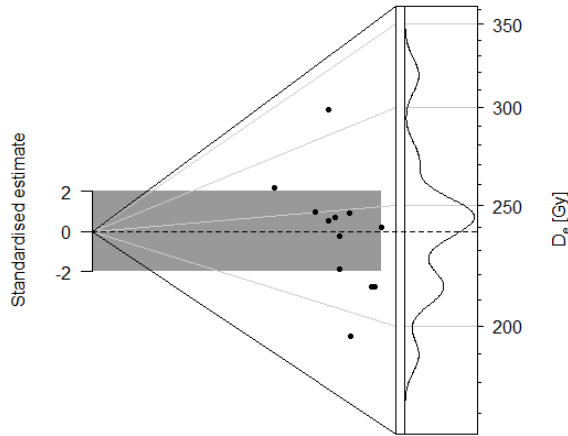


Fig. 1 Signal Calibration Natural blue and laboratory-induced infrared (IR) OSL signals. Detectable IR signal decays are diagnostic of feldspar contamination. Inset, the natural blue OSL signal (open triangle) of each aliquot is calibrated against known laboratory doses to yield equivalent dose ( $D_0$ ) values. Repeats of low and high doses (open diamonds) illustrate the success of sensitivity correction.

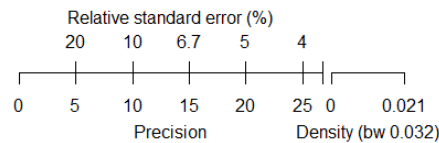
Fig. 2 Dose Recovery The acquisition of  $D_0$  values is necessarily predicated upon thermal treatment of aliquots succeeding environmental and laboratory irradiation. The Dose Recovery test quantifies the combined effects of thermal transfer and sensitisation on the natural signal using a precise lab dose to simulate natural dose. Based on this an appropriate thermal treatment is selected to generate the final  $D_0$  value.

Fig. 3 Inter-aliquot  $D_0$  distribution Abanico plot of inter-aliquot statistical concordance in  $D_0$  values derived from natural irradiation. Discordant data (those points lying beyond  $\pm 2$  standardised  $\ln D_0$ ) reflect heterogeneous dose absorption and/or inaccuracies in calibration.

Fig. 4 Signal Analysis Statistically significant increase in natural  $D_0$  value with signal stimulation period is indicative of a partially-bleached signal, provided a significant increase in  $D_0$  results from simulated partial bleaching followed by insignificant adjustment in  $D_0$  for simulated zero and full bleach conditions. Ages from such samples are considered maximum estimates. In the absence of a significant rise in  $D_0$  with stimulation time, simulated partial bleaching and zero/full bleach tests are not assessed.

Fig. 5 U Activity Statistical concordance (equilibrium) in the activities of the daughter radioisotope  $^{226}\text{Ra}$  with its parent  $^{238}\text{U}$  may signify the temporal stability of  $D_0$  emissions from these chains. Significant differences (disequilibrium;  $>50\%$ ) in activity indicate addition or removal of isotopes creating a time-dependent shift in  $D_0$  values and increased uncertainty in the accuracy of age estimates. A 20% disequilibrium marker is also shown.

Fig. 6 Age Range The Cumulative frequency plot indicates the inter-aliquot variability in age. It also shows the mean age range: an estimate of sediment burial period based on mean  $D_0$  and  $D_0$  values with associated analytical uncertainties. The maximum influence of temporal variations in  $D_0$  forced by minima-maxima variation in moisture content and overburden thickness is outlined and may prove instructive where there is uncertainty in these parameters. However the combined extremes represented should not be construed as preferred age estimates.



Sample: GL18024

Fig. 5 U Decay Activity

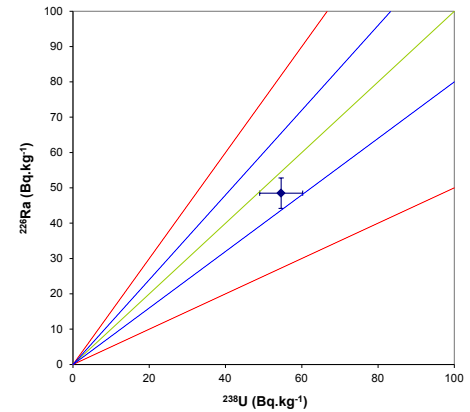
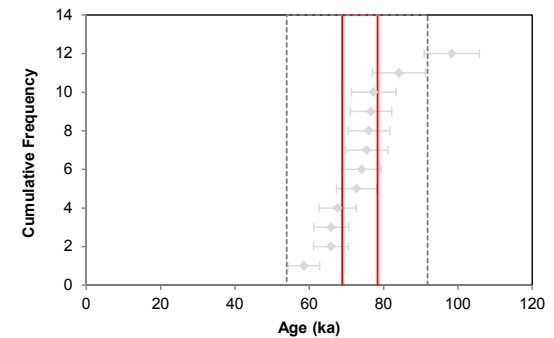


Fig. 6 Age Range





## References

- Adamiec, G. and Aitken, M.J. (1998) Dose-rate conversion factors: new data. *Ancient TL*, 16, 37-50.
- Agersnap-Larsen, N., Bulur, E., Bøtter-Jensen, L. and McKeever, S.W.S. (2000) Use of the LM-OSL technique for the detection of partial bleaching in quartz. *Radiation Measurements*, 32, 419-425.
- Aitken, M. J. (1998) An introduction to optical dating: the dating of Quaternary sediments by the use of photon-stimulated luminescence. Oxford University Press.
- Bailey, R.M., Singarayer, J.S. , Ward, S. and Stokes, S. (2003) Identification of partial resetting using  $D_e$  as a function of illumination time. *Radiation Measurements*, 37, 511-518.
- Bateman, M.D., Frederick, C.D., Jaiswal, M.K., Singhvi, A.K. (2003) Investigations into the potential effects of pedoturbation on luminescence dating. *Quaternary Science Reviews*, 22, 1169-1176.
- Bateman, M.D., Boulter, C.H., Carr, A.S., Frederick, C.D., Peter, D. and Wilder, M. (2007) Detecting post-depositional sediment disturbance in sandy deposits using optical luminescence. *Quaternary Geochronology*, 2, 57-64.
- Berger, G.W., Mulhern, P.J. and Huntley, D.J. (1980). Isolation of silt-sized quartz from sediments. *Ancient TL*, 11, 147-152.
- Bøtter-Jensen, L., Mejdahl, V. and Murray, A.S. (1999) New light on OSL. *Quaternary Science Reviews*, 18, 303-310.
- Bøtter-Jensen, L., McKeever, S.W.S. and Wintle, A.G. (2003) *Optically Stimulated Luminescence Dosimetry*. Elsevier, Amsterdam.
- Dietze, M., Kreutzer, S., Burow, C., Fuchs, M.C., Fischer, M., Schmidt, C. (2016) The abanico plot: visualising chronometric data with individual standard errors. *Quaternary Geochronology*, 31, 1-7.
- Duller, G.A.T (2003) Distinguishing quartz and feldspar in single grain luminescence measurements. *Radiation Measurements*, 37, 161-165.
- Galbraith, R. F., Roberts, R. G., Laslett, G. M., Yoshida, H. and Olley, J. M. (1999) Optical dating of single and multiple grains of quartz from Jinmium rock shelter (northern Australia): Part I, Experimental design and statistical models. *Archaeometry*, 41, 339-364.
- Glignac, L.A., May, J.-H. and Cohen, T.J. (2015). All mixed up: using single-grain equivalent dose distributions to identify phases of pedogenic mixing on a dryland alluvial fan. *Quaternary International*, 362, 23-33.
- Glignac, L.A., Cohen, T.J., Slack, M. and Feathers, J.K. (2016) Sediment mixing in Aeolian sandsheets identified and quantified using single-grain optically stimulated luminescence. *Quaternary Geochronology*, 32, 53-66.
- Huntley, D.J., Godfrey-Smith, D.I. and Thewalt, M.L.W. (1985) Optical dating of sediments. *Nature*, 313, 105-107.
- Hubbell, J.H. (1982) Photon mass attenuation and energy-absorption coefficients from 1keV to 20MeV. *International Journal of Applied Radioisotopes*, 33, 1269-1290.

- Hütt, G., Jaek, I. and Tchonka, J. (1988) Optical dating: K-feldspars optical response stimulation spectra. *Quaternary Science Reviews*, 7, 381-386.
- Jackson, M.L., Sayin, M. and Clayton, R.N. (1976). Hexafluorosilicic acid reagent modification for quartz isolation. *Soil Science Society of America Journal*, 40, 958-960.
- Jacobs, A., Wintle, A.G., Duller, G.A.T, Roberts, R.G. and Wadley, L. (2008) New ages for the post-Howiesons Poort, late and finale middle stone age at Sibdu, South Africa. *Journal of Archaeological Science*, 35, 1790-1807.
- Lombard, M., Wadley, L., Jacobs, Z., Mohapi, M. and Roberts, R.G. (2011) Still Bay and serrated points from the Umhlatuzana rock shelter, Kwazulu-Natal, South Africa. *Journal of Archaeological Science*, 37, 1773-1784.
- Markey, B.G., Bøtter-Jensen, L., and Duller, G.A.T. (1997) A new flexible system for measuring thermally and optically stimulated luminescence. *Radiation Measurements*, 27, 83-89.
- Mejdahl, V. (1979) Thermoluminescence dating: beta-dose attenuation in quartz grains. *Archaeometry*, 21, 61-72.
- Murray, A.S. and Olley, J.M. (2002) Precision and accuracy in the Optically Stimulated Luminescence dating of sedimentary quartz: a status review. *Geochronometria*, 21, 1-16.
- Murray, A.S. and Wintle, A.G. (2000) Luminescence dating of quartz using an improved single-aliquot regenerative-dose protocol. *Radiation Measurements*, 32, 57-73.
- Murray, A.S. and Wintle, A.G. (2003) The single aliquot regenerative dose protocol: potential for improvements in reliability. *Radiation Measurements*, 37, 377-381.
- Murray, A.S., Olley, J.M. and Caitcheon, G.G. (1995) Measurement of equivalent doses in quartz from contemporary water-lain sediments using optically stimulated luminescence. *Quaternary Science Reviews*, 14, 365-371.
- Olley, J.M., Murray, A.S. and Roberts, R.G. (1996) The effects of disequilibria in the Uranium and Thorium decay chains on burial dose rates in fluvial sediments. *Quaternary Science Reviews*, 15, 751-760.
- Olley, J.M., Caitcheon, G.G. and Murray, A.S. (1998) The distribution of apparent dose as determined by optically stimulated luminescence in small aliquots of fluvial quartz: implications for dating young sediments. *Quaternary Science Reviews*, 17, 1033-1040.
- Olley, J.M., Caitcheon, G.G. and Roberts R.G. (1999) The origin of dose distributions in fluvial sediments, and the prospect of dating single grains from fluvial deposits using -optically stimulated luminescence. *Radiation Measurements*, 30, 207-217.
- Olley, J.M., Pietsch, T. and Roberts, R.G. (2004) Optical dating of Holocene sediments from a variety of geomorphic settings using single grains of quartz. *Geomorphology*, 60, 337-358.
- Pawley, S.M., Toms, P.S., Armitage, S.J., Rose, J. (2010) Quartz luminescence dating of Anglian Stage fluvial sediments: Comparison of SAR age estimates to the terrace chronology of the Middle Thames valley, UK. *Quaternary Geochronology*, 5, 569-582.

- Prescott, J.R. and Hutton, J.T. (1994) Cosmic ray contributions to dose rates for luminescence and ESR dating: large depths and long-term time variations. *Radiation Measurements*, 23, 497-500.
- Singhvi, A.K., Bluszcz, A., Bateman, M.D., Someshwar Rao, M. (2001). Luminescence dating of loess-palaeosol sequences and coversands: methodological aspects and palaeoclimatic implications. *Earth Science Reviews*, 54, 193-211.
- Smith, B.W., Rhodes, E.J., Stokes, S., Spooner, N.A. (1990) The optical dating of sediments using quartz. *Radiation Protection Dosimetry*, 34, 75-78.
- Spooner, N.A. (1993) The validity of optical dating based on feldspar. Unpublished D.Phil. thesis, Oxford University.
- Templer, R.H. (1985) The removal of anomalous fading in zircons. *Nuclear Tracks and Radiation Measurements*, 10, 531-537.
- Wallinga, J. (2002) Optically stimulated luminescence dating of fluvial deposits: a review. *Boreas* 31, 303-322.
- Wintle, A.G. (1973) Anomalous fading of thermoluminescence in mineral samples. *Nature*, 245, 143-144.
- Zimmerman, D. W. (1971) Thermoluminescent dating using fine grains from pottery. *Archaeometry*, 13, 29-52.



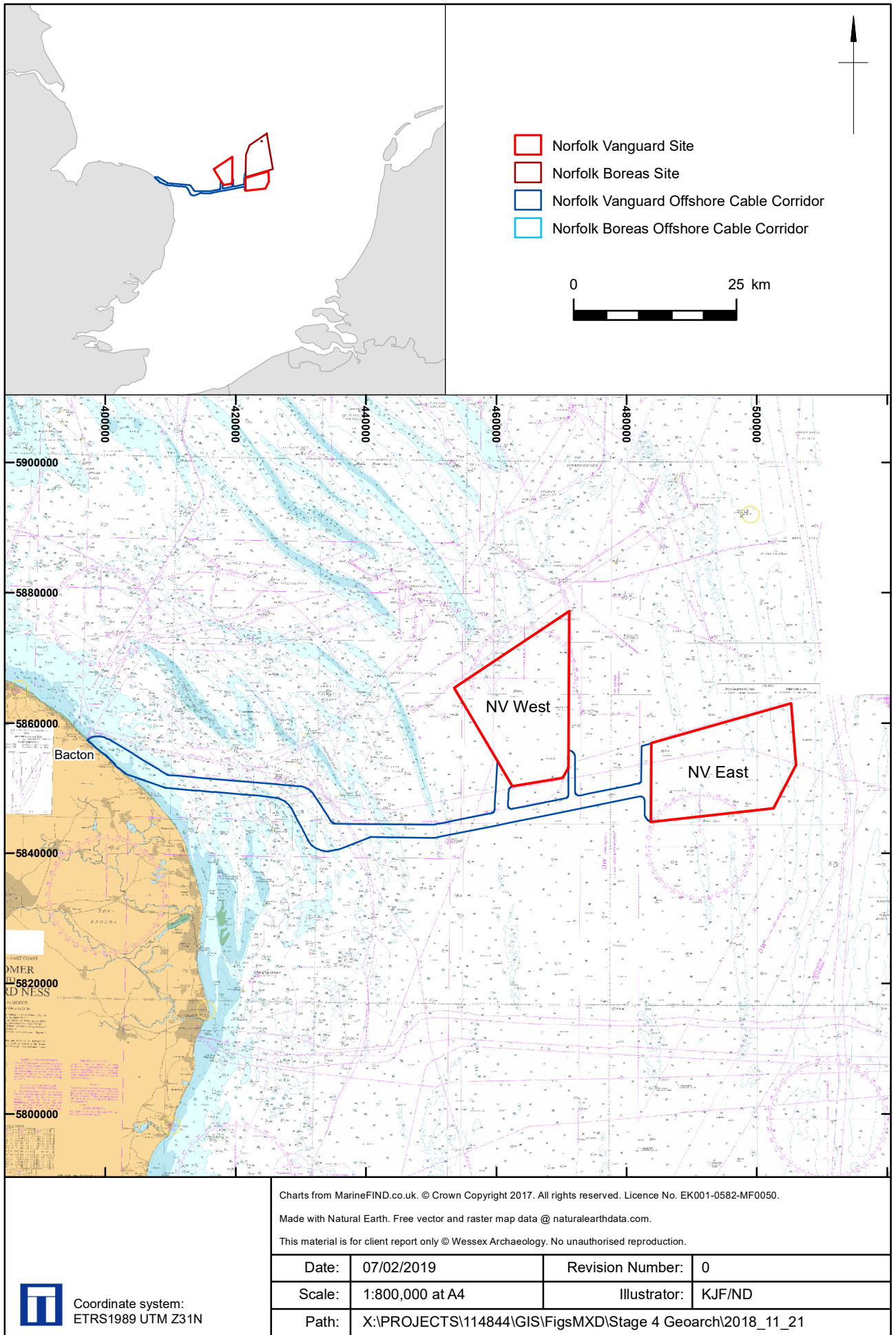
## Appendix 6 – Norfolk Vanguard site stratigraphy (deposit model)

WA Deposit Model (Stage 2) <sup>1</sup>		Fugro Soil Stratigraphy <sup>2</sup>		BGS Lithostratigraphy <sup>3</sup>	WA Deposit Model (Stage 4)		
Unit No	Unit Name	Soil Unit	Soil Unit Name	Formation	Unit No	Unit Name	Age
8	Holocene seabed sediments	A1	Bligh Bank	Southern Bight Formation	8	Seabed sediments	Holocene post-transgression (MIS 1)
7	Holocene sediments	A2	Elbow	Elbow Formation	7c	Elbow Formation – intertidal	Early Holocene (MIS 1)
					7b	Elbow Formation – organic	Late Devensian to Early Holocene (MIS 2-1)
					7a	Elbow Formation – fluvial	Late Devensian to Early Holocene (MIS 2-1)
6	Twente Formation	B	Twente	Twente Formation	6	Twente Formation	Late Devensian (MIS 2)
5	Upper Brown Bank Formation	C	Brown Bank	Brown Bank Formation	5	Upper Brown Bank	Early Devensian (MIS 5d-3)
4	Lower Brown Bank Formation/Eem Formation	C/D	Brown Bank	Brown Bank Formation and Eem Formation	4	Lower Brown Bank/Eem Formation	Ipswichian or Early Devensian (MIS 5e - 5d)
3	Swarte Bank Formation	E	Swarte Bank	Swarte Bank Formation	3	Swarte Bank Formation	Anglian (MIS 12)
2	Yarmouth Roads Formation	F	Yarmouth Roads	Yarmouth Road Formation	2	Yarmouth Roads Formation	Early to Middle Pleistocene (MIS >13)
1	Westkapelle Ground Formation	I	Westkapelle Ground Formation	Westkapelle Ground Formation	1	Westkapelle Ground Formation	Late Pliocene to Early Pleistocene (MIS 63-103)

<sup>1</sup> Wessex Archaeology (2018a)

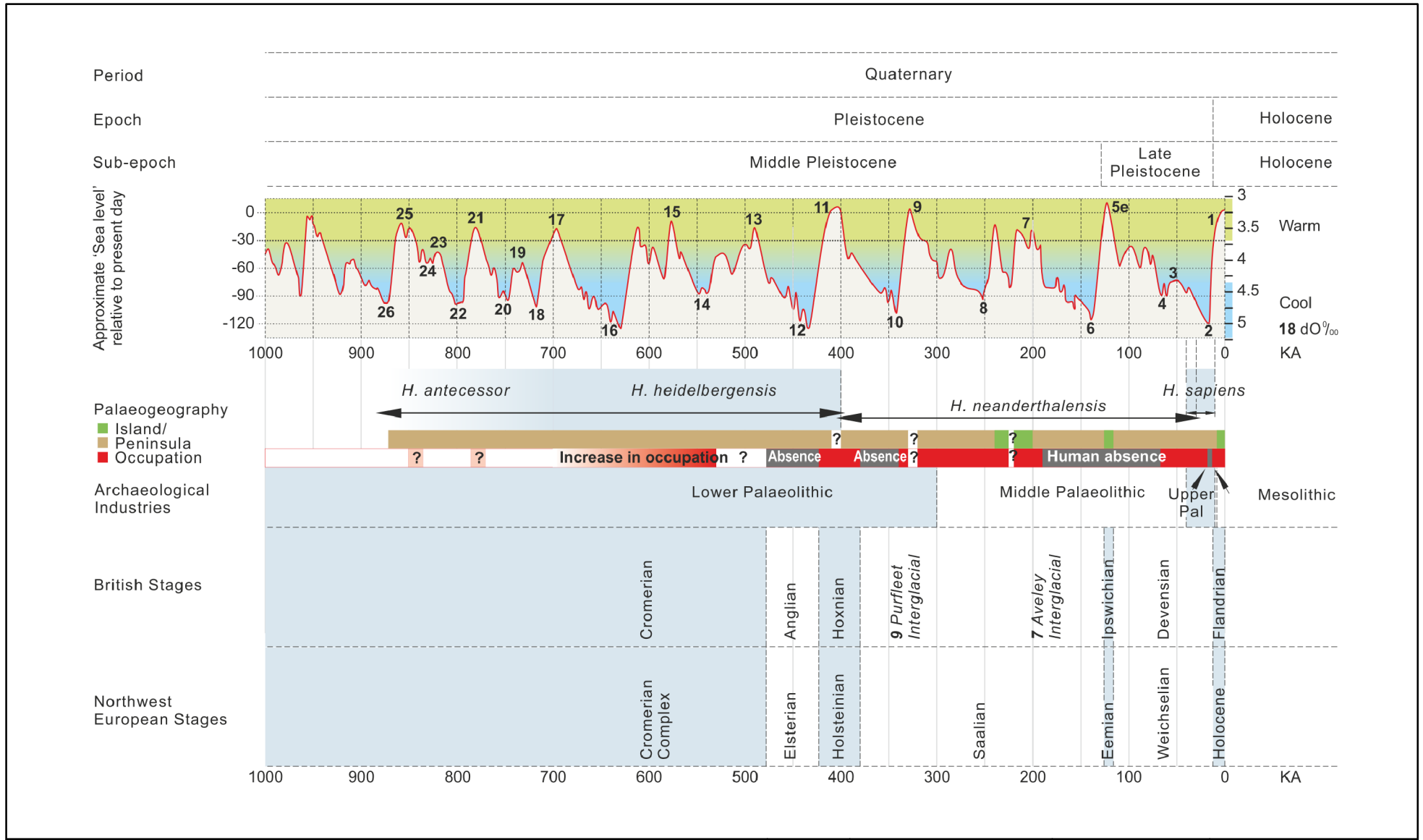
<sup>2</sup> Fugro (2017)

<sup>3</sup> Stoker et al. (2011)



Location of Norfolk Vanguard site

Figure 1



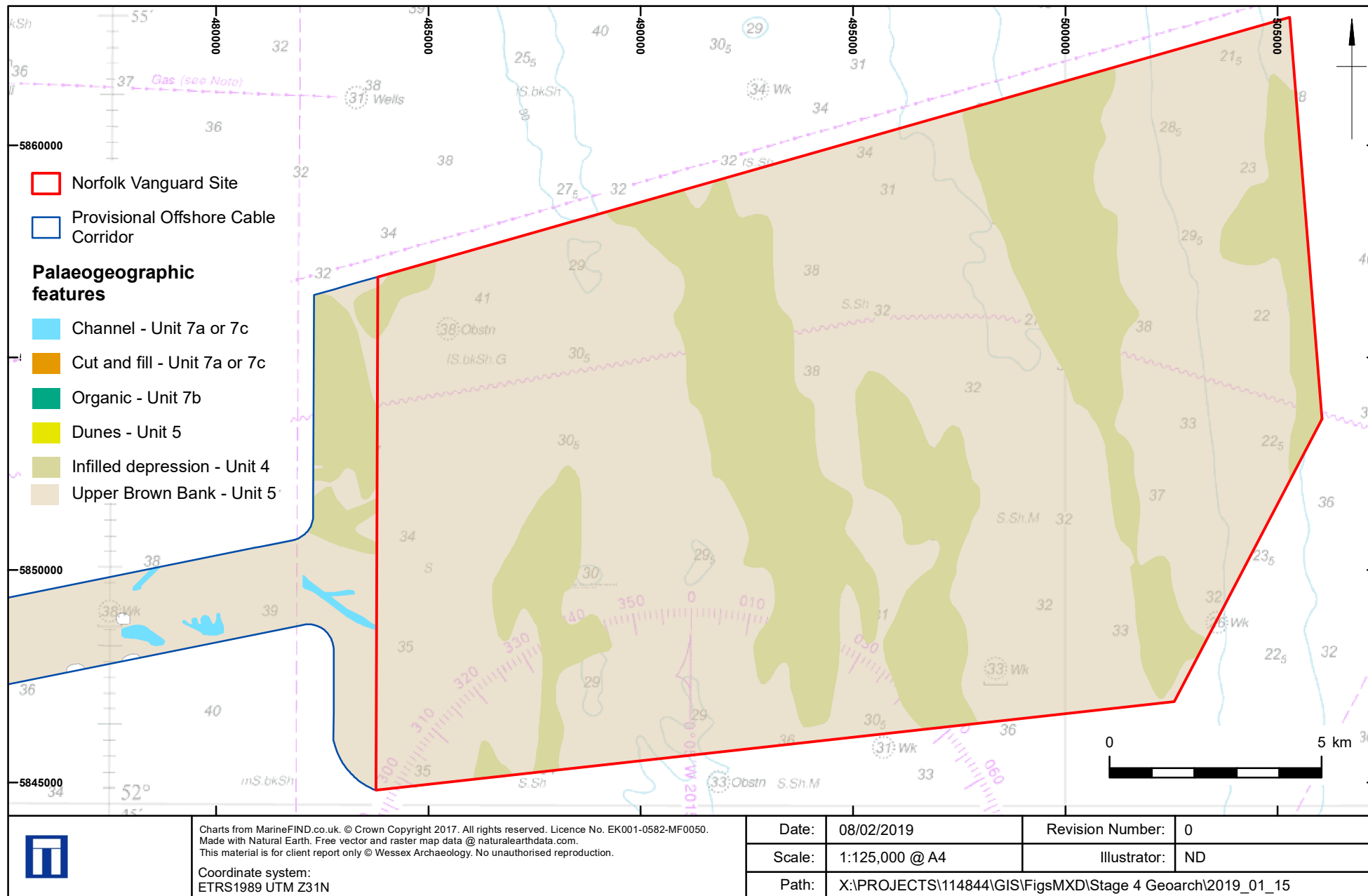
The figure presents information derived from several references: the global sea-level curve is from Lisiecki and Raymo (2005) and Jelgersma (1979). Details on the geology and archaeology were provided by Dix and Westley (2004); Funnel (1995); Gibbard and van Kolfschoten (2004); Kukla et al. (2002); Lee et al. (2006); Lowe and Walker (1997) and Wymer (1999).

This material is for client report only © Wessex Archaeology. No unauthorised reproduction.

Date:	21/11/2018	Revision Number:	0
Scale:	N/A	Illustrator:	RAM
Path:	X:\PROJECTS\114844\GIS\FigsMXD\Stage 4 Geoarch\2018_11_21		

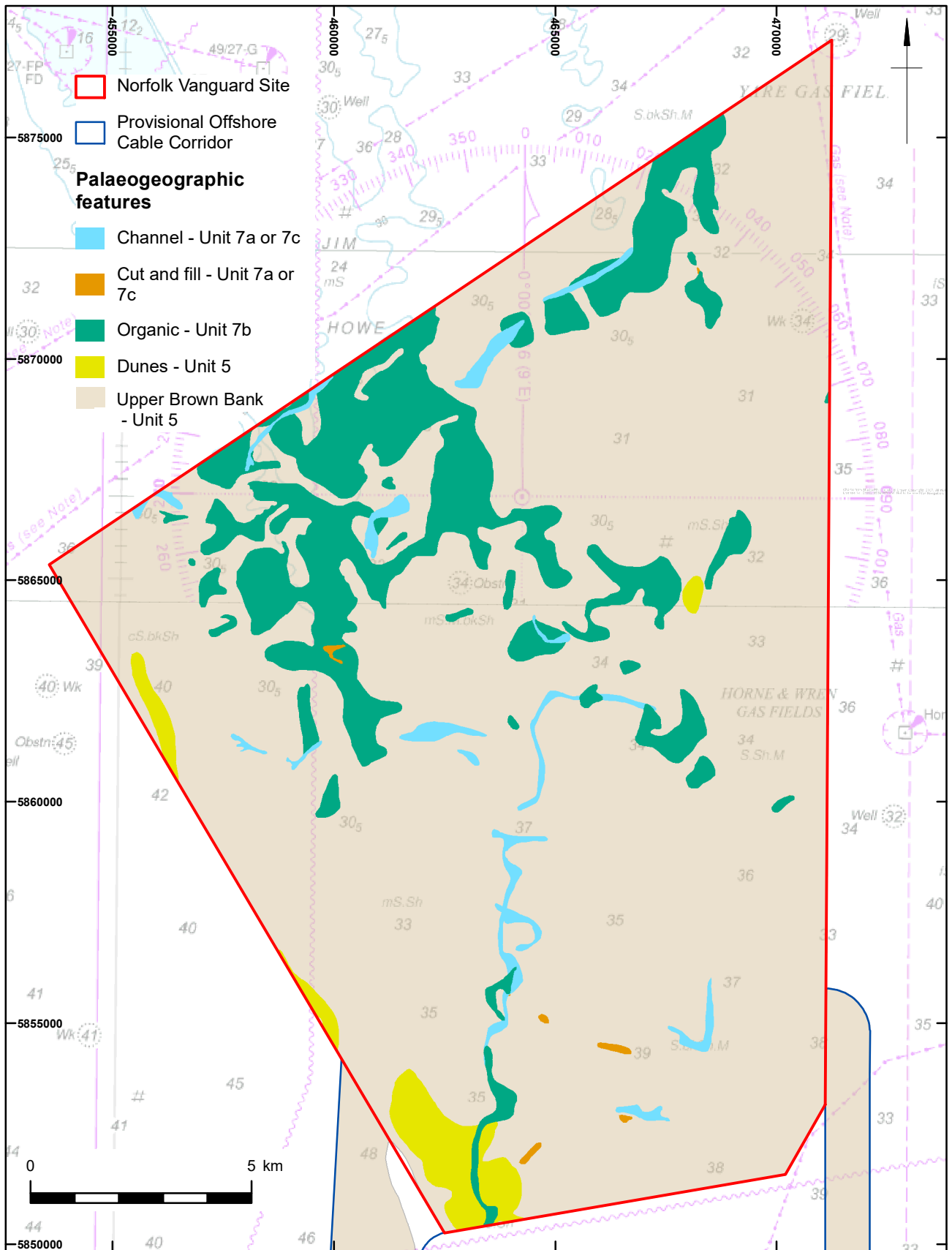
Chronostratigraphic timeline for the last 1 million years


Figure 2



Norfolk Vanguard East extent and location of deposits showing palaeogeographic features mapped from geophysical data

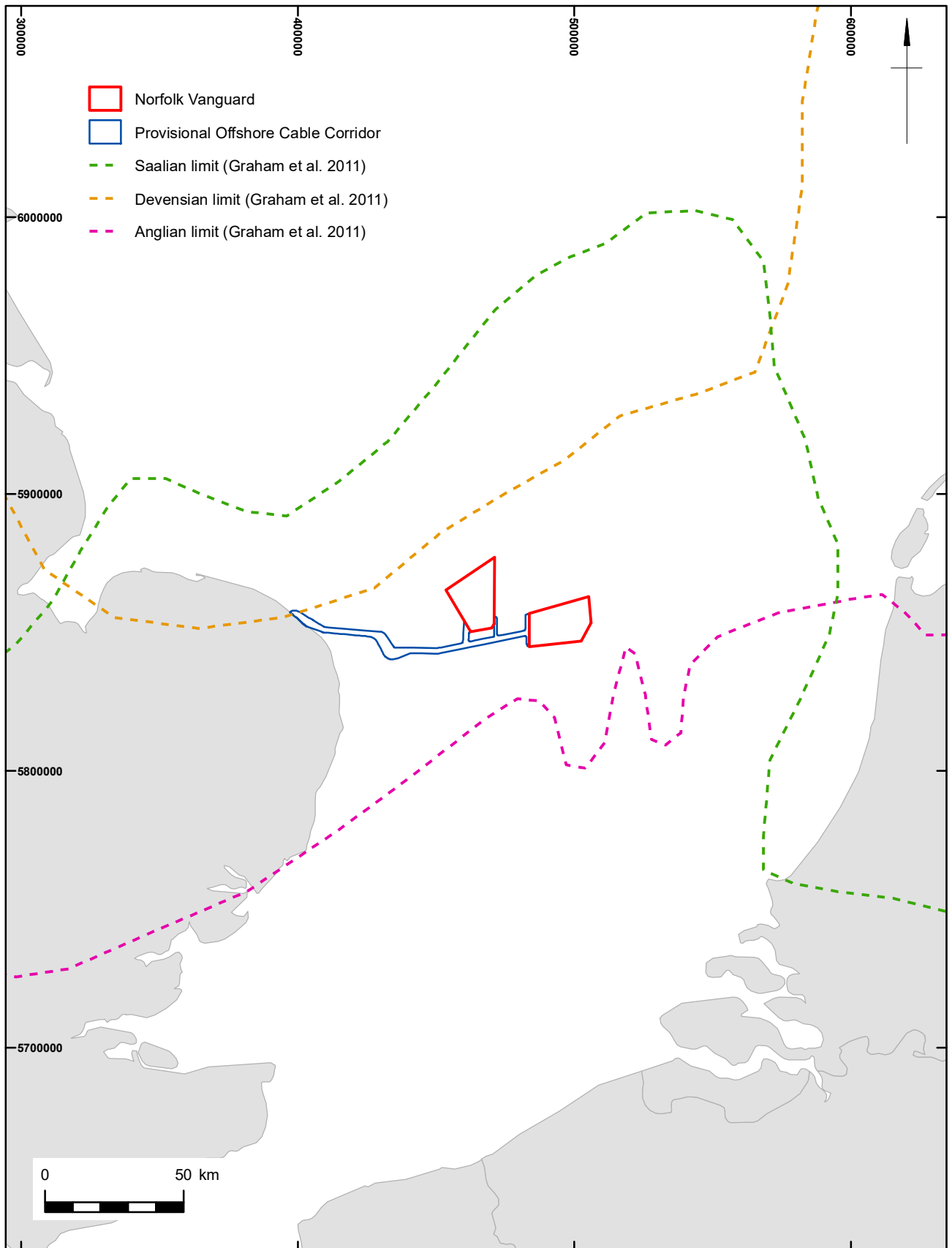
Figure 3a




	Coordinate system: ETRS1989 UTM Z31N		Charts from MarineFIND.co.uk. © Crown Copyright 2017. All rights reserved. Licence No. EK001-0582-MF0050. Made with Natural Earth. Free vector and raster map data @ naturalearthdata.com. This material is for client report only © Wessex Archaeology. No unauthorised reproduction.	
	Date:	08/02/2019	Revision Number:	0
	Scale:	1:125,000 at A4	Illustrator:	ND
	Path:	X:\PROJECTS\114844\GIS\FigsMXD\Stage 4 Geoarch\2019_01_15		

Norfolk Vanguard West extent and location of deposits showing palaeogeographic features mapped from geophysical data Figure 3b

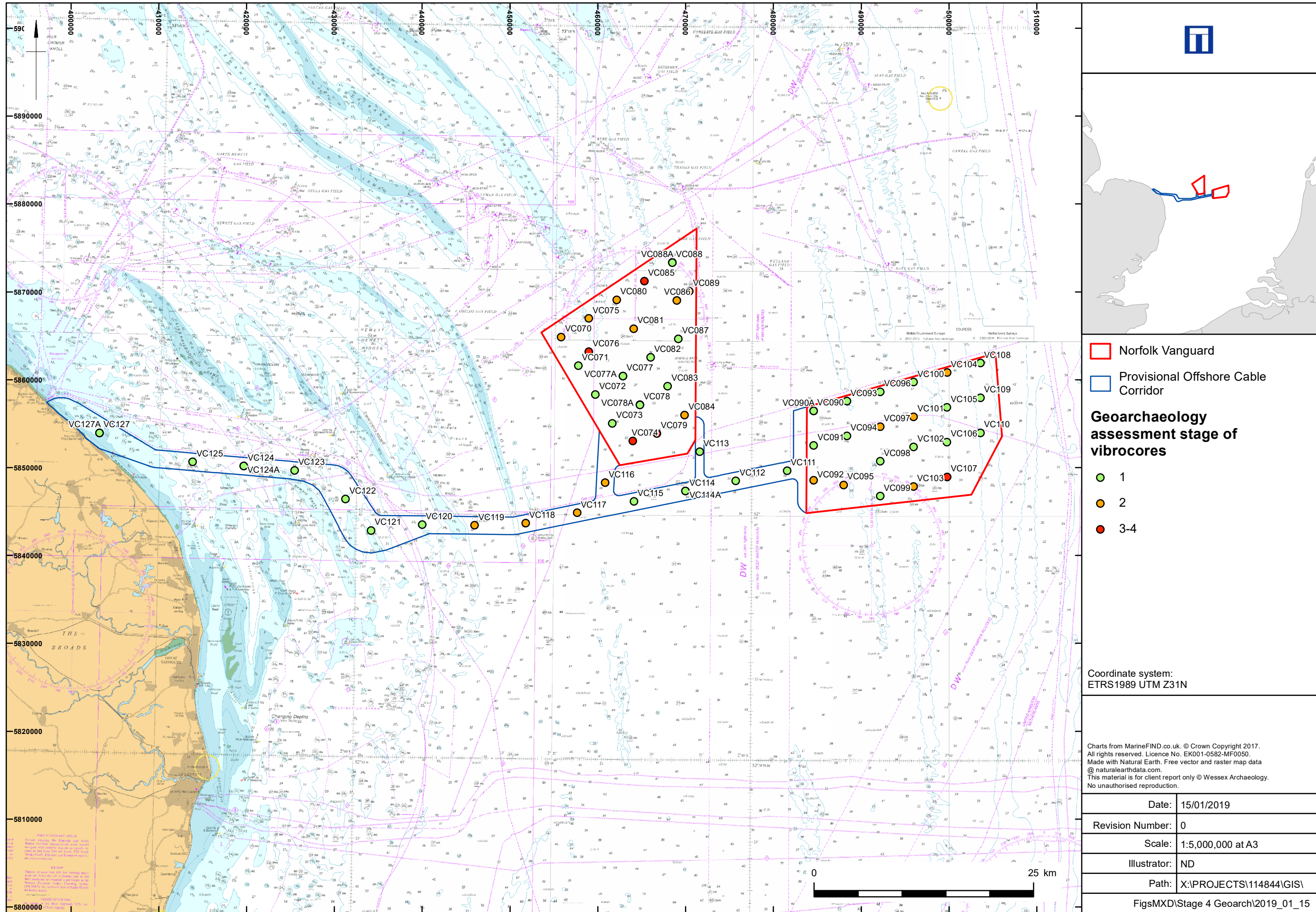




 Coordinate system: ETRS1989 UTM Z31N	Made with Natural Earth. Free vector and raster map data @ <a href="http://naturalearthdata.com">naturalearthdata.com</a> .			
	This material is for client report only © Wessex Archaeology. No unauthorised reproduction.			
	Date:	15/01/2019	Revision Number:	0
	Scale:	1:2,000,000 at A4	Illustrator:	KJF/ND
Path:		X:\PROJECTS\114844\GIS\FigsMXD\Stage 4 Geoarch\2019_01_15		

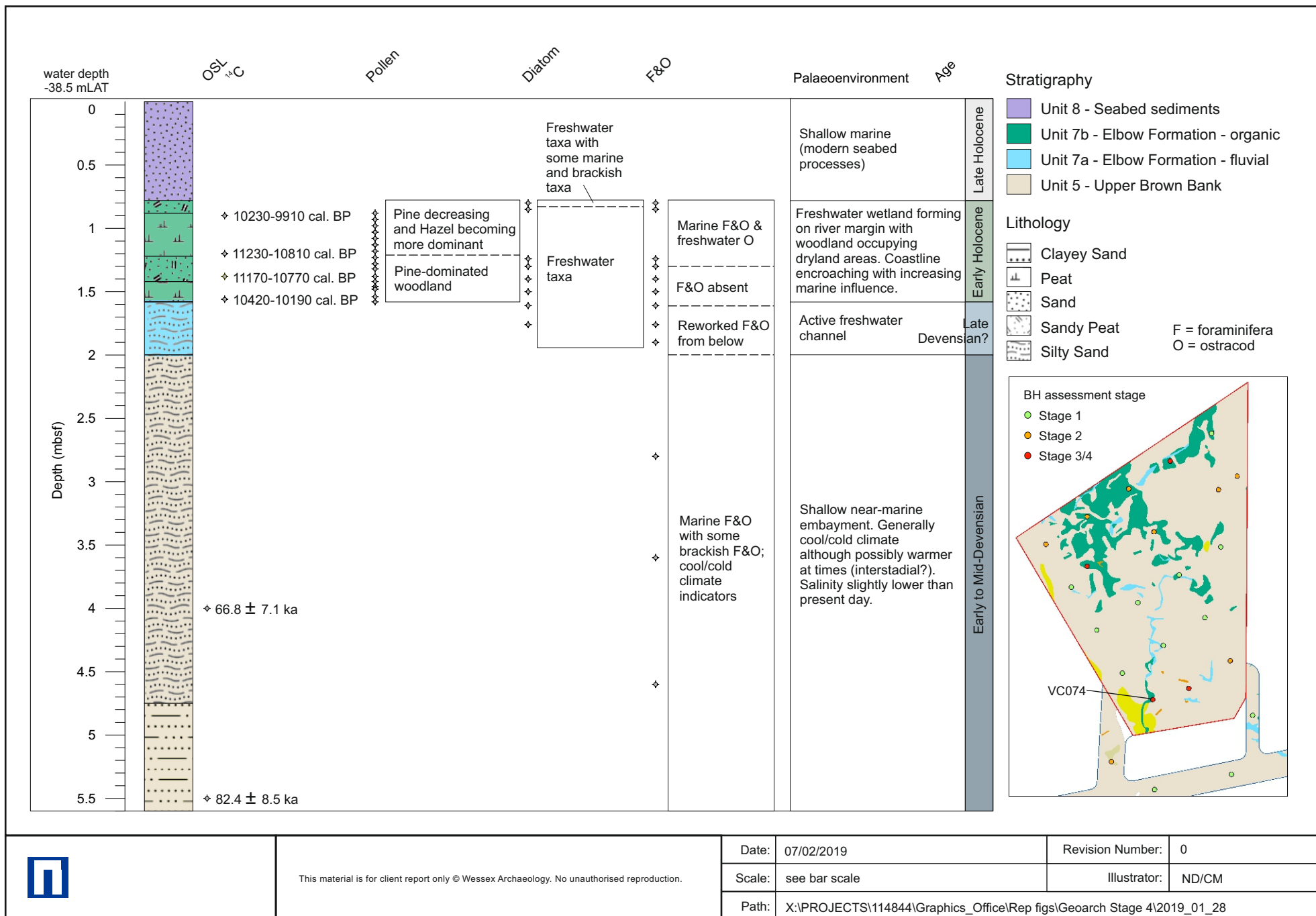
Pleistocene ice limits

Figure 4



Location of geotechnical boreholes showing stages of geoarchaeological assessment/analysis

Figure 5



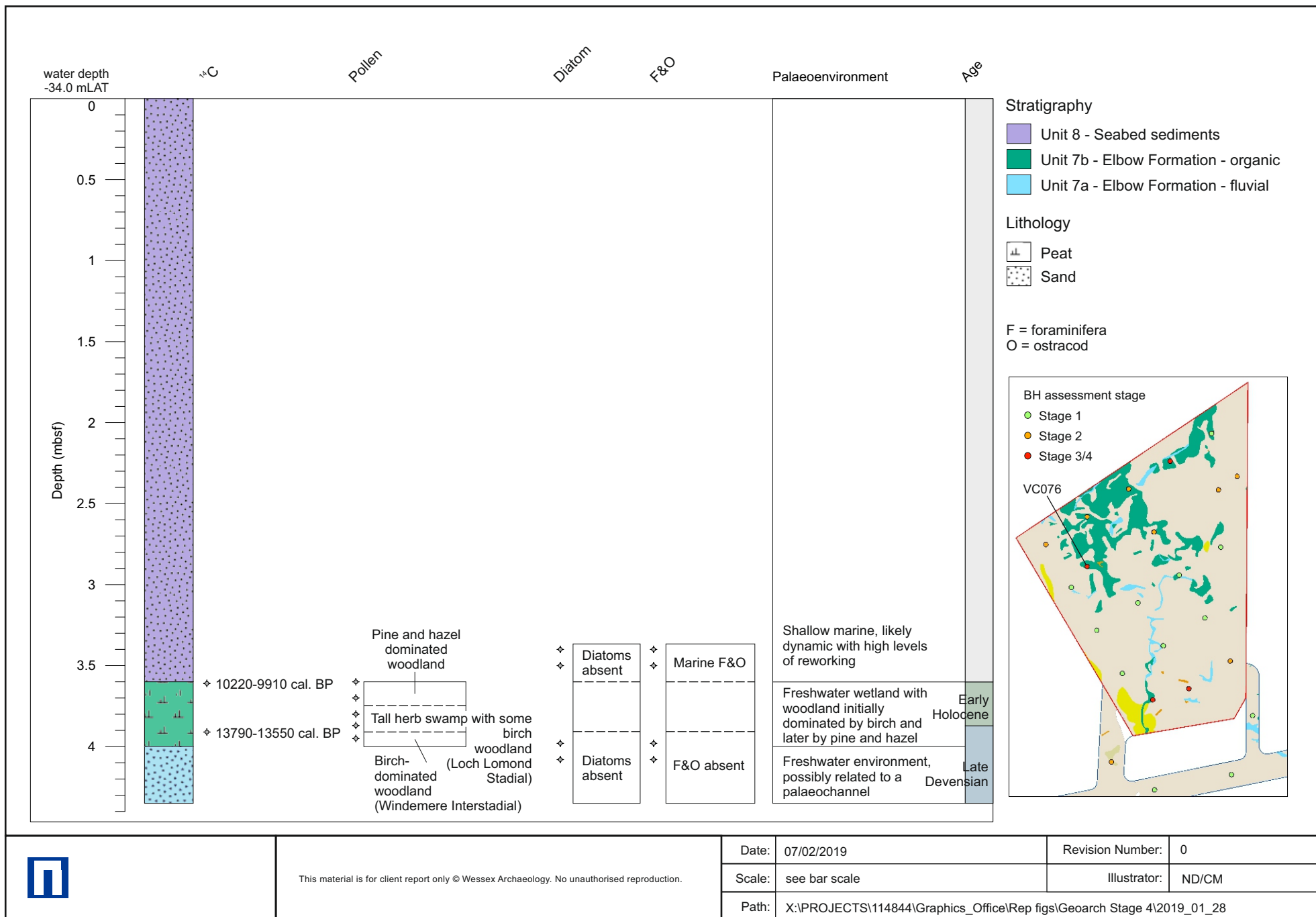
This material is for client report only © Wessex Archaeology. No unauthorised reproduction.

Date:	07/02/2019	Revision Number:	0
Scale:	see bar scale	Illustrator:	ND/CM
Path:	X:\PROJECTS\114844\Graphics_Office\Rep figs\Geoarch Stage 4\2019_01_28		

Vibrocore log and geophysical palaeolandscapes assessment showing palaeoenvironmental and dating, results and interpretation, for VC074

Figure 6





This material is for client report only © Wessex Archaeology. No unauthorised reproduction.

Date: 07/02/2019

Revision Number: 0

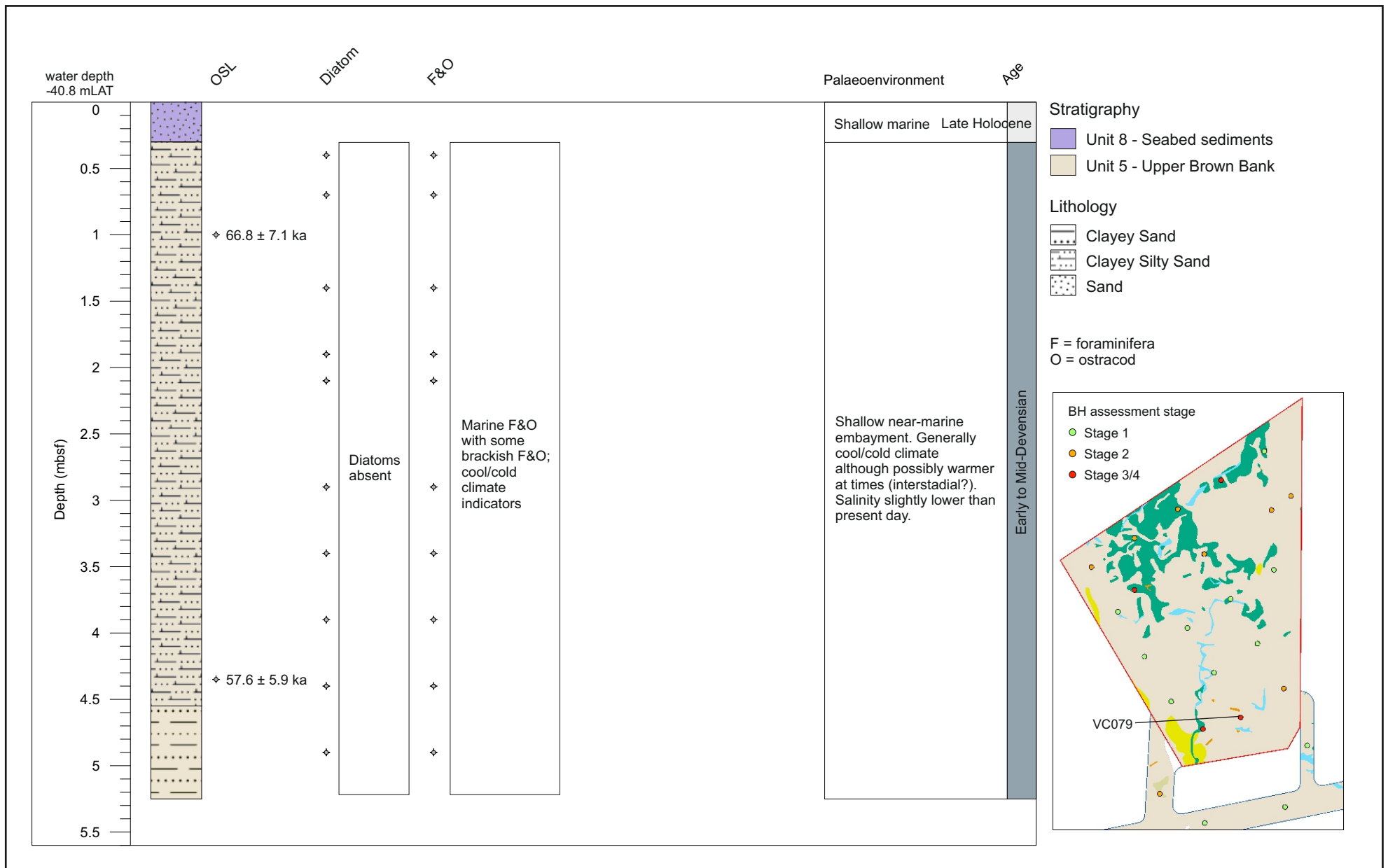
Scale: see bar scale


Illustrator: ND/CM

Path: X:\PROJECTS\114844\Graphics\_Office\Rep figs\Geoarch Stage 4\2019\_01\_28

Vibrocore log and geophysical palaeolandscape assessment showing palaeoenvironmental and dating, results and interpretation, for VC076

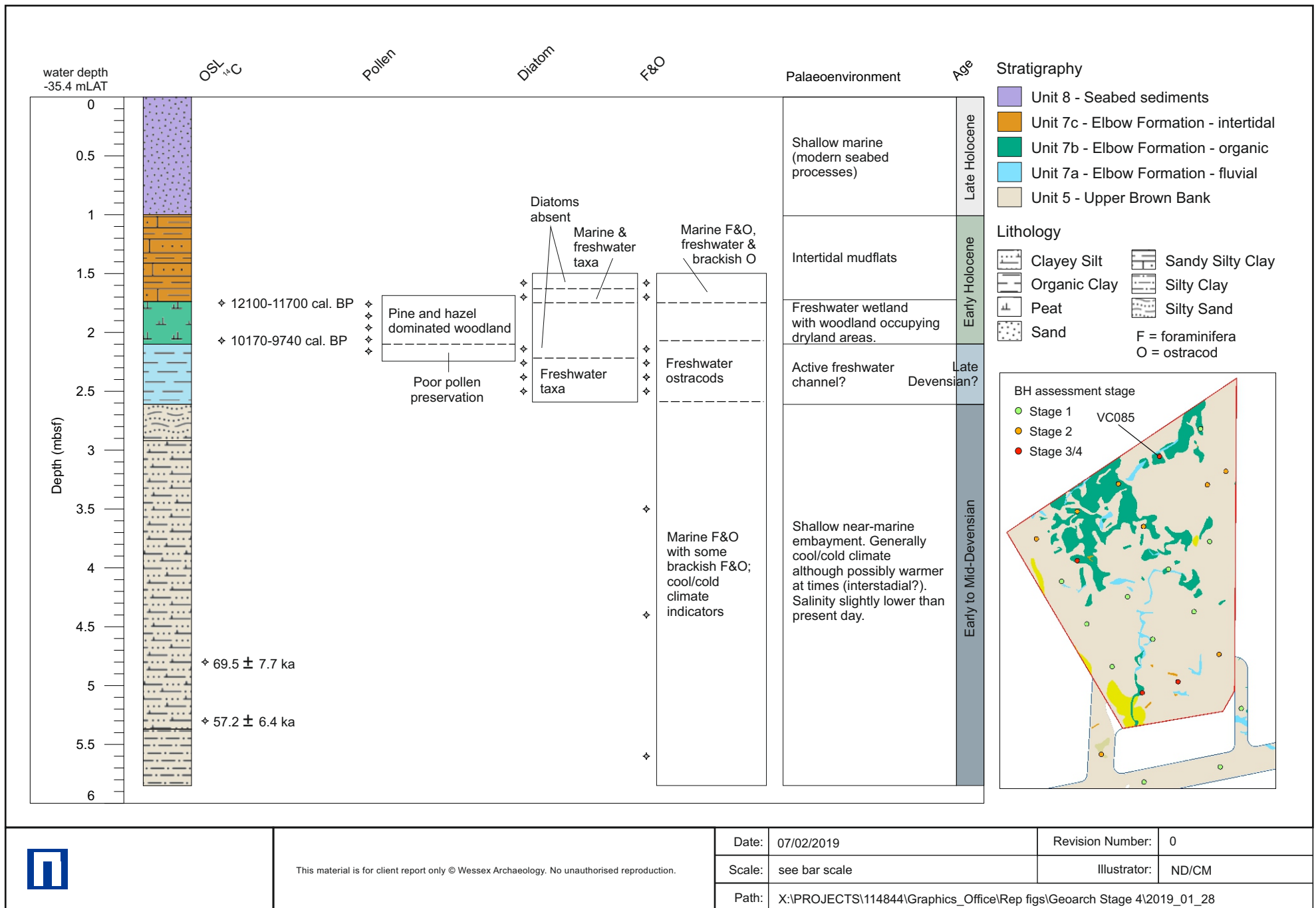
Figure 7



	This material is for client report only © Wessex Archaeology. No unauthorised reproduction.	Date: 07/02/2019	Revision Number: 0
		Scale: see bar scale	Illustrator: ND/CM
		Path: X:\PROJECTS\114844\Graphics_Office\Rep figs\Geoarch Stage 4\2019_01_28	

Vibrocore log and geophysical palaeolandscapes assessment showing palaeoenvironmental and dating, results and interpretation, for VC079

Figure 8



This material is for client report only © Wessex Archaeology. No unauthorised reproduction.

Date: 07/02/2019

Revision Number: 0

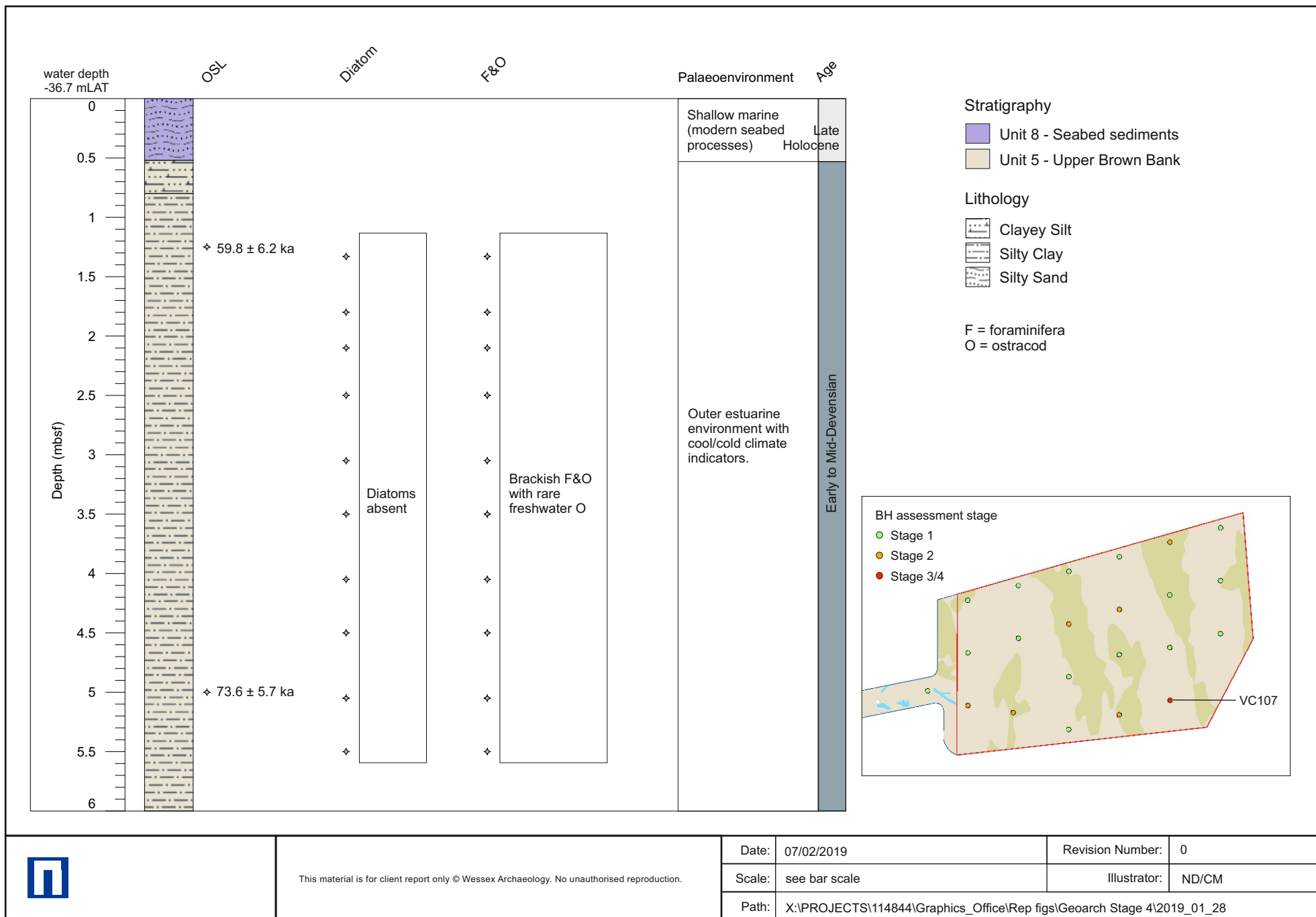
Scale: see bar scale

Illustrator: ND/CM

Path: X:\PROJECTS\114844\Graphics\_Office\Rep figs\Geoarch Stage 4\2019\_01\_28

Vibrocore log and geophysical palaeolandscapes assessment showing palaeoenvironmental and dating, results and interpretation, for VC085

Figure 9



This material is for client report only © Wessex Archaeology. No unauthorised reproduction.

Date: 07/02/2019

Revision Number: 0

Scale: see bar scale

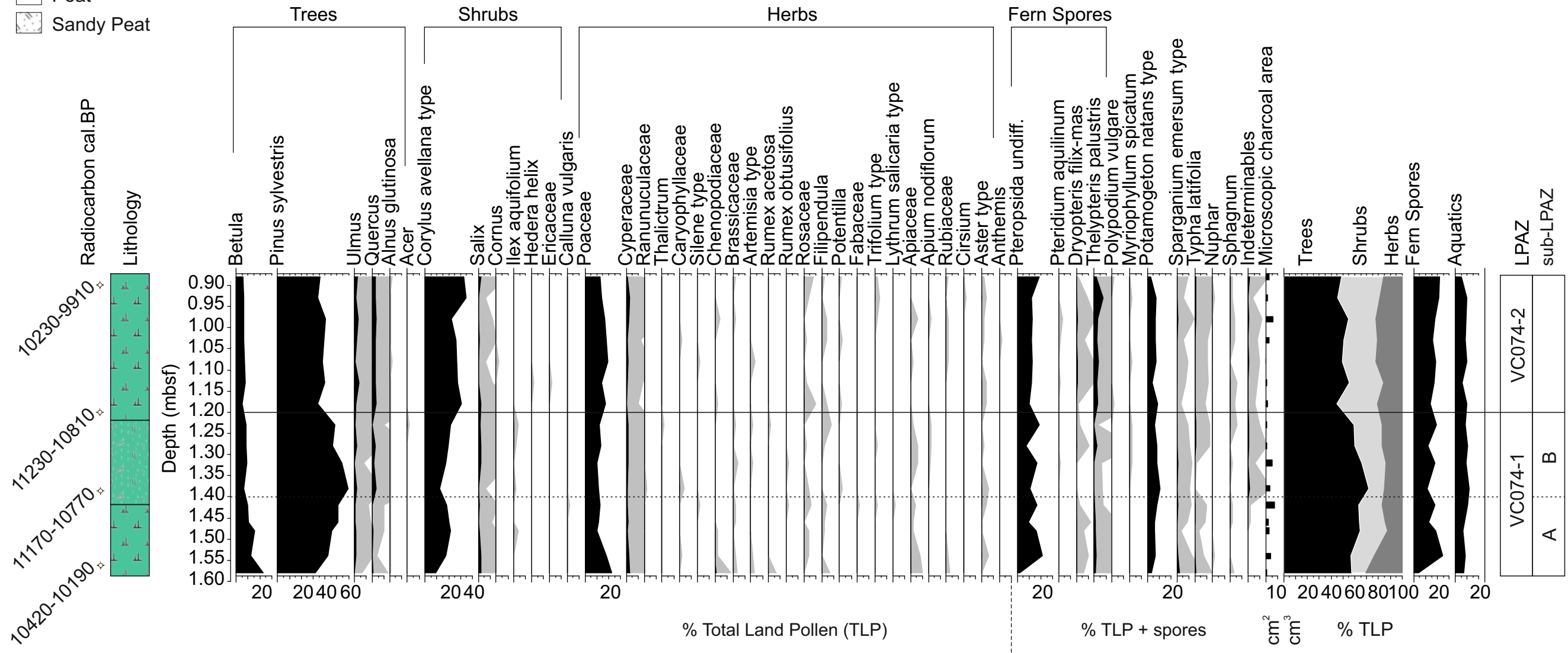
Illustrator: ND/CM

Path: X:\PROJECTS\114844\Graphics\_Office\Rep figs\Geoarch Stage 4\2019\_01\_28

Vibrocore log and geophysical palaeolandscape assessment showing palaeoenvironmental and dating, results and interpretation, for VC107

Figure 10

- Unit 7b
- Elbow Formation - organic
- Peat
- Sandy Peat



This material is for client report only © Wessex Archaeology.  
No unauthorised reproduction.

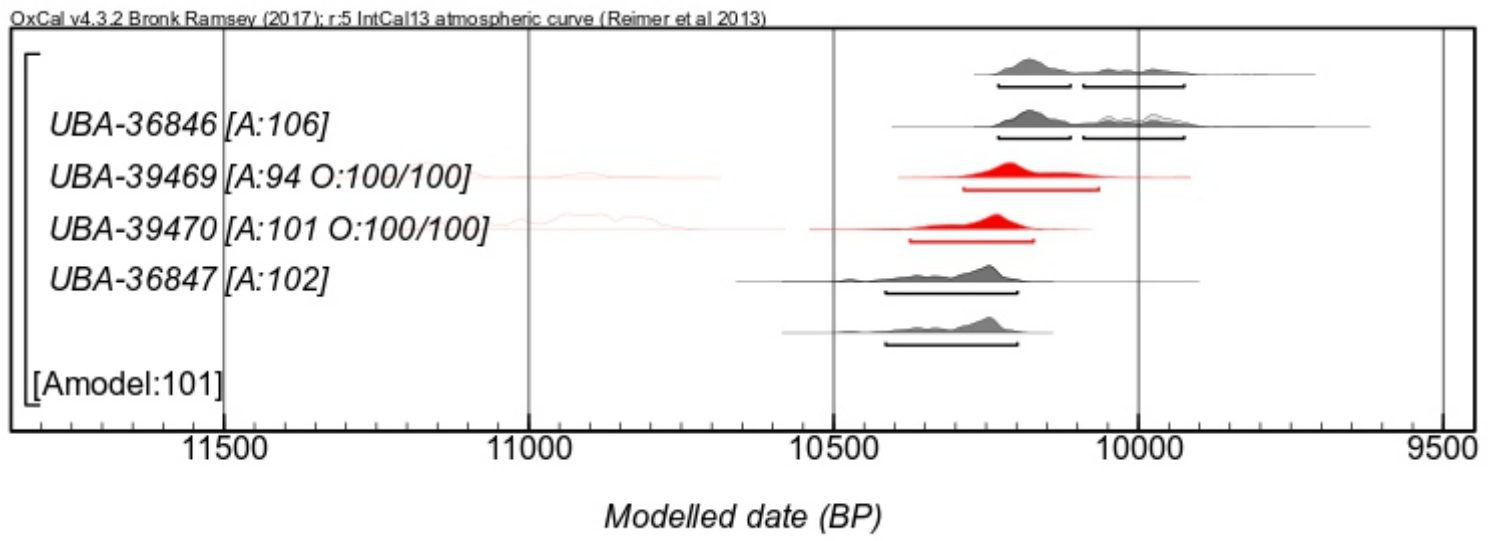
Date:	07/02/2019	Revision Number:	0
Scale:	NTS	Illustrator:	CM/ND
Path:	X:\PROJECTS\114844\Graphics_Office\Rep figs\Geoarch Stage 4\2019_01_28		

Pollen diagram VC074

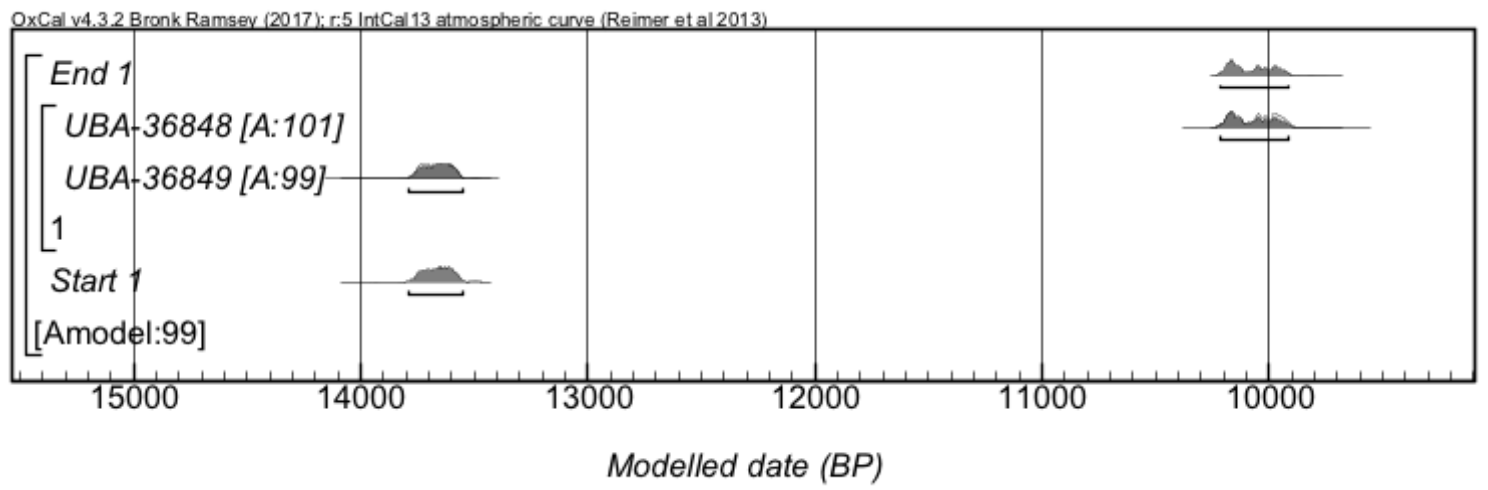
Figure 11



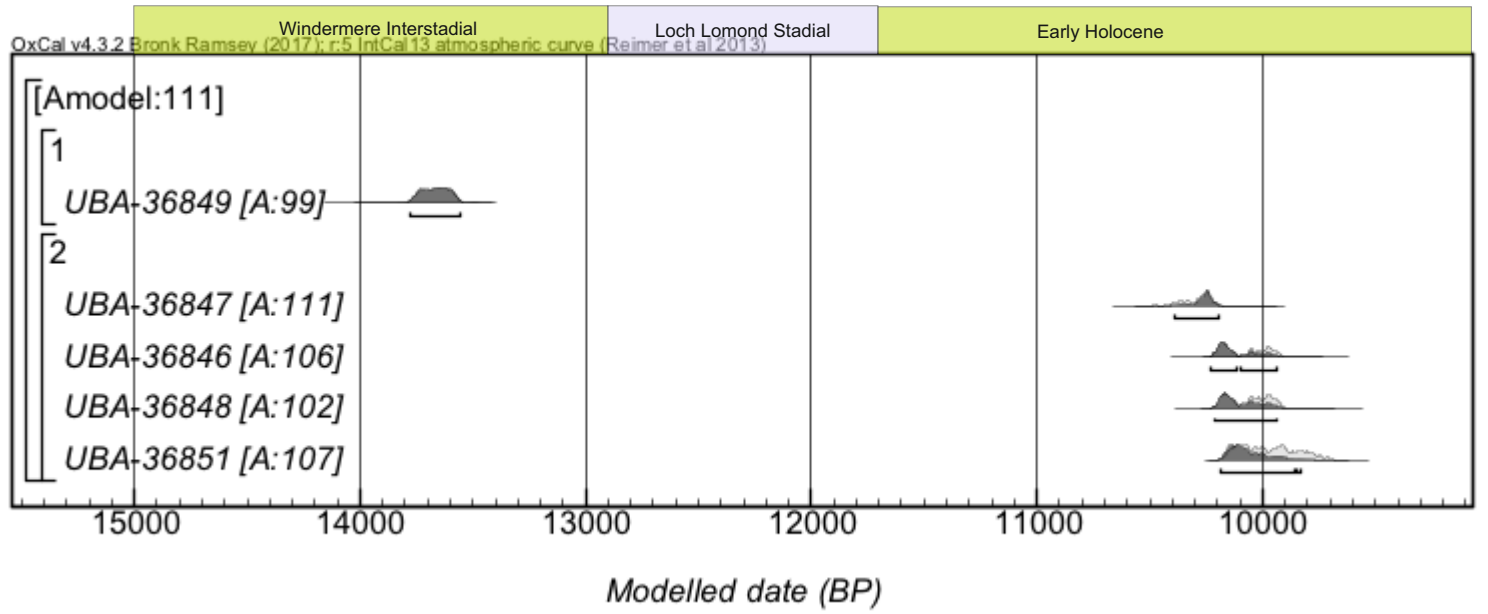
A. VC076



B. VC074



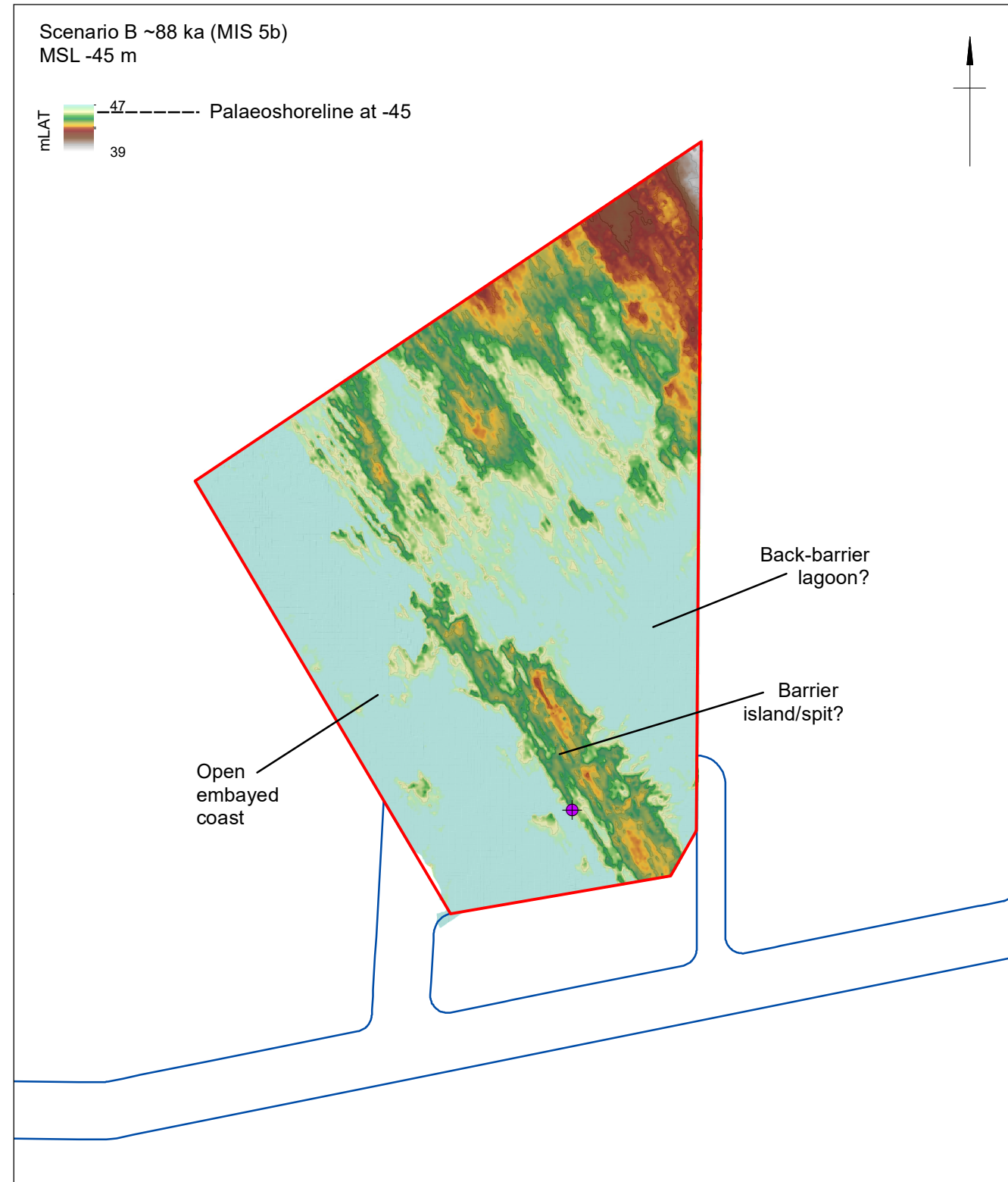
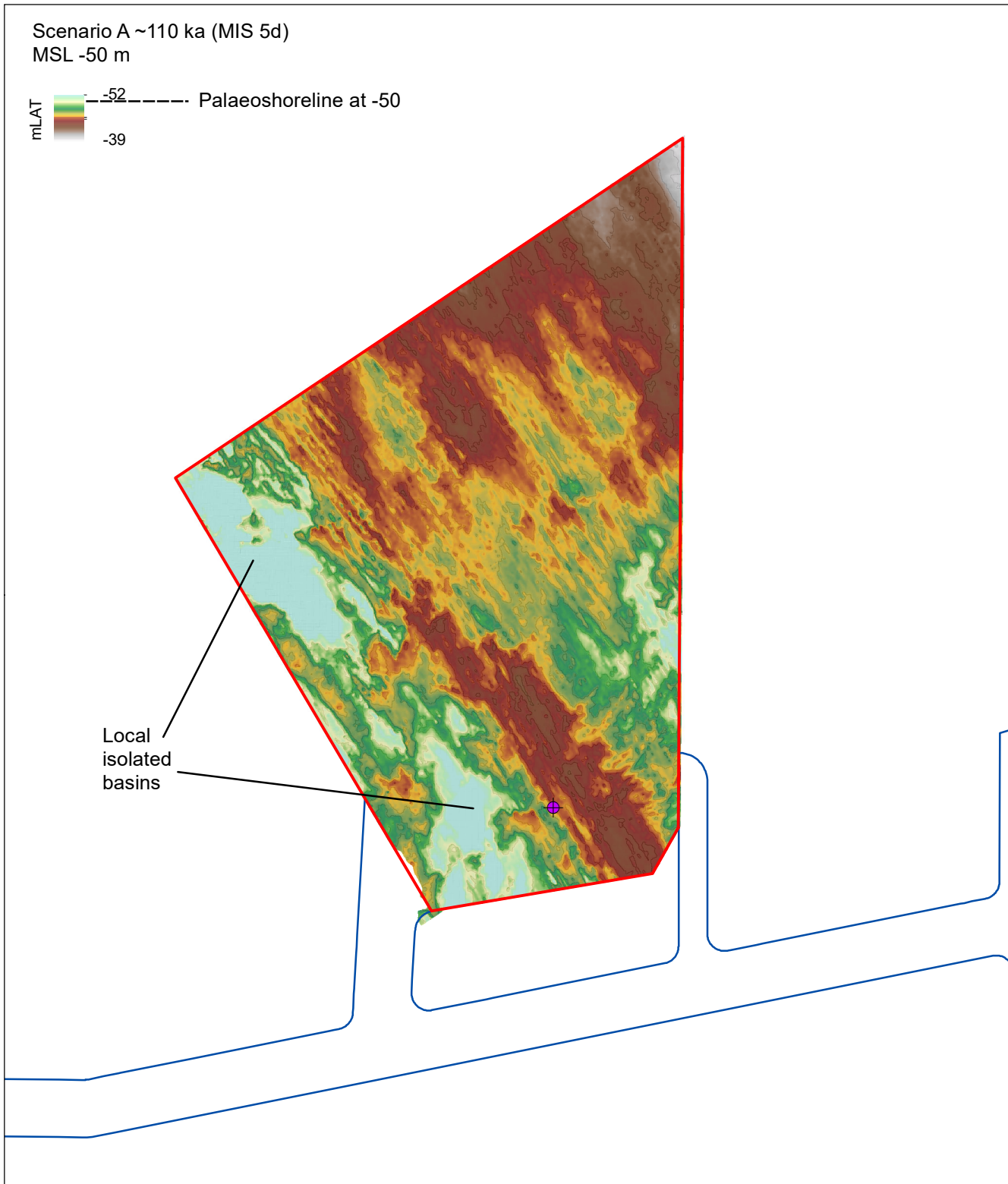
C. All accepted radiocarbon dates



This material is for client report only © Wessex Archaeology. No unauthorised reproduction.

Date:	28/01/2019	Revision Number:	0
Scale:	N/A	Illustrator:	ND
Path:	X:\PROJECTS\114844\Graphics_Office\Rep figs\Geoarch Stage 4\2019_01_28		





Coordinate system:  
ETRS 1989 UTM Z31N

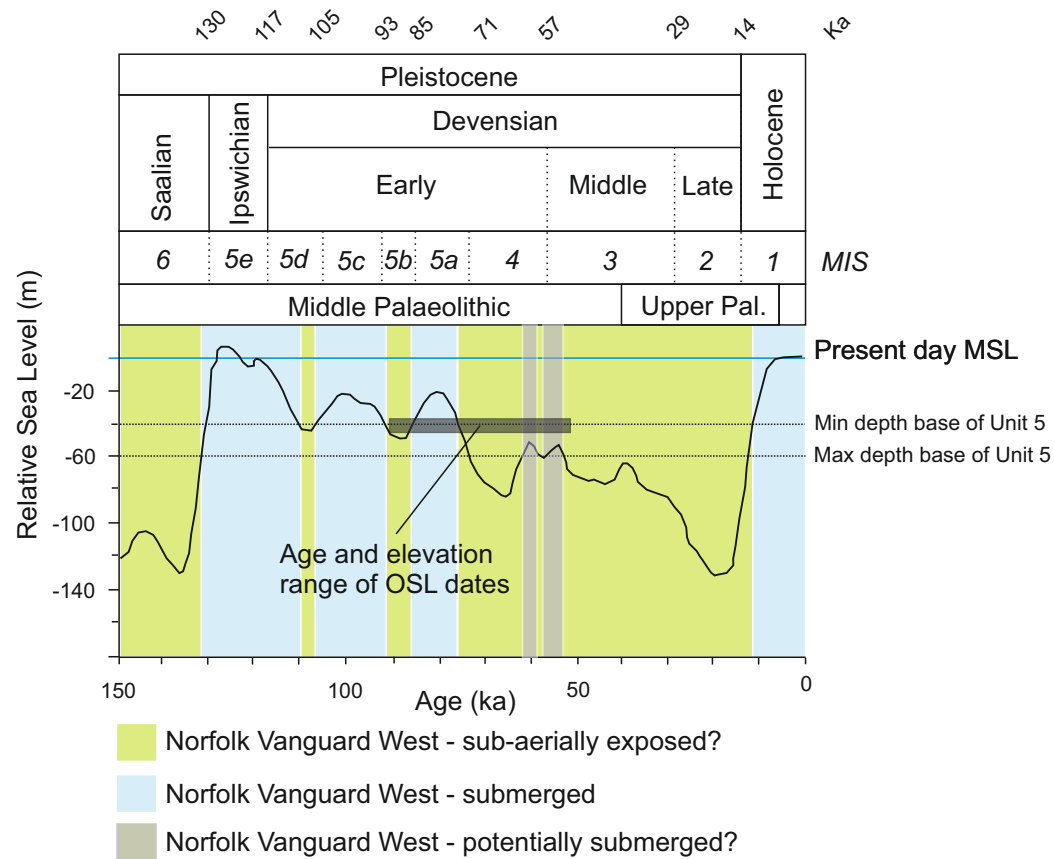
This material is for client report only © Wessex Archaeology.  
No unauthorised reproduction.

Norfolk Vanguard

Provisional Offshore Cable Corridor

VC079

Date:	28/01/2019	Revision Number:	0
Scale:	1:200,000 @ A3	Illustrator:	ND
Path:	X:\PROJECTS\114844\GIS\FigsMXD\Stage 4 Geoarch\2019_01_28		

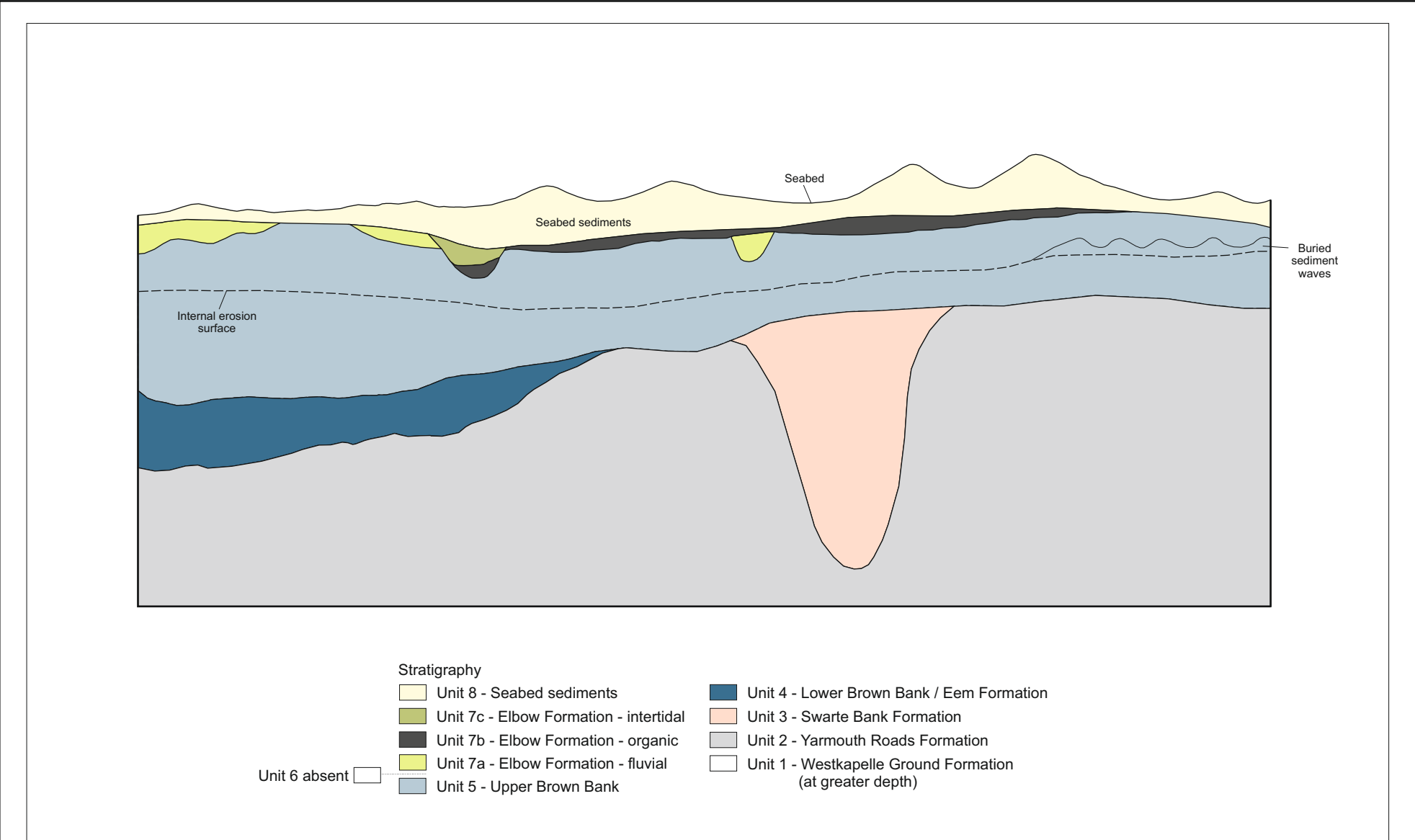



Sea-level data taken from Waelbroeck et al. (2002)  
 and elevation of the base of Unit 5 taken from Fugro (2017)



This material is for client report only © Wessex Archaeology. No unauthorised reproduction.

Date:	07/02/2019	Revision Number:	0
Scale:	N/A	Illustrator:	CM/ND
Path:	X:\PROJECTS\114844\GO\Rep figs\Geoarch Stage 4\2019_01_28\114844_Fig14.cdr		

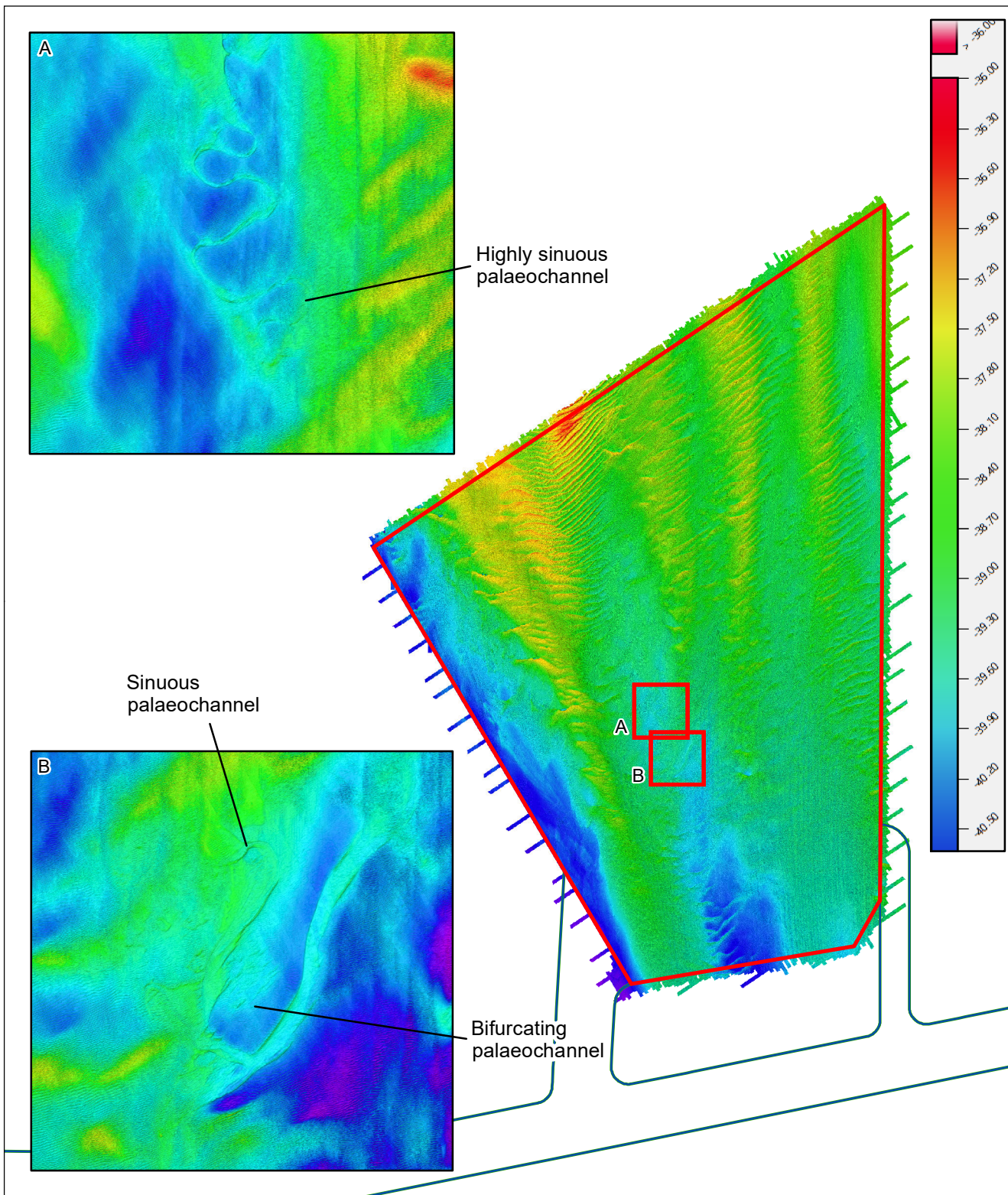


	This material is for client report only © Wessex Archaeology. No unauthorised reproduction.	Date:	07/02/2019	Revision Number:	0
		Scale:	NTS	Illustrator:	ND
		Path:	X:\PROJECTS\114844\GO\Rep figs\Geoarch Stage 4\2019_01_15\114844_Fig15.cdr		

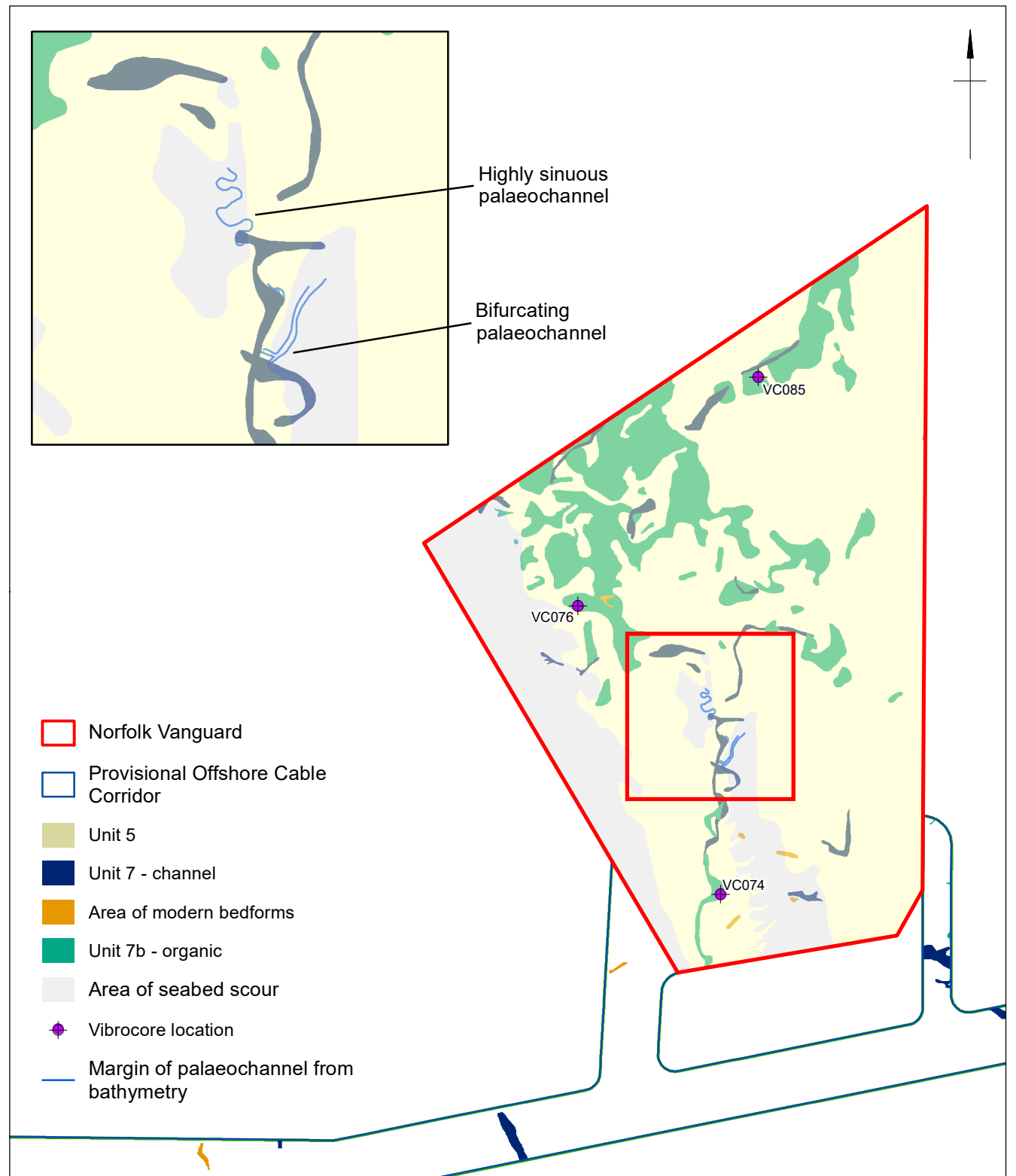
Schematic cross section of site stratigraphy (deposit model)

Figure 15





A. Palaeolandscape features identified from bathymetry



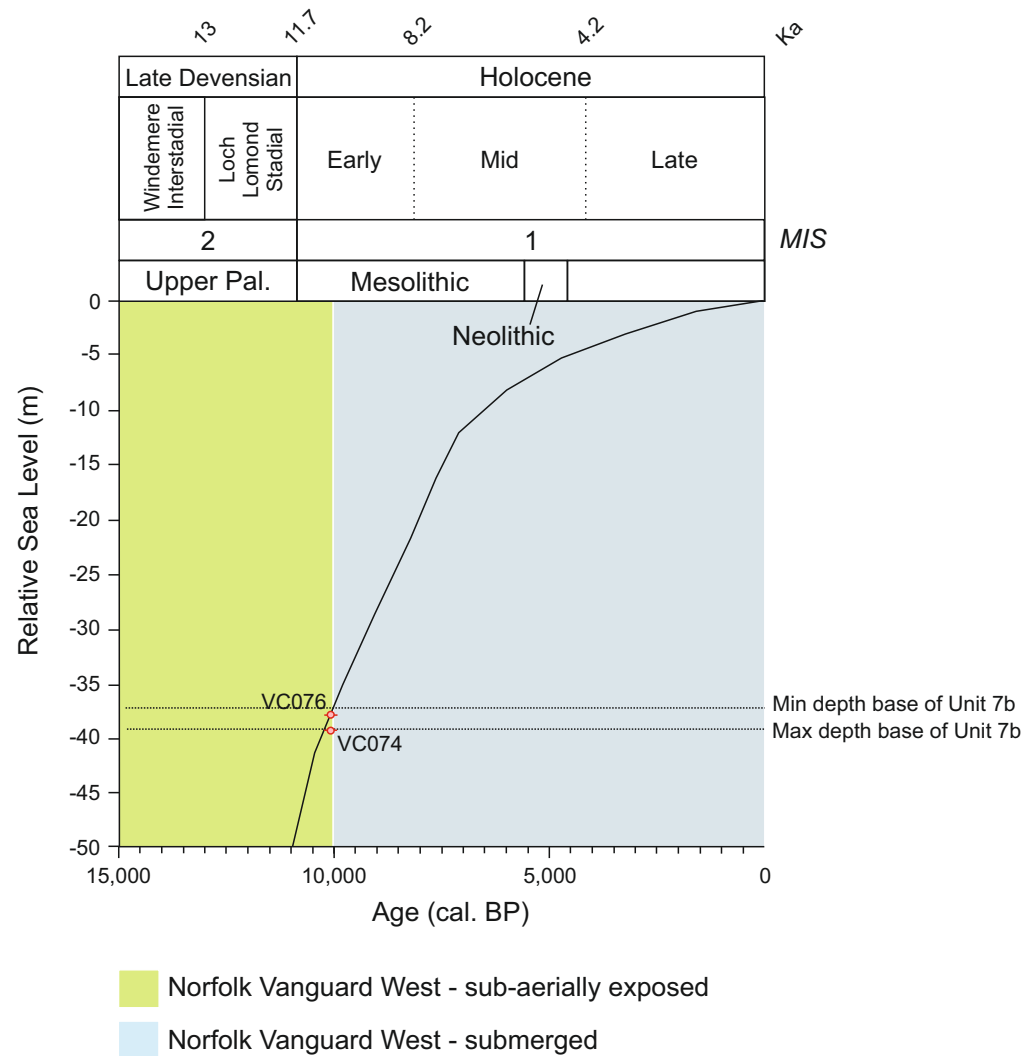
B. Interpretation



Coordinate system:  
ETRS 1989 UTM Z31N

This material is for client report only © Wessex Archaeology. No unauthorised reproduction.

Date:	08/02/2019	Revision Number:	0
Scale:	1:200,000 at A3	Illustrator:	ND
Path:	X:\PROJECTS\114844\GIS\FigsMXD\Stage 4 Geoarch\2019_01_28		



This material is for client report only © Wessex Archaeology. No unauthorised reproduction.

Date: 07/02/2019

Revision Number: 0

Scale: N/A

Illustrator: CM/ND

Path: X:\PROJECTS\114844\Graphics\_Office\Rep figs\Geoarch Stage 4\2019\_01\_28



Wessex Archaeology Ltd registered office Portway House, Old Sarum Park, Salisbury, Wiltshire SP4 6EB  
Tel: 01722 326867 Fax: 01722 337562 info@wessexarch.co.uk www.wessexarch.co.uk

